NAVAL POSTGRADUATE SCHOOL

MONTEREY, CALIFORNIA

THESIS

GUNSHOT DIRECTION OF ARRIVAL DETERMINATION USING BIO-INSPIRED MEMS SENSORS

by

Ionatan A. Soule

June 2022

Thesis Advisor: Fabio Durante Pereira Alves
Co-Advisor: Gamani Karunasiri

THIS PAGE INTENTIONALLY LEFT BLANK

REPORT DOCUMENTATION PAGE			*Form Approved OMB No. 0704-0188*

1. AGENCY USE ONLY *(Leave blank)*	**2. REPORT DATE** June 2022	**3. REPORT TYPE AND DATES COVERED** Master's thesis

4. TITLE AND SUBTITLE GUNSHOT DIRECTION OF ARRIVAL DETERMINATION USING BIO-INSPIRED MEMS SENSORS	**5. FUNDING NUMBERS** RPL4Y
6. AUTHOR(S) Ionatan A. Soule	
7. PERFORMING ORGANIZATION NAME(S) AND ADDRESS(ES) Naval Postgraduate School Monterey, CA 93943-5000	**8. PERFORMING ORGANIZATION REPORT NUMBER**
9. SPONSORING / MONITORING AGENCY NAME(S) AND ADDRESS(ES) ONR, Arlington, VA 22203	**10. SPONSORING / MONITORING AGENCY REPORT NUMBER**

11. SUPPLEMENTARY NOTES The views expressed in this thesis are those of the author and do not reflect the official policy or position of the Department of Defense or the U.S. Government.

12a. DISTRIBUTION / AVAILABILITY STATEMENT	**12b. DISTRIBUTION CODE**
Approved for public release. Distribution is unlimited.	A

13. ABSTRACT (maximum 200 words)

A key component of battle space awareness is direction of arrival (DoA) determination of gunshots. In the initial stages of an engagement, quick and reliable DoA determination enhances a Marine's ability to execute the observe-orient-decide-act (OODA) loop, increasing chances of survival and mission success. Naval Postgraduate School (NPS) has developed a novel, biomimetic acoustic sensor modeled after the auditory system of the Ormia Ochracea fly. This microelectromechanical system (MEMS)-based directional sound sensor, which consists of two wings connected to a substrate using two torsional legs in the middle, is well documented in previous NPS theses. Each sensor has a uniform dipole beam pattern. By combining two crossed MEMS sensors (crossed-dipoles) with an omni-directional microphone, 360° DoA determination can be fully resolved. The objective of this thesis is to evaluate, optimize, and develop DoA estimators for gunshots in the time- and frequency-domain, specifically for the crossed-dipoles sensors plus an omni-directional microphone configuration.

14. SUBJECT TERMS Ormia Ochracea, fly, angle of arrival, AOA, direction of arrival, DoA, gunshot, microelectromechanical system, MEMS, acoustic, detection, direction, bio-inspired, biomimetic, arctan estimator	**15. NUMBER OF PAGES** 115
	16. PRICE CODE

17. SECURITY CLASSIFICATION OF REPORT	**18. SECURITY CLASSIFICATION OF THIS PAGE**	**19. SECURITY CLASSIFICATION OF ABSTRACT**	**20. LIMITATION OF ABSTRACT**
Unclassified	Unclassified	Unclassified	UU

NSN 7540-01-280-5500

Standard Form 298 (Rev. 2-89)
Prescribed by ANSI Std. 239-18

THIS PAGE INTENTIONALLY LEFT BLANK

Approved for public release. Distribution is unlimited.

GUNSHOT DIRECTION OF ARRIVAL DETERMINATION USING BIO-INSPIRED MEMS SENSORS

Ionatan A. Soule
Ensign, United States Navy
BS, United States Naval Academy, 2021

Submitted in partial fulfillment of the
requirements for the degree of

MASTER OF SCIENCE IN APPLIED PHYSICS

from the

NAVAL POSTGRADUATE SCHOOL
June 2022

Approved by: Fabio Durante Pereira Alves
Advisor

Gamani Karunasiri
Co-Advisor

Joseph P. Hooper
Chair, Department of Physics

THIS PAGE INTENTIONALLY LEFT BLANK

ABSTRACT

A key component of battle space awareness is direction of arrival (DoA) determination of gunshots. In the initial stages of an engagement, quick and reliable DoA determination enhances a Marine's ability to execute the observe-orient-decide-act (OODA) loop, increasing chances of survival and mission success. Naval Postgraduate School (NPS) has developed a novel, biomimetic acoustic sensor modeled after the auditory system of the Ormia Ochracea fly. This microelectromechanical system (MEMS)-based directional sound sensor, which consists of two wings connected to a substrate using two torsional legs in the middle, is well documented in previous NPS theses. Each sensor has a uniform dipole beam pattern. By combining two crossed MEMS sensors (crossed-dipoles) with an omni-directional microphone, 360° DoA determination can be fully resolved. The objective of this thesis is to evaluate, optimize, and develop DoA estimators for gunshots in the time- and frequency-domain, specifically for the crossed-dipoles sensors plus an omni-directional microphone configuration.

THIS PAGE INTENTIONALLY LEFT BLANK

Table of Contents

List of Figures

List of Tables

THIS PAGE INTENTIONALLY LEFT BLANK

List of Acronyms and Abbreviations

AOR Area of Operations

DAC data acquisition instrument

DFT discrete Fourier Transform

DoA Direction of Arrival

DOD Department of Defense

FFT fast Fourier Transform

FOP Figures of Performance

FT Fourier Transform

MEMS microelectromechanical system

NPS Naval Postgraduate School

SNR signal-to-noise ratio

SOI silicon-on-insulator

THIS PAGE INTENTIONALLY LEFT BLANK

Acknowledgments

I would like to thank my advisor, Dr. Alves, for always pushing me to work harder and to think deeper. His high expectations motivated me throughout the process and, without him, this thesis would not have been possible.

I would like to thank my co-advisor, Dr. Karunasiri, for always asking insightful and thought-provoking questions. They encouraged me to look for creative solutions.

I would like to thank Dr. Rabelo for helping me navigate the complicated world of data collection. Without his guidance and expertise, troubleshooting would have been measured in days and not hours.

I would like to thank Dr. Crooker for always being available to discuss different approaches to codes and algorithms.

I would like to thank all of the students in the Sensors Research Lab for making the whole experience enjoyable and memorable.

Thank you all.

THIS PAGE INTENTIONALLY LEFT BLANK

CHAPTER 1:
Introduction

1.1 Background

In modern warfare, gunshots often serve as a soldier's first warning of enemy presence and an imminent engagement. As such, the issue of gunshot location is of critical importance to the defense and civil law enforcement industries for applications in sniper and enemy engagement detection, passive crime detection, as well as anti-poaching efforts in Africa to name a few [1]–[3]. Much research is being conducted on this matter. In military applications, gunshot detection technology can be a deciding factor in the initial stages of an engagement or anti-sniper operations. Quick and accurate Direction of Arrival (DoA) determination of a gunshot directly contributes to battlespace awareness allowing for quick, effective, and actionable decisions and deployment of countermeasures which will increase the probability of mission completion with minimal casualties.

In actuality, various gunshot DoA determination methods exist including non-acoustic and acoustic means. Non-acoustic means center around electro-optic detection of the flash of a gunshot and/or the heat emitting from the firearm or the body of the enemy assailant [4]. Another source is the retro-reflective lights off of rifle scopes [5]. All of these can be searched for through various imaging techniques such as regular daylight cameras and more likely, infrared imaging devices. Localization can be achieved via a single imaging device or an array of such devices. One critical limitation of an electro-optical approach is requiring a direct line of sight from the sensor to the thermal source since light diffracts little around thermally opaque objects. Other limitations include background radiation that could hide features required for localization [4], [5] as well as the narrow field of view of current imaging methods requiring sensors to be pointing in the right direction. Though many electro-optical detection systems are available to detect and locate a variety of battlefield relevant objects serving a critical role in many tasks, acoustic detection is better suited for gunshot detection and localization.

Acoustics is a much more common approach to gunshot DoA determination and has been the focus of many recent research efforts as discussed in Chapter 2. Many commercial systems also exist including Raytheon's Boomerang III, which is currently being deployed in the battlespace to support and protect our troops [6]. Acoustic systems have several advantages, the greatest being their ability to detect and locate gunshots coming from any direction even if the source is occluded behind an obstacle [7]. On the battlefield, this omni-directional detection is critical because a sensor system is incapable of missing a shot because it happened to be pointed in a different direction. This allows for an easy setup-and-forget system that will passively work in the background without requiring additional Marines to control and direct.

Current acoustic systems rely almost exclusively on arrays of omni-directional microphones, as established in Chapter 2. Omni-directional microphones are readily available and provide that passive 360° listening capability discussed earlier. As such, they seem an obvious choice for DoA determination applications. Unfortunately, their omni-directional quality is exactly what makes them incapable of determining incident direction by themselves. As such, multiple omni-directional microphones must be joined in a distributed array to allow for DoA determination capabilities. Multiple methods are available to determine incident angle of a sound on an array of microphones such as phased power steering, but the most common and easy to implement is what is called a time difference of arrival algorithm. Applying this technique requires that the microphones be spatially distributed. Unfortunately, this results in gunshot DoA determination systems that are relatively large, cumbersome, and often too heavy or impractical to be carried by an individual combatant requiring instead to be fixed site or vehicle mounted. While they are still incredibly capable systems, a smaller soldier-transported system that provides the same coverage and abilities would be highly beneficial to increasing battlespace awareness, command and control, and survivability in the battlefield.

At the Naval Postgraduate School (NPS), researchers are currently working on developing such a system. The system relies on microelectromechanical system (MEMS) sensors inspired by the parasitoid fly *Ormia Ochracea*. These MEMS sensors show promise in being able to detect the azimuth of an incoming gunshot with just two collocated *Ormia Ochracea* inspired sensors and one commercial MEMS omni-directional microphone. This means that, unlike the distributed arrays of current commercial systems, this DoA determination

system will be small, light, and easily carried by an individual on the ground as a rifle/helmet attachment or a separate handheld device.

1.2 Thesis Objective

In this context, the objective of this thesis is to develop the means of calculating gunshot DoA using a combination of two *Ormia*-inspired MEMS sensors and one commercial MEMS microphone, all collocated, and evaluate its performance under various gunshot stimuli in a research setting as well as in the field.

This development includes:

- understand the frequency response of the *Ormia*-inspired sensors, their differences and limitations,
- study and adapt DoA determination algorithms as well as,
- apply corrective signal processing to improve accuracy.

The study research questions are:

1. Can the collocated sensor combination be used to provide 360° DoA determination?
2. Can DoA be determined in the frequency domain to allow for the application of more processing techniques?
3. Can different sensor responses be corrected in the frequency domain to increase accuracy of DoA algorithms?
4. Assuming questions provide affirmative answers, what is the achievable accuracy of the system?

THIS PAGE INTENTIONALLY LEFT BLANK

CHAPTER 2:
Literature Review

2.1 Acoustic Signature of a Gunshot

In order to acoustically determine the DoA of a gunshot, a basic understanding of a gunshot's acoustic signatures and the main contributing factors is required. Both will be explored in the subsequent sections.

Characteristics

When fired, a gun produces sound in three distinct ways: muzzle blast, mechanical action, and Mach cone [1]. The muzzle blast is produced by the detonation of the cartridge propelling the projectile out of the barrel. Most of the energy released from this action is in the direction of the barrel, but sound still propagates in all directions from the gun [1]. The sound wave produced usually lasts about 3 milliseconds [8] and is loud, typically on the order of 120-160 dB [9]. If the microphone receiver is close enough to the gun, it may be able to pick up the mechanical action of the gun which is comprised of all mechanical sounds such as the bolt, trigger, or cartridge. Finally, if the projectile leaves the barrel at a supersonic speed it will produce a shockwave propagating at the speed of sound perpendicular to the direction of travel in the shape of a Mach cone [1]. The mechanical action is negligible at any appreciable distance and the Mach cone is only detectable perpendicular to the path of the projectile when it is at supersonic speeds. This provides limited coverage, as shown in Figure 2.1. The primary acoustic source for gunshot detection is the muzzle blast as is evident in Figure 2.2. Due to their near instant pressure changes both Mach cone and muzzle blast can be considered impulsive sounds, which, unfortunately, suffer the most from environmental effects [1].

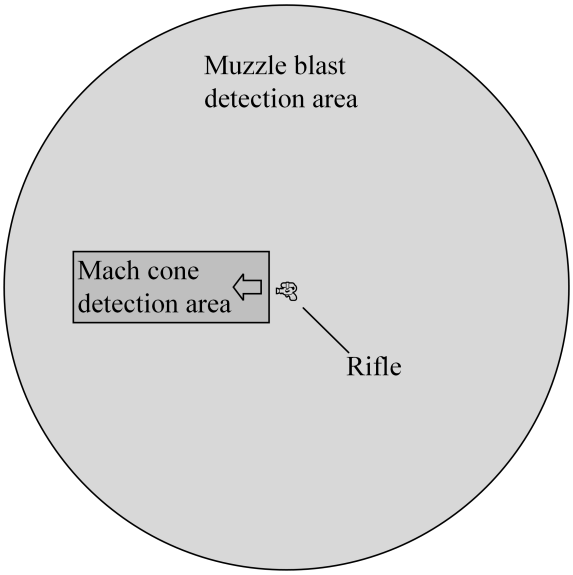

Figure 2.1. Diagram depicting advantages of muzzle blast over Mach cone detection. Mach cone can only be detected with a sensor positioned in the dark gray box, while muzzle blast is detectable in the larger light gray circle.

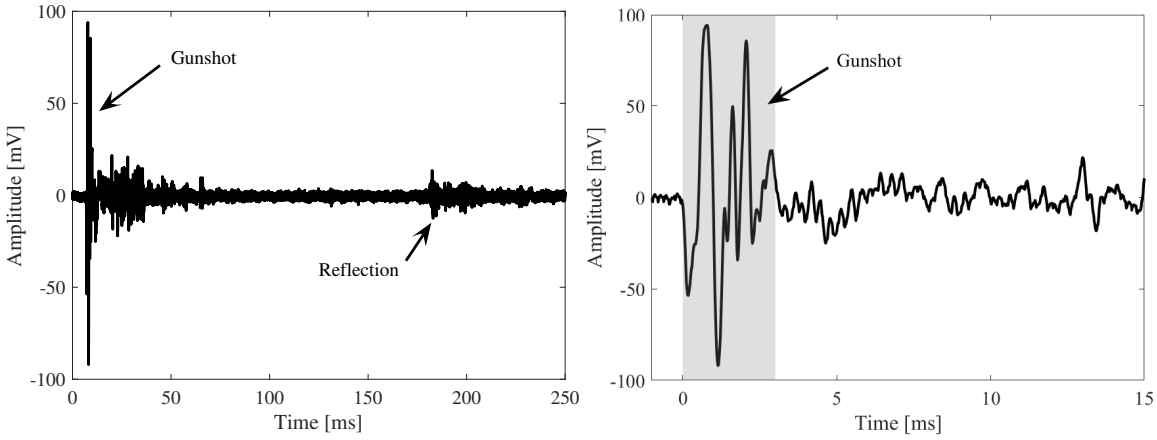

(a) (b)

Figure 2.2. Audio file of 9mm gunshot in an open field in the vicinity of an obstacle. Reflection from obstacle is visible in (a). Short 3 ms duration of gunshot highlighted in (b). Recording was taken during the Paso Robles field exercise discussed in detail in Section 4.2.

Environmental Effects

Environmental effects must be taken into consideration as they can significantly alter propagating sound waves between source and receiver. Maher et al. [1] summarizes key environmental factors in a 2007 paper. The most significant impacting factor in free space propagation is wind. A crosswind will produce an apparent origin shift introducing error into a DoA determination; a tail- or headwind will cause a doppler shift. The magnitude of these effects increases with propagation distance and may not be constant along the path. Vertical temperature gradients along the ground can bend sound much like they affect light propagation, causing an up- or downwards curve to the propagation path [1]. Propagating sound will also be affected by obstacles in its path which cause energy loss, scattering, reverberation, and multi-path reflections all of which add increased complexity to the problem at hand—gunshot detection and DoA.

2.2 Current Direction-Finding Technology for Gunshot DoA Determination

Gunshot detection and localization sensors can serve as force multipliers in many spaces including military battlespace and civilian law enforcement. On the Department of Defense (DOD) side, their implementation has the potential of greatly increasing a unit's combat effectiveness, safety, lethality, and survivability. With the aid of such a system, units will be provided with critical and actionable information within seconds of a sniper engagement or ambush, significantly accelerating the deployment of countermeasures. Furthermore, with the implementation of wireless networks, offsite chain of command, commanders and support teams will have access to valuable and time sensitive information without hampering the engaged unit's efficiency by requiring status reports. In the civilian sector, but also with clear DOD relevance, passive sensors can be used as gunshot surveillance units in high-crime areas capable of alerting the proper authorities of the nature and location of gunfire. Current commercial systems available include Boomerang, ShotSpotter, and EARS SWATS, PEARL, PILAR, and ACLOGUS.

2.2.1 Commercial systems

Boomerang

Boomerang is an acoustic gunshot detection system developed for defense applications by Raytheon Intelligence & Space [website]. The current system, Boomerang III, is a passive acoustic listening system with an array of seven omni-directional microphones utilizing a time-of-arrival algorithm for DoA determination [6]. The standard sensor array must be site- or vehicle-mounted as it is too large and heavy to be carried by an individual soldier, but a vest-integrated version, the Boomerang Warrior X, is also available though it suffers from decreased performance [10]. It boasts a $> 95\%$ shot detection rate with no false positives in less than one second of processing time [10]. Key Figures of Performance (FOP) for both the Boomerang III and Boomerang Warrior X systems are summarized in Table 2.1. Other features of the system include motion compensation for mobile mounts and friendly fire filtering [10]. Furthermore, multiple sensor arrays can be linked to provide heightened large-area coverage allowing for the application of multi-angulation techniques [10]. Bullet Ears, a well-known system that popularized acoustic gunshot detection, was Boomerang's predecessor [11].

Table 2.1. FOP for Raytheon's Boomerang III and Warrior-X systems. Adapted from [10].

Performance Accuracy:	Boomerang III	Boomerang Warrior-X
Azimuth	$< 2.5°$	$< 7.5°$
Elevation	$< 2.5°$	$< 15°$
Range	$\pm 10\%$	$\pm 20\%$

ShotSpotter

ShotSpotter [website] is a company developing a proprietary acoustic gunshot detection and localization sensor system of the same name. The sensor system is developed primarily for civilian law enforcement to aid them in detecting, locating, and reporting gunshots over large areas [12]. Single point sensors suffer from azimuthal, elevation, and range ambiguities and can be easily mislead by multi-path propagation common in urban environments where the sensor is primarily deployed [13]. To overcome these limitations, ShotSpotter has developed an integrated wide-area distributed array of passive acoustic omni-directional

microphones [13]. Microphones are fixed throughout the Area of Operations (AOR) and listen passively for a gunshot. Once a gunshot is detected, two DoA determination methods are employed: 1) multi-lateration based on time difference of arrival, and 2) multi-angulation based on angle of arrival [13]. ShotSpotter can then localize the gunshot within 80 feett of where the shot was actually fired [12]. Due to the distributed nature of the network shot-to-localization takes 2-3 seconds making it unfeasible for most military operations such as counter-sniper operations [13]. The distributed array, however, helps improve other FOP; by imposing a multi-sensor activation requirement, ShotSpotter has a > 97% shot detection accuracy. A 3% error over 360° results in approximately 10° of error [12]. It also achieved a < 0.5% false positive rate across all reported gunfire incidents [12].

EARS

EARS (Early Attack Reaction Sensor) is another commercially available acoustic gunshot detection and localization sensor developed by QinetiQ Inc. [website] for defense applications. It comes in three variants: EARS SWATS (Shoulder-Worn Acoustic Targeting System), EARS VMS (Vehicle Mounted System), and EARS FSS (Fixed Site Sensor) [14]. The focus of QinetiQ Inc. in developing this sensor was light weight and portability for soldier worn applications in their SWATS variant [15]. The sensor is a passive acoustic sensor that consists of a two-dimensional array of omni-directional microphones [16]. Once a gunshot is detected, time-of-arrival calculations are performed on the muzzle blast and the supersonic shockwave if present to get DoA and range estimates [16]. It has a > 95% gunshot detection rate with a processing time of a quarter second [15]. Range and bearing FOP are summarized in Table 2.2. Compared to Raytheon's soldier-worn Boomerang Warrior-X system, the EARS SWATS sensor is superior in accuracy and processing time at a decreased weight and size while providing similar features such as friendly fire filtering [14]. Furthermore, multiple sensors can be linked in a network to provide heightened accuracy for larger area coverage [14].

Table 2.2. FOP for QinetiQ's EARS. Adapted from [15].

Performance Accuracy:	EARS SWATS
Azimuth	±7.5°
Range	±10%

PEARL and PILAR

Metravib Defense [website] has produced a family of acoustic gunshot detection and localization systems based around the same sensor. The family includes the PEARL (Personal Equipment Add-on for Reactive Localization) system which is rifle-mounted, and the PILAR system which has vehicle-, helicopter-, and site-mounted variants [17]–[19]. Each system is comprised of at least one acoustic array with four omni-directional microphones arranged to form a tetrahedral antenna [20]. The PEARL system relies on one such sensor, while the different PILAR systems rely on two or more [20]. Once a gunshot is detected, each system estimates the wave vector of the incoming pressure wave through time-of-arrival calculations on muzzle blast and supersonic crack signatures to provide an azimuth and elevation estimate [20]. Since the PILAR system has multiple acoustic arrays, it is also capable of estimating range [18]. From the moment of detection, response time takes less than two seconds and it has a $> 95\%$ gunshot detection rate which are slower and comparable to previous systems respectively [21]. FOPs for each system are summarized in Table 2.3.

Table 2.3. FOP for Metravib's PILAR and PEARL systems. Adapted from [17]–[19].

Performance Accuracy:	PILAR V	PILAR Helicopter	PEARL
Azimuth	±2°	±15°	±7.5°
Elevation	±3°	±15°	±7.5°
Range	±10%		

ACLOGUS

Microflown AVISA [website] has produced the first dedicated acoustic vector microphone currently deployed in gunshot detection and localization systems for ground- and vehicle-mounted defense applications [22]. The basic sensor contained in their systems is a MEMS acoustic vector transducer with dipole directionality capable of detecting sound pressure and particle velocity [22]. The ACLOGUS (ACoustic LOcalization of GUnshotS) system is comprised of four sub-arrays each containing four crossed-dipole transducers for a total of 32 sensors [22]. DoA and range estimates are determined using time-of-arrival and direction-of-arrival algorithms on both the shockwave and muzzle blast of the detected

gunshot [22], [23]. A summary of ACLOGUS's advertised FOPs is provided in Table 2.4, but controlled experiments have achieved $< 0.5^\circ$ azimuth and $< 2\%$ range accuracy [21]. The entire system provides various additional features such as filtering vehicle noise and reflections due to mount surfaces [23].

Table 2.4. FOP for Microflown AVISA's ACLOGUS system. Adapted from [22].

Performance Accuracy:	ACLOGUS
Azimuth	$< 2^\circ$
Range	$\pm 10\%$

Conclusions

As established above, current gunshot localization technology is advanced and capable, but there is still significant room for improvement. For the most part, systems rely heavily on distributed arrays of many sensors as shown in the Boomerang III, ShotSpotter, EARS VMS, PILAR, and ACLOGUS systems making them impractical, if not impossible, for an individual soldier to carry. Though various systems come in soldier transportable variants—Boomerang Warrior-X, EARS SWATS, and PEARL—their performance is severely reduced as seen in the FOP tables making them less effective in providing capabilities that would increase the effectiveness, response time, and survivability of our troops. Ideally, an acoustic sensor or group of collocated sensors capable of detecting DoA accurately is desirable.

2.2.2 Research Systems

Research into acoustic gunshot DoA determination is a current and ongoing effort. Although various systems are commercially available as discussed in 2.2.1, research is still required to improve accuracy, robustness, and reliability in all environments especially the non-ideal. Current lines of effort in research can be subdivided into two categories. The first involves DoA determination via traditional algorithms which includes time delay of arrival calculations between separate microphones [7], [24]–[28]. The second attempts to take advantage of the adaptability of artificial neural networks and other advanced computing techniques [29], [30].

Localization via Traditional Methods

Many commercial systems rely on the presence of both a muzzle blast and supersonic shock wave to localize a gunshot [24]. This presents a serious limitation as both acoustic components must be detected by the sensor system requiring clear path propagation for the shockwave [24]. Furthermore, subsonic guns do not produce a shock wave [1]. In 2017, Fernandes et al. [24] published a paper to address this limitation and propose a solution: a drone-mounted system. Such a system presents various advantages including a wider surveillance area and better chances of clear path propagation [24]. They utilized a planar array of five omni-directional microphones arranged in a rectangle with one central microphone [24]. The array was mounted on the belly of the quad-copter and the microphones were shielded to minimize the effect of the vibration and incurred wind caused by the propellers [24]. Once a gunshot was detected, DoA was determined by a generalized cross correlation algorithm with phase transformation (GCC-PHAT) to determine the time delay of arrival between different microphones [24], [31]. Both 3-dimensional and 2-dimensional solutions were explored, but only the 2-dimensional solution was applied under the assumption that the gunshot source was at the same elevation as the drone [24]. Experimental DoA results produced a max error of $< 19^\circ$ with a mean value of -2.94° and a standard deviation of 5.13° [24].

Another limitation in current acoustic DoA determination technology is the presence of obstacles that disrupt the propagation path of a gunshot [7], [24]. This is especially present in current urban war fighting environments. Sinha et al. [7] attempt to find a more robust method for handling this issue published in a 2018 paper. Using a virtual array of three microphones they were able to simulate various indirect propagation path scenarios with rectangular obstacles. To do this, they solved the two-dimensional linearized Euler equations in the presence of rectangular obstacles while preserving the dispersion relations [7]. The detected wavefront curvature at the three sensors was then used to estimate the gunshot source location [7]. The scenario only requires muzzle blast detection which also helps increase robustness as set forth by Fernandes et al. [24]. The approach proved effective for azimuth determination, but was ineffective for range calculations [7]. Simulated scenarios resulted in a maximum error of $\leq 3^\circ$ over all cases analyzed and $\leq 8^\circ$ when random noise was artificially added [7]. The simulation also demonstrated that larger obstacles induce increased error [7].

Noise can be a formidable limitation especially in real world application of acoustic DoA determination of gunshots. As such, much research focuses on mitigating its impact on sensor systems. In 2019, Svatos et al. [26] published research showing increased effectiveness of DoA determination in high noise environments. The sensor being tested consisted of a four acoustic microphone array arranged in a tetrahedral pattern [26]. The three microphones forming the base allowed for determining azimuth while the peak microphone in conjunction with the base provided elevation [26]. These sensors were attached to an analog pre-processing unit and then to a data processing unit that ran a modified time delay of arrival algorithm to determine gunshot location [26]. The time delay of arrival of the gunshot signature also aided in overcoming noise by comparing the time delay between microphones to the maximum time delay possible, a geometric property. Unless all four sensors detected a gunshot within the maximum time delay possible, the potential gunshot was discarded [26]. The setup was fine tuned in an anechoic chamber and then tested in the field at a shooting range [26]. Experimental results show an accuracy of $\pm 1.8^\circ$ and $\pm 3.8^\circ$ for azimuth and elevation, respectively [26]. Furthermore, the sensor was able to detect 100% of gunshots with an $SNR \geq 5dB$ with only 12% of doors slamming registering as false positives [26]. This paper is proof that even a simple microphone setup can achieve impressive DoA results in the presence of high noise with the proper data processing.

While most DoA determination systems rely on a single closely spaced microphone array [1], [7], [24], [26], [28]–[30], Tran et al. [27] decided to try a slightly different approach in a 2020 paper. Instead of a localized microphone array, [27] decided to create a distributed network of four smaller acoustic arrays located at the corners of a large rectangular working array in which gunshots could be localized [27]. Each array consisted of three acoustic microphones arranged in a planar equilateral triangle [27]. Each sub-array would detect and localize the gunshot using a time delay of arrival algorithm and then the final location was determined by finding the quadrilateral center of the four crossing points [27]. The researchers computed time delay of arrival algorithms using four different features: when threshold is first triggered between sensors, when maximum excitation occurs between sensors, using the Akaike's Information Criterion, and using the cross correlation function [24], [27], [31]. Without noise, all four techniques produced comparable results with errors of $\approx 1.5\%$ in a $500m \times 500m$ working area [27]. With added noise, the time delay of arrival of the maximum amplitude provided the best results with an average relative error of 1.5%

and the added benefit of low computational cost [27]. One limitation the paper discussed is the added necessity of wireless synchronization between the distributed array elements which is required for time delay of arrival calculations to be effective and accurate [27].

Most recently, Park et al. [28] have attempted a novel acoustic gunshot DoA determination by combining steered response power phase transformation (SRP-PHAT) and an interaural level difference (ILD). ILD is another term for a time delay of arrival approach since it relies on physical separation of the microphones. By combining the two methods they hoped to supplement SRP-PHAT's high angular accuracy with ILD's ability to improve an insufficient range accuracy [28]. The experiment was carried out in an anechoic chamber with two acoustic arrays of 6 microphones each arranged at the corners of a regular hexagon [28]. Each array was steered and the ILD was established between both arrays as well as between the microphones of each individual array [28]. Measurements were taken by moving the speaker in 10° increments to a maximum of 60° on each side of a beam-fired array for a total of 120° of DoA determination [28]. Range and the distance between arrays was also varied [28]. Results show that including ILD (time delay of arrival) calculations significantly improved the gunshot localization ability, for azimuth and range, of the sensor setup compared to just including an SRP-PHAT algorithm [28]. Furthermore, it was determined that error increases with range and that the method needed testing in high-noise reverberant methods, a limitation explored previously by Svatos et al. [26], [28].

Localization via Advanced Computing

A new line of investigation has appeared due to the advent of advanced computing techniques such as machine learning and artificial neural networks (ANN). A recent 2018 study conducted by Ding et al. [29] applies deep learning algorithms to acoustic gunshot localization problems. The hope is that such a method will be more accurate and prove more adaptable to varying environments especially those with low signal-to-noise ratios [29]. Instead of applying the deep neural network (DNN) to solving an intensive acoustic modeling problem, the task set forth to the DNN is a less computationally intensive categorical identification task [29]. This is achieved by dividing the azimuth into subspaces [29]. This experiment assumes a linear array of two microphones setup against the wall of a room [29]. The 180°'s of azimuth is subdivided into ten 18° subspaces [29]. Gunshot recordings were then played through a loudspeaker and the data recorded by the microphones was passed to the DNN as

the input [29]. The output of the DNN was one of the indexed subspaces [29]. These results were compared to the GCC-PHAT algorithm developed by Knapp and discussed earlier [29], [31]. The DNN approach achieved high accuracy in subspace determination especially in high SNR and reverberant environments which is advantaguous for possible DOD applications [29]. Another advantage is that the audio data is passed directly to the DNN and does not require any additional computational power to pre-process the signal [29]. Once trained for its location, the DNN process presents a low computational requirement [29]. One limitation is that subspace size determines maximum azimuth resolution; more subspaces would result in a higher resolution at the cost of an incorrect categorization [29].

Galangque et al. [30] performed a similar neural net study in 2019 in which they used an ANN to both distinguish and locate a gunshot [30]. For gunshot identification, spatial and frequency features of the recorded gunshot were used as inputs to determine whether or not a muzzle blast and shock wave were present [30]. This method achieved a 99% identification rate for M16 gunshots against a background of firecrackers [30]. More interestingly, the gunshot localization approach utilized both time delay of arrival calculations and an ANN [30]. The experiment was carried out using an array of four acoustic omni-directional microphones arranged in a planar square [30]. Once a gunshot was detected, the time delay of arrival calculations were determined for all possible microphone pairs and these values were fed to the ANN as the input layer [30]. Much like Ding et al., Galangque et al. decided to approach localization as a categorization problem as opposed to an intensive acoustic modeling problem [29], [30]. They divided the 360° of azimuth into 24 subspaces which set a maximum resolution of 15° [29]. The resulting ANN was able to determine the correct azimuth subspace [30]. Like the previous study involving machine learning techniques, a major limitation is the trade-off between tighter subspaces and increased false categorizations [29], [30].

2.3 Bio-Inspired MEMS Sensors for DoA Determination

In 1995, Robert Miles [32] published an article in the Journal of the Acoustical Society of America. The title read "Mechanically coupled ears for directional hearing in the parasitoid fly *Ormia Ochracea*," and it presented a possible solution for an ultra-small sensor capable of DoA determination.

Mammalian hearing relies on careful spacing between individual ears and ears' canal shape to help determine DoA for incoming sounds [32]. They use a combination of directional amplification provided by the physical structure of the ear and time-delay provided by the interaural spacing between the ears to resolve a bearing on the sound. This type of auditory system is observed throughout the animal kingdom and appears to be standard, but it is not the only one.

The fly *Ormia Ochracea* is a small parasitoid fly whose size does not allow for two separate auditory sensors to be placed far enough apart to experience sufficient changes in incoming acoustic events [32]. This is because the span of its hearing organ is approximately 50 times smaller than the wavelength of sound they are trying to localize [32]. Despite this seeming limitation they can detect a cricket's, their host's, chirp with an accuracy below two degrees [32]. Since it lacks the required size to determine DoA based on interaural time delays, it instead, must rely on a separate mechanism.

Instead, the most notable difference is that the left and right hearing organs are coupled together through a mechanical pivot. Through an in-depth analysis, Miles et al. [32] shows that the behavior of this structure can be modeled accurately as two stiff wings coupled by a torsional bridge. This torsional pressure allows the motion of one side to affect the motion of the other, thereby permitting two oscillatory modes, a rocking and a bending mode. This setup results in an incident sound wave of 45 degrees having an effective time delay of approximately 2.5 micro-seconds. Essentially, the mechanical system amplifies the time delay despite the small size [32].

Researchers at the Naval Postgraduate School have successfully produced a MEMS sensor modeled after the fly's torsional bridge hearing organ [33]–[36]. The sensor is manufactured out of a silicon-on-insulator (SOI) substrate and includes two wings connected via a thin bridge and support to the substrate by torsional legs. This concept is fully customizable to be resonant at a designated frequency. The wings are terminated with comb finger capacitors, interdigitated with the substrate allowing transduction between vibration to capacitance oscillation and then to voltage through charge amplification [33]. A detailed description of the sensor can be found in [33]–[36].

The fly *Ormia Ochracea* has inspired other approaches to biomimetic MEMS sensors designed for DoA determination. These variations are being designed and tested by re-

searchers all over the world. Michael Kuntzman et al. [37] reported on a similar approach using paddles suspended by a torsional bridge [33]–[36]. However, their biomimetic MEMS sensor includes four springs mounted to the outer edges of the paddles which are meant to enhance the rocking mode of the sensor. Additionally, piezoelectric transducers are used instead of combed-finger capacitors to sense vibration. Instead of using rectangular paddles, Ishfaque et al. [38] used a circular diaphragm. This sensor used piezoelectric transducers to detect vibration and claimed a higher signal-to-noise ratio (SNR) than compared literature and demonstrated a similar dipole response as shown in [33]–[37]. In 2020, Rahaman et al. [39] successfully broadened the traditionally narrow-band response of *Ormia*-inspired biomimetic sensors. This was accomplished by suspending coupled rectangular paddles by four torsional bridges instead of two and utilizing a piezoelectric readout scheme. This construction was able to achieve a working frequency range of $1 - 13$ kHz which is greater than the previously reported maximum of < 3 kHz [40], [41].

Another concept inspired by the *Ormia Ochracea* fly is being developed at University of Maryland College Park and the Army Research Laboratories. Instead of directly imitating the wing-bridge structure of the hearing organ, they developed a different configuration that still utilizes the mechanical coupling of the bridge. The configuration involves three coupled circular membranes in an equilateral triangle configuration whose oscillatory motion is detected optically. This configuration allows for two-dimensional azimuthal and elevation acoustic source localization [42].

In general, current sub-wavelength approaches to DoA determination inspired by the *Ormia Ochracea* fly include optical readouts such as diffraction gratings and optical fibers, piezoelectric readouts of different piezoelectric transducers, and capacitive readouts such as the combed-finger approach [43]. Support structures also vary with the principle methods being torsional bridges and centrally supported diaphragms [44]. Furthermore, the *Ormia Ochracea* fly is not the only animal that has inspired biomimetic MEMS sensors capable of DoA determination. Other research efforts are underway that study the hearing mechanism of geckos, elephant mosquitoes, and desert locusts [44]. Each idea presents particular advantages, challenges, and limitations. Table 2.5 summarizes the FOP, unique feature, and readout scheme for various research efforts.

Table 2.5. FOP and unique characteristics for current *Ormia*-inspired DoA determination sensors.

Works	Azimuth	Unique Feature	Readout scheme
Rahaman et al. [39]	±7°	Four torsional bridges	Piezoelectric
Kuntzman et al. [37]	±6.5°	Four additional springs	Piezoelectric
Lisiewski et al. [42]	±2°	Coupled circular diaphragms	Fiber-optic

Conclusions

The *Ormia Ochracea* fly presents a novel auditory system capable of determining DoA of incident acoustic events with wavelengths much larger than the dimensions of the organ itself. This ability is due in large part to the mechanical coupling between two wing-like membranes. This mechanism can be reproduced allowing for the development of small MEMS sensors with promising directional capabilities. The development and employment of such sensors could eliminate the need for large, cumbersome, and expensive sensor arrays that are currently being used and allow for the development of smaller units with similar if not better capabilities that are light, and easily transported by an individual soldier.

CHAPTER 3:
Theory

3.1 Sensor

As discussed in Section 2.3, Researchers at NPS have developed a MEMS sensor that imitates the unique hearing capabilities of the *Ormia Ochracea* fly [35], [36]. A diagram of the basic sensor can be seen in Figure 3.1. More information about the sensor design can be found in [33]–[36]. The critical characteristics of the sensor are its frequency response and directional response which together these define the sensor's capability and effectiveness in gunshot DoA determination.

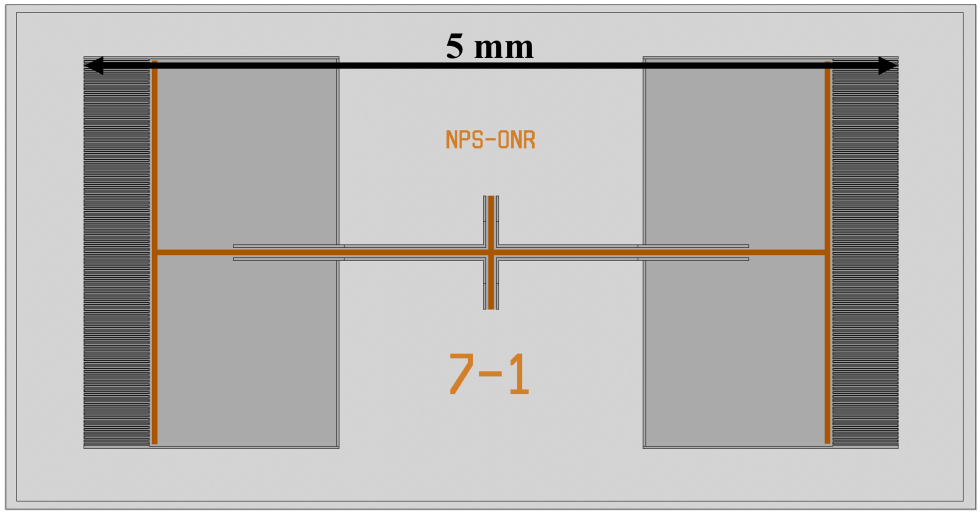

Figure 3.1. Diagram of MEMS sensor. Paddles, torsional bridge, and comb-finger capacitor are clearly visible.

3.1.1 Frequency Response

The frequency response of the sensor is key to obtaining a functional DoA determination system. The magnitude of the frequency responses are for two sensors with identical layouts

fabricated in the same lot, named Sin and Cos shown in Figure 3.2. They closely resembles a harmonic oscillator. Key features of the response curve include the peak frequency, magnitude, and quality factor which all correspond to the bending mode of the sensor [33], [35]. These quantities are determined in large part by the dimensions and design of the individual sensor shown in Figure 3.1. Other features to note include the low and high frequency response regimes since a gunshot will contribute to frequencies over a broadband spectrum. Additionally, a local minimum is visible at the left tail of the peak which corresponds to the rocking mode of the sensor. The rocking mode's contribution is insignificant compared to the main peak for sensors operating with an open back.

One important fact to note is that these values will vary from sensor to sensor. Although frequency response can be tailored through design parameter selection, small imperfections in the manufacturing process will induce variation amongst sensors with the same design parameters. This variation impacts the accuracy of a system's capabilities in gunshot DoA determination and must be corrected for as discussed in Section 3.4.3.

In addition to the ormia-inspired sensor characteristics, Figure 3.2 shows the frequency response of the employed commercial omni-directional microphone. Since this sensor exhibits resonance at higher frequencies ($>$ 15 kHz), it shows flat response in the range of interest.

Figure 3.3 shows the phase of the frequency response for the Sin and Cos sensors. The most important feature of the phase response is the 180° phase shift shown in Figure 3.3. The feature is centered over the peak frequency and significant phase change occurs approximately over the width of the resonant peaks.

This 180° phase shift is a typical feature of resonant vibratory systems and is usually avoided by operating away from resonance. In our case, the sensors are operated at resonance in order to increase the SNR. It can be shown that an increase of the square root of the quality factor can be obtained [45].

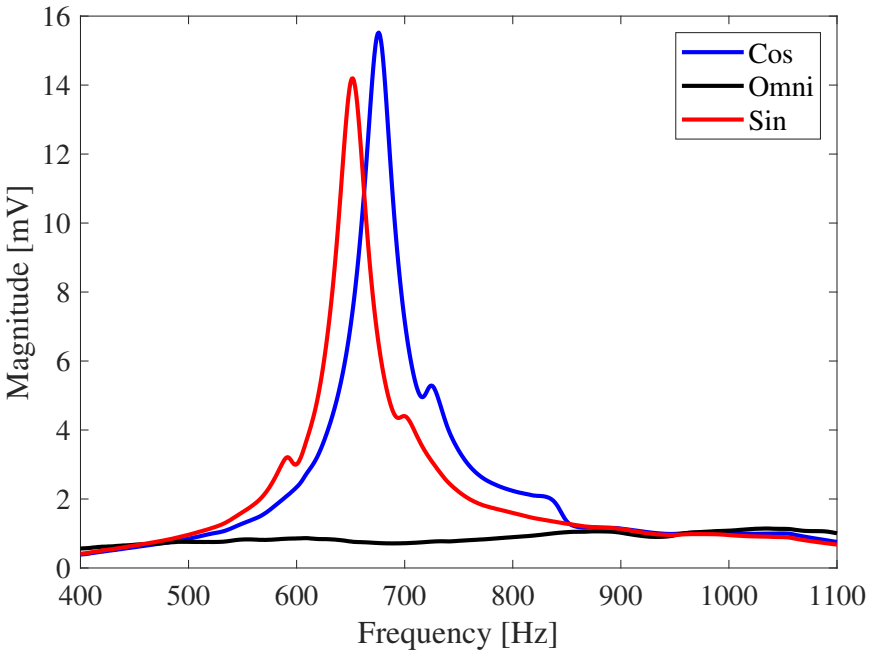

Figure 3.2. Measured magnitude response of the two MEMS sensors and one omni-directional microphone. Note resemblance with a harmonic oscillator.

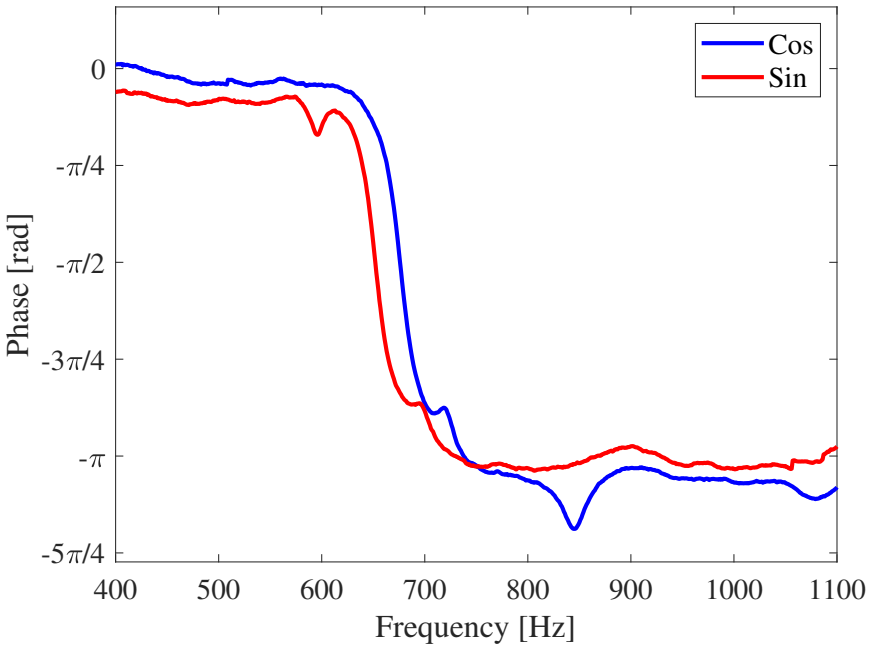

Figure 3.3. Measured phase response of the MEMS sensors with respect to the omni-directional microphone. Note resemblance with a harmonic oscillator.

Benefiting from this improvement, it is desirable to operate the sensors near resonance and phase must be taken into account in signal processing. This means that the phase behavior will have a large impact in the accuracy of the desired frequency-domain DoA determination algorithm discussed in Section 3.4.2 and must be accounted for.

3.1.2 Directional Response

By nature of the design, the sensor exhibits directional behavior similar to a pressure gradient microphone. As incident angle increases away from the face normal, the sensor response decreases producing a dipole beam pattern as shown in Figure 3.4.

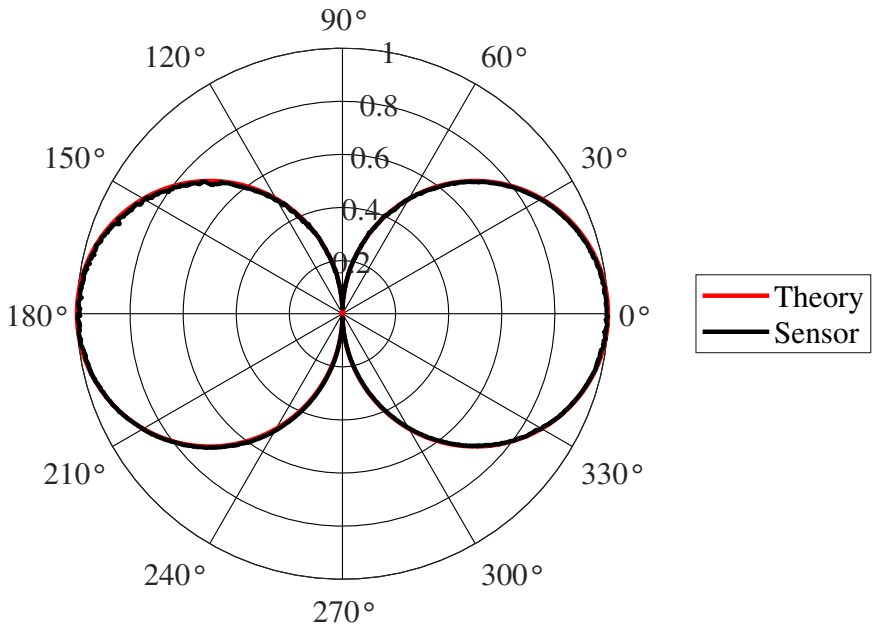

Figure 3.4. Normalized measured beam pattern of single MEMS sensor against a theoretical dipole. The close match is critical for DoA determination as discussed in Section 3.4.

The dipole directional response of the sensor is essential to the system and its ability to determine DoA of a gunshot accurately, quickly, and efficiently, as will be discussed later in Section 3.4.

3.2 System

The system tested required two *Ormia*-inspired MEMS sensors and one omni-directional microphone. The collocated MEMS sensors were aligned along a vertical axis and arranged orthogonal to each other. The omni-directional microphone was centrally located along the axis and between the two sensors facing upwards. A diagram of the completed system is shown in Figure 3.5.

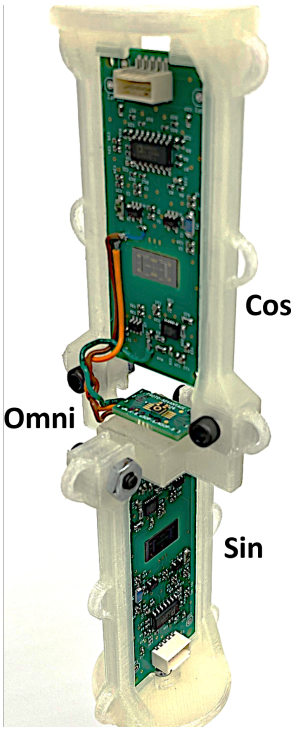

Figure 3.5. Assembled crossed-dipole MEMS sensors with centrally collocated omni-directional microphone.

The overall beam pattern of the array closely resembles that of a four-leaf clover and is shown in Figure 3.6. The crossed-dipole arrangement allows for determination of incident angle of acoustic sounds as discussed subsequently.

3.3 Method

As seen in Chapter 2, current research and commercial acoustic gunshot DoA location systems rely heavily on distributed arrays capable of performing time delay of arrival calculations. While these prove to be effective, they can be large requiring fixed mounts on buildings or vehicles [6], [13], [18]. Variants small enough to be carried by soldiers suffer from significant losses in accuracy and effectiveness [17], [46]. Therefore, a different approach is required to solve these problems and create a small, compact, lightweight sensor capable of quick and accurate DoA determination via acoustic means.

In 1987, Stephen W. Davies [47] published an article analyzing the effectiveness and accuracy of an arctan bearing estimator [47]. This approach to DoA determination requires a single crossed dipole array and one centrally located omni-directional microphone. Though originally developed for radio direction finding, the method is easily adapted to acoustic DoA determination providing sensors with the appropriate dipole beam pattern.

3.4 DoA Determination Algorithm

3.4.1 Arctan Estimator in the Time Domain

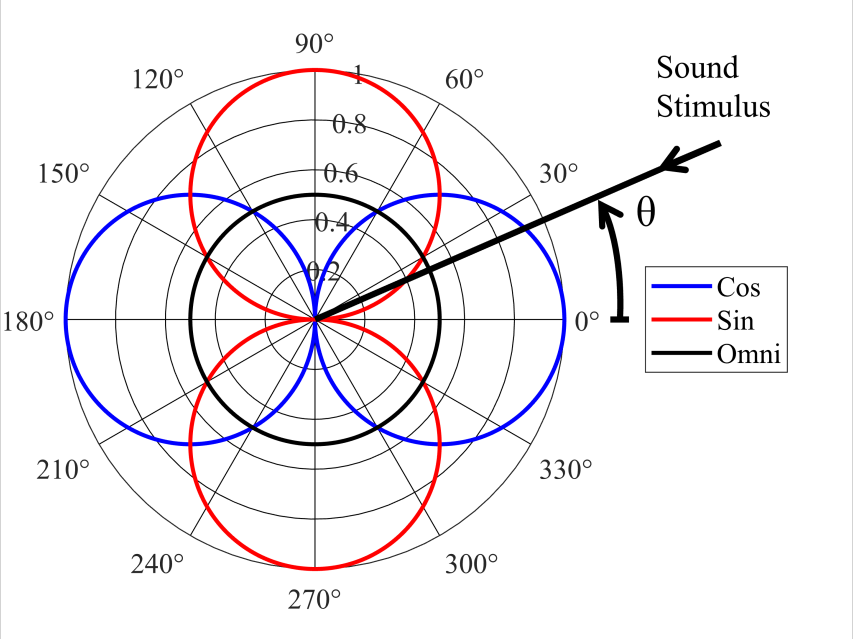

Figure 3.6. Directional response of collocated crossed-dipoles array with centrally located omni-directional microphone required for arctan DoA determination.

A dipole beam pattern is useful because it has axial symmetry and preferentially weighs signals received along the axis. The weighting decreases to a minimum for signals received along the beam. By crossing two collocated dipoles, the total beam pattern resembles a

four-leaf clover as shown in Figure 3.6. Each dipole will detect an incident acoustic event on its own and the strength of the produced signal will depend on the incident angle of the stimulus. The Cos sensor exhibits minima at 90° and 270° and the Sin sensor at 0° and 180° as shown in Figure 3.6. Consider an acoustic signal $s(t_i)$ sampled at a specific sampling frequency f_s such that $\Delta t = 1/f_s$ with an incident angle θ as measured from the axis of the Cos sensor. Each dipole will detect the signal with the appropriate weight while the omni-directional microphone will detect the signal without any azimuth dependence.

$$c(t_i, \theta) = s(t_i)\cos(\theta) \quad \rightarrow \quad \text{cosine} \tag{3.1}$$

$$o(t_i) \quad = s(t_i) \quad \rightarrow \quad \text{omni} \tag{3.2}$$

$$s(t_i, \theta) = s(t_i)\sin(\theta) \quad \rightarrow \quad \text{sine} \tag{3.3}$$

The crossed dipole sensors are enough for a functional arctan estimator as shown below.

$$\theta = \tan^{-1}\left(\frac{s(t_i)\sin(\theta)}{s(t_i)\cos(\theta)}\right) \tag{3.4}$$

Though the dipole sensors alone are enough to determine an incident angle, the arctan estimator is unable to resolve quadrant on its own as any determined DoA could also be incident at an angle $\theta \pm 180°$. To resolve this ambiguity, the omni-directional microphone is utilized to help determine the sign of each dipole measurement, thereby allowing for additional conditionals that will remove the ambiguity as shown in Figure 3.6 [47]. To do this, one must take the product of the Sin and Cos sensors with the omni-directional microphone for each sample point. Then the products must be summed over the relevant time interval. Mathematically, the numerator and denominator of the tangent estimator are:

$$N = \sum_{i=1}^{n_f} s(t_i, \theta) o(t_i) \tag{3.5}$$

$$D = \sum_{i=1}^{n_f} c(t_i, \theta) o(t_i) \tag{3.6}$$

where the sum is taken over the interval of interest from 1 to n_f. The angle of incidence θ can be computed as [47]:

$$\theta = \begin{cases} \tan^{-1}\left(\frac{N}{D}\right), & D \geq 0 \\ \tan^{-1}\left(\frac{N}{D}\right) + \pi, & D < 0, N \geq 0 \\ \tan^{-1}\left(\frac{N}{D}\right) - \pi, & D < 0, N < 0 \end{cases} \tag{3.7}$$

Equations 3.5 through 3.7 form the basis of a robust acoustic DoA localization algorithm capable of unambiguously detecting incident azimuth over the full 360°. Though simple, this approach to the arctan estimator operates on the received signal in the time domain [47]. Unfortunately, this comes with significant limitations in post detection signal processing techniques that would be possible in the frequency domain.

Figure 3.7 shows the time series of the summands, N and D, in each quadrant for Equations 3.5 and 3.6. This data was obtained by measuring the The sums are taken over the red and blue regions respectively and the sign of each uniquely determine the quadrant as shown in Equation 3.7.

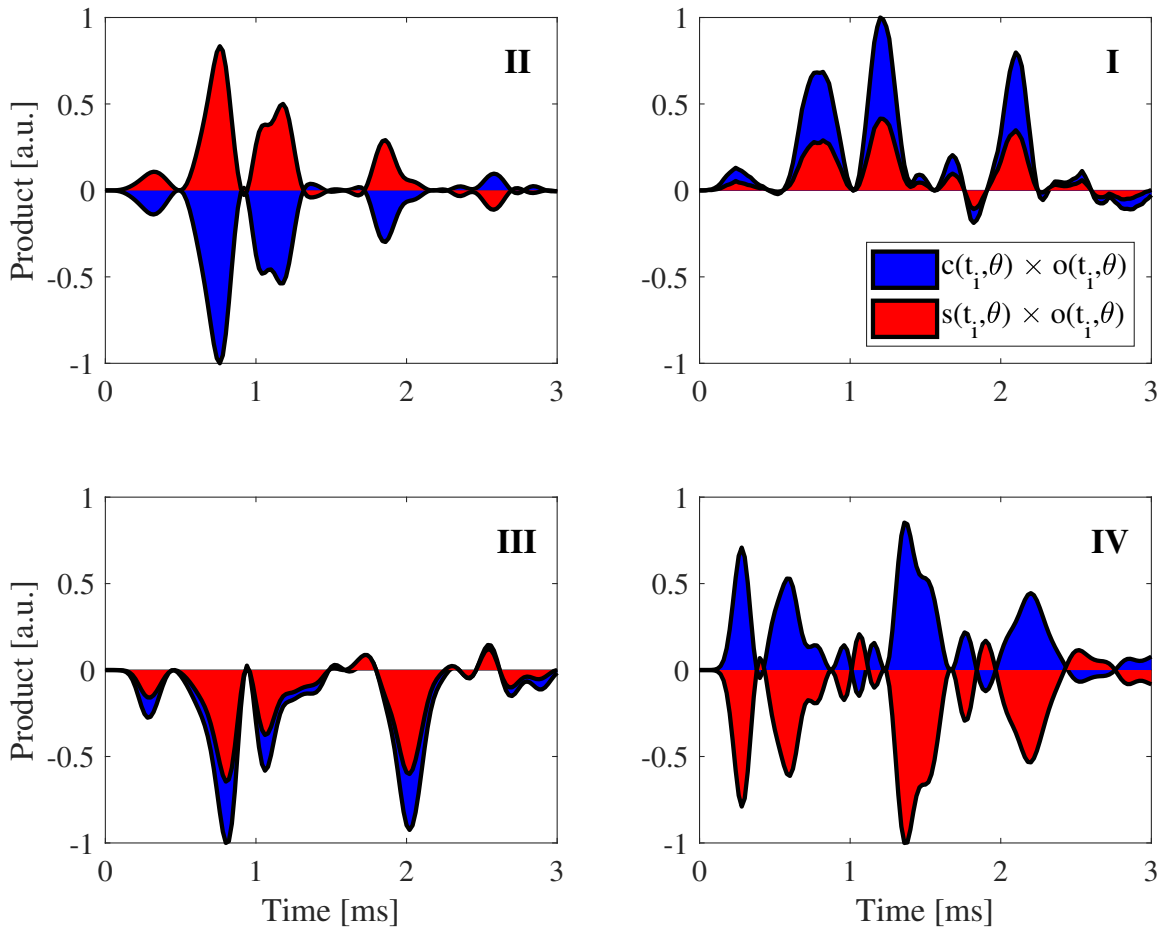

Figure 3.7. A visual representation of how the product of each sensor's response and the omni-directional microphone's response allows one to determine quadrant of incident signal. Notice the unique orientations of the blue and red regions in each quadrant that allow quadrant to be resolved.

3.4.2 Arctan Estimator in the Frequency Domain

Building on Davies' work, Dini et al. expanded the arctan estimator algorithm into the frequency domain for applications in underwater target tracking in a 2012 publication [48]. This approach opens up various post detection signal processing possibilities and requires few alterations from the approach outlined in Section 3.4.1.

Consider the same incident acoustic signal $s(t_i)$. The signal will be weighted by the crossed-dipoles, as described earlier. To move from the time to the frequency domain, $s(t_i)$ must be

passed through a Fourier Transform (FT) resulting in $S(\omega_i)$. The frequency domain version of Equations 3.1 to 3.3 are then written as:

$$C(\omega_i, \theta) = S(\omega_i)\cos(\theta) \quad \rightarrow \quad \text{cosine} \tag{3.8}$$

$$O(\omega_i) \quad = S(\omega_i) \quad \rightarrow \quad \text{omni} \tag{3.9}$$

$$S(\omega_i, \theta) = S(\omega_i)\sin(\theta) \quad \rightarrow \quad \text{sine} \tag{3.10}$$

where capital functions represent the FT of the signal at some frequency ω_i [48]. As before, the numerator and denominator of the arctan estimator's argument must be evaluated for n_f frequency bins created by the FT, and are given by:

$$N = \Re\left\{\sum_{i=1}^{n_f} S(\omega_i, \theta)O^*(\omega_i)\right\} \tag{3.11}$$

$$D = \Re\left\{\sum_{i=1}^{n_f} C(\omega_i, \theta)O^*(\omega_i)\right\} \tag{3.12}$$

where * represent the complex conjugate and the real component $\Re$ must be taken after the sum $\sum$ [48]. Equations 3.11 and 3.12 are equivalent to 3.5 and 3.6 and can be substituted into the conditionals of Equation 3.7 resulting in the same DoA localization algorithm capable of unambiguously detecting incident azimuth over the full 360° [29], [47].

3.4.3 Correction Factor

Due to imperfections in the manufacturing process, variations will exist between MEMS sensors of the same layout even when fabricated in the same batch. Therefore, it is challenging to select two that exhibit the exact same frequency response. Unfortunately, this means that a given crossed-dipole assembly will have mismatched dipole responses to an incident acoustic stimulus, compromising the DoA determination accuracy. Therefore, a solution must be found to correct sensor response.

Correction Factor

Consider two sensors with different frequency responses.

$$R_1 = F_1(\omega)e^{i\Phi_1(\omega)} \tag{3.13}$$

$$R_2 = F_2(\omega)e^{i\Phi_2(\omega)} \tag{3.14}$$

where $F_n(\omega)$ and $\Phi_n(\omega)$ represent the magnitude and phase at frequency ω for sensor n. R_1 and R_2 are sensor characteristics and must be experimentally determined for each sensor. This is performed using appropriate instrumentation (to be described) in an anechoic environment. The calibration frequency response must be measured with both sensors at 45° with the source. In this condition, if they were a perfect match, the frequency response should be exactly the same. This is rarely the case and a possible correction factor is:

$$CF_{2\to1}(\omega) = \frac{R_1(\omega)}{R_2(\omega)} = \frac{F_1(\omega)}{F_2(\omega)}e^{i[\Phi_1(\omega)-\Phi_2(\omega)]} \tag{3.15}$$

where $CF_{2\to1}(\omega)$ will correct the signal received by sensor 2 and put it on equal footing with the signal received by sensor 1. A visual representation of the magnitude and phase components of the correction factor is shown in Figure 3.8.

This correction factor can be applied in the frequency domain arctan estimator of Section 3.4.2. An incident gunshot produces signals $C(\omega_i, \theta)$ and $S(\omega_i, \theta)$ from Equations 3.8 and 3.10. Since each sensor has a different response, these to signals cannot be directly compared in Equation 3.7. Instead, the predetermined correction factor $CF_{C\leftrightarrow S}$ must be applied where $\leftrightarrow$ implies the correction can be applied directly to the FT of the detected signal of one of the MEMS sensors. Once applied, both magnitude and phase are corrected as if the detection occured by the sensors with the exact same frequency response, as shown in Figure 3.9. This correction should reduce the error of the arctan estimator due to mismatched frequency responses. Remaining errors from a diversity of factors, such as noise, obstacles, multi-path propagation, environmental factors, and more, must be addressed using different techniques, beyond the scope of this thesis.

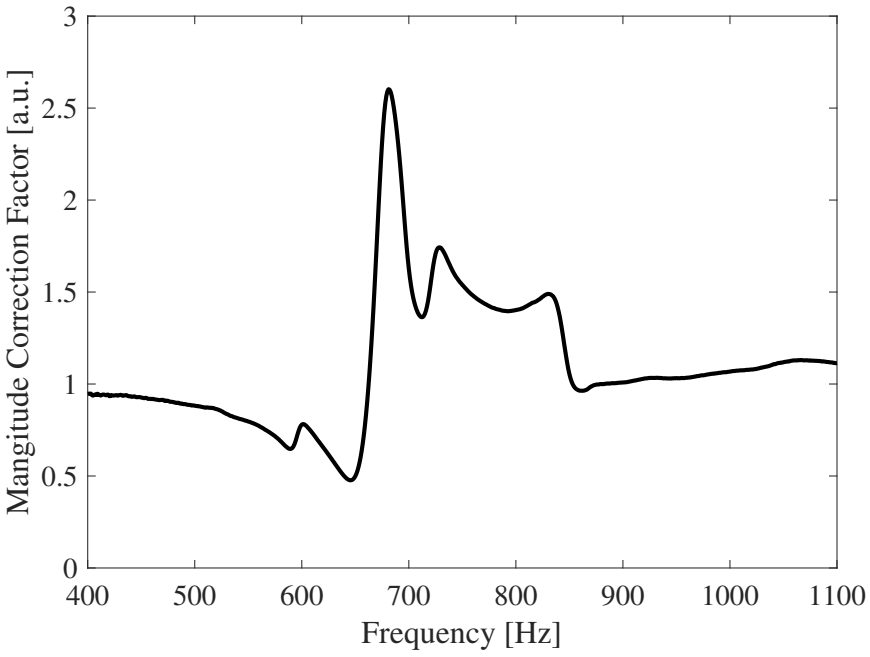

(a)

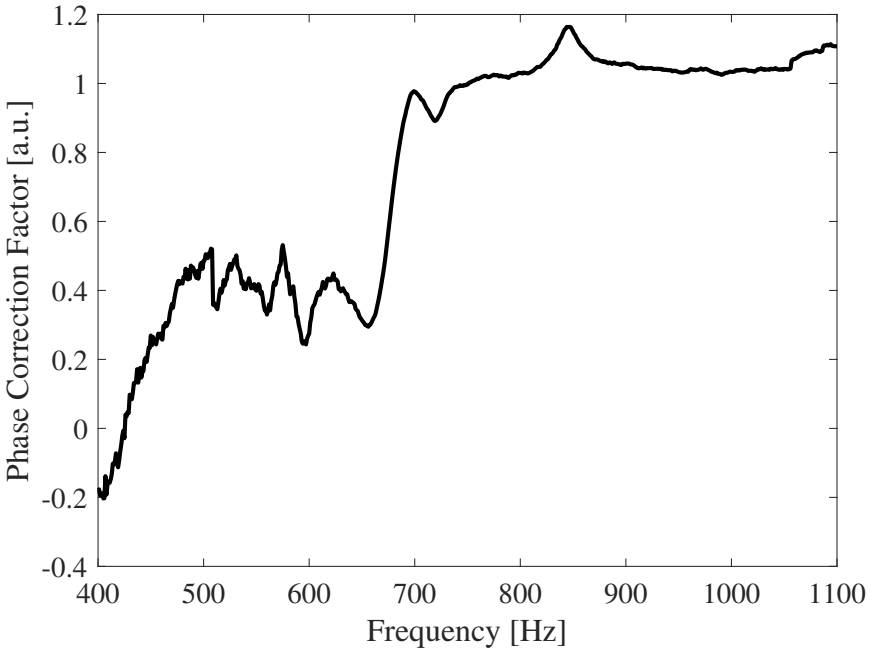

(b)

Figure 3.8. Magnitude (a) and phase (b) components of the correction factor to correct the response of the sine sensor to make it comparable with the cosine sensor, $CF_{\cos \rightarrow \sin}$.

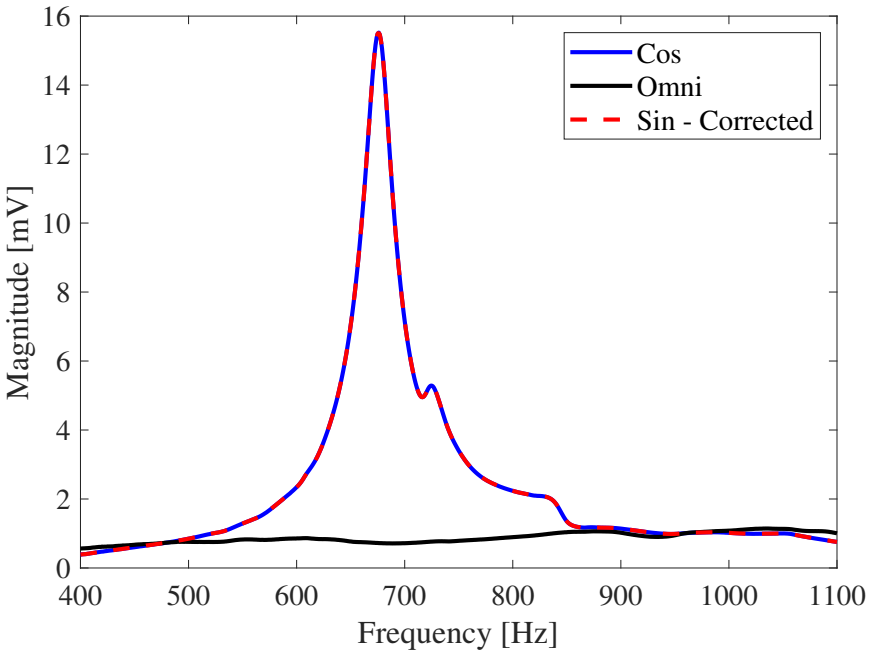

(a)

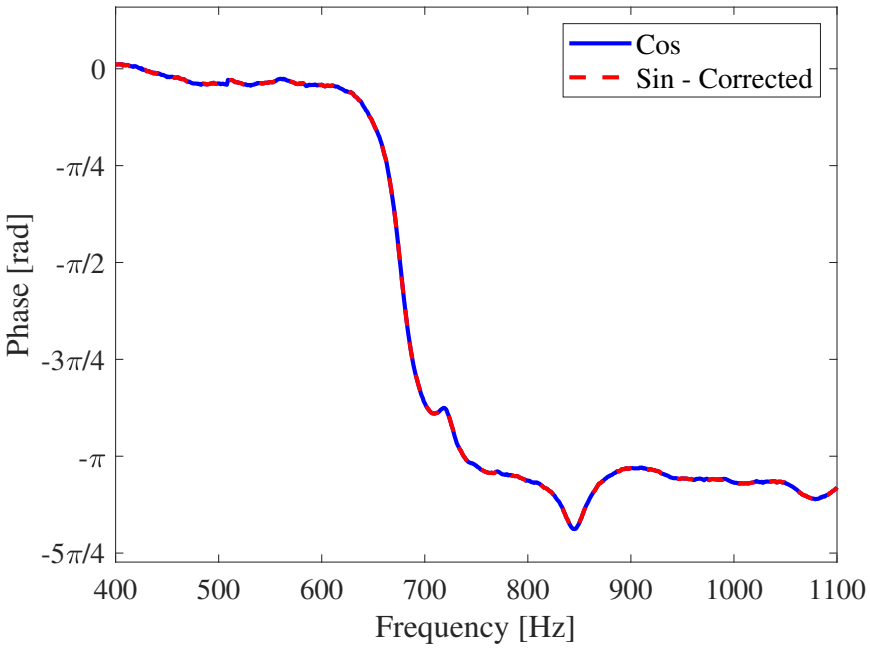

(b)

Figure 3.9. Corrected magnitude (a) and phase (b) response of the sine sensor after applying the correction factor, $CF_{\cos \rightarrow \sin}$, from Figure 3.8.

CHAPTER 4:
Tests and Results

4.1 Proof of Concept: Simulation

The first step in evaluating the arctan estimator proposed by Davies [47], was to simulate the system's response to a gunshot stimulus incident at a known angle. Successful DoA determination will serve as an initial proof of concept.

4.1.1 Description and Setup

The initial test was developed in MATLAB. A gunshot recording acquired from an online audio library served as the stimulus. The time series of the recording was multiplied by $\cos(\theta)$, $\sin(\theta)$, and a constant for all angles θ in a 360° azimuthal, emulating the response of the cosine, sine, and omni-directional sensors, respectively. Since this would provide a perfect directional and spectral response, artificial noise was included by adding normally distributed random numbers through the `randn()` function in MATLAB. Noise contribution was scaled as a percentage of maximum sensor response and was added individually to each sensor to avoid noise correlation across sensors. These three sets of data constitute a complete simulation of the systems response to an incident gunshot and are all that is required to test the arctan estimator discussed in Section 3.4.

The time-domain approach described in Section 3.4.1 is directly executable with the simulated sensor responses, but the frequency-domain approach described in Section 3.4.2 requires taking the Fourier Transform of each sensor, accomplished here by taking the discrete Fourier Transform (DFT) of each signal using MATLAB's `fft()` function. Note that the spectrum response of each sensor is not taken into account. Flat and broadband sensor response is assumed. Both approaches are illustrated as block-diagrams in Figures 4.1 and 4.2.

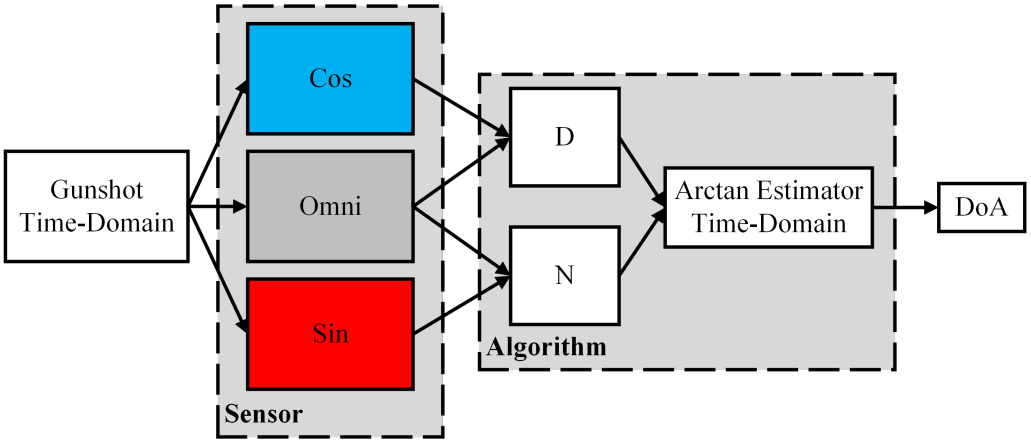

Figure 4.1. Time-domain DoA determination algorithm.

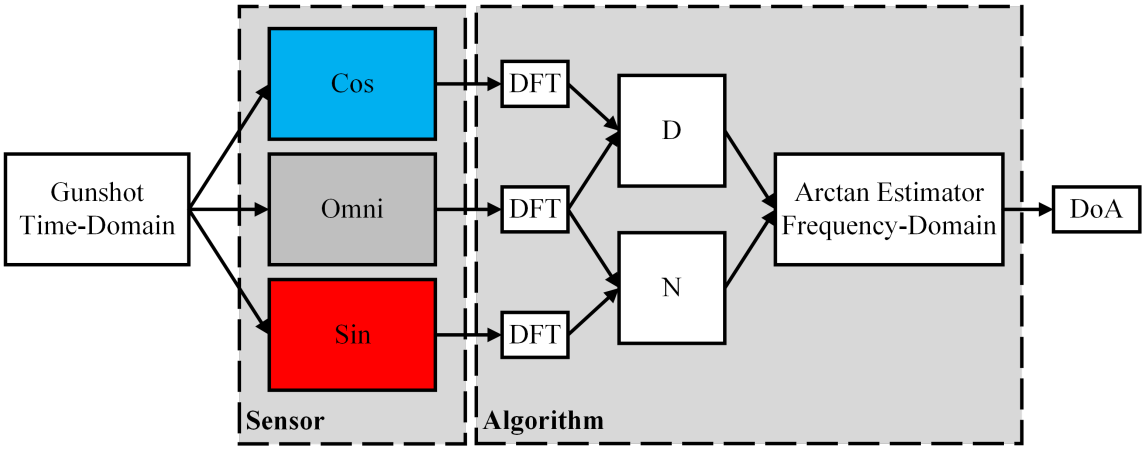

Figure 4.2. Frequency-domain DoA determination algorithm.

4.1.2 Results

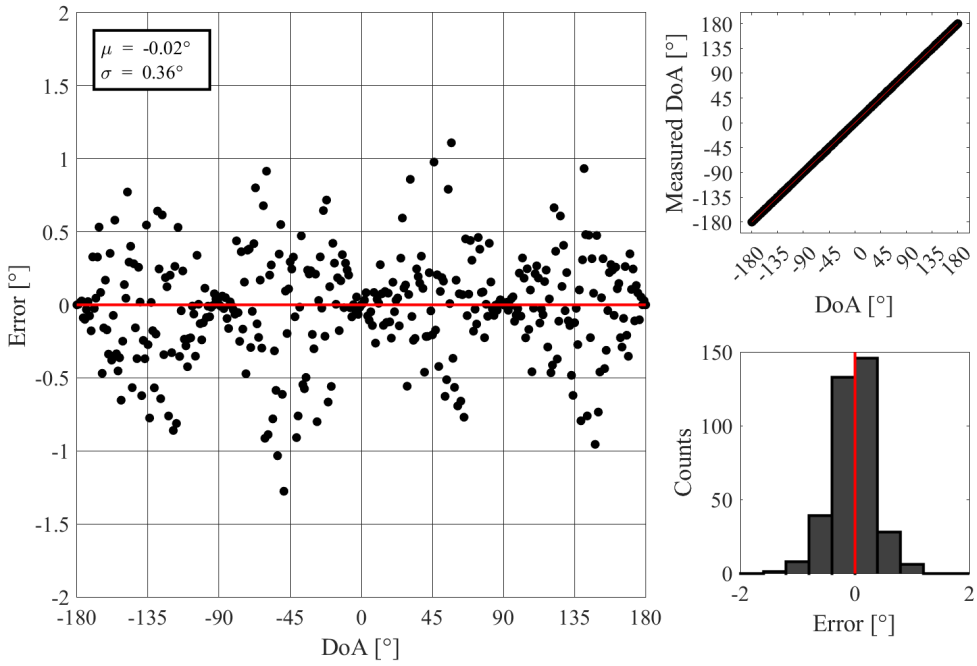

Figure 4.3. DoA error of simulated gunshot with 10% noise added using the frequency-domain algorithm. Note the sinusoidal nature and normal distribution of the error.

The simulation shows that this estimation method works under controlled circumstances. Figure 4.3 clearly shows the error over the entire azimuthal range, obtained by subtracting the estimated DoA by the actual. Also shown is the histogram of the error and a direct correspondence between the estimated and actual angle of arrival. Error is minimized for incident angles of 0°, ±90°, and ±180°. At these angles, one sensor is at maximum, thus less susceptible to error, whereas the other is at a minimum and the noise is almost negligible. Furthermore, simulation of the frequency-domain arctan estimator shows that error increases as the SNR decreases as shown in 4.4. Below an SNR of approximately 8.5 dB, results are no longer reliable.

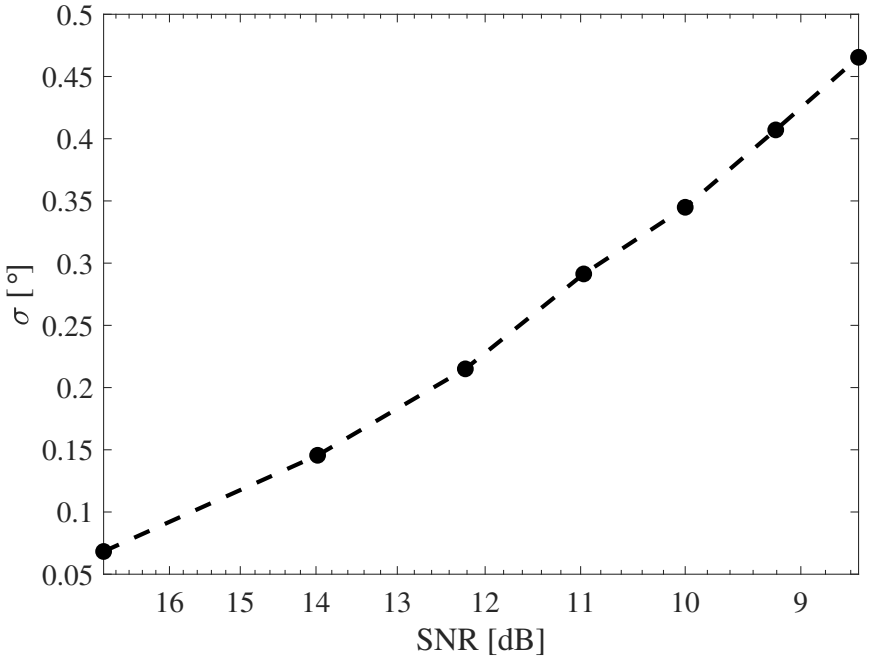

Figure 4.4. Error increases as SNR decreases.

4.1.3 Discussion

This theoretical proof of concept shows significant promise in the arctan estimator's ability to determine DoA of an incident gunshot with significant noise.

Of note, is how the error in DoA behaves. Observing Figure 4.3, it is clear that error behaves in a sinusoidal manner with respect to incident angle. This makes sense when considering the arctan estimator approach. As incident angle passes through 90° and 270°, the cosine sensor's response passes through zero. This means that Equation 3.6 becomes very small causing $\frac{N}{D}$ to diverge, thus increasing the impact noise has on the final DoA determination. It also is most likely a direct result of the added noise having a normal distribution which is clearly seen in the histogram of Figure 4.3.

4.2 Field Test: Paso Robles, CA

4.2.1 Description and Setup

The Paso Robles, CA, field test was the system's first test against live fire. The test took place on 10-13 November, 2021, in an open field with a gun range approximately 20 minutes outside of Paso Robles, CA. A satellite view of the testing site is shown in Figure 4.5 with important dimensions labeled. The firing range is located around the sand berm and the sensor and testing equipment were setup in the red box approximately 220 m away from the center of the berm. The field itself was flat and clear of any obstacles making it an ideal location for testing the sensor. Of note, a small mountain range extends from the Southwest to Northwest, but the distance was sufficient such that gunshot reflections would not overlap with the the direct propagation path we were attempting to detect. An illustration of the reflection is visible in Figure 2.2. An airport was also located near by requiring periodic pausing of testing to allow planes to pass nearby.

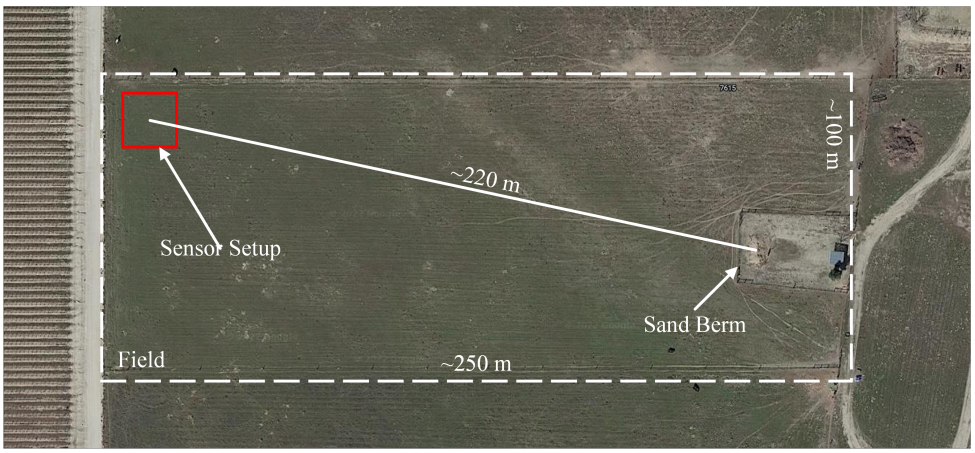

Figure 4.5. Satellite view of Paso Robles testing site with important dimensions and locations marked. North is oriented upwards.

A block diagram of the sensor setup is shown in Figure 4.6. System response was passed through a data acquisition instrument (DAC) allowing all three sensor signals to be recorded simultaneously as WAVE formatted files. Incident angle was controlled manually by rotating

the swivel on which the sensor was mounted and for which degrees were marked on the bevel. Only the 9mm handgun and M4 rifle were tested for 360° DoA in 10° increments. Multiple guns, Table 4.1, were recorded to build a database of acoustic signatures for later testing.

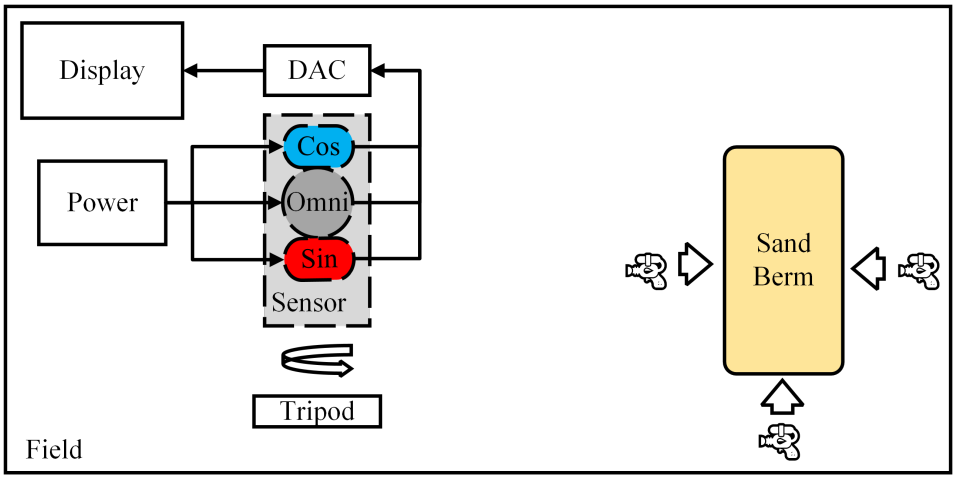

Figure 4.6. Block diagram depicting Paso Robles field exercise setup.

Table 4.1. Guns used and recorded at the Paso Robles field test. Complete gun information can be found in Appendix A.

Gun	**Caliber**	**Type**
45 Smith & Wesson	45 cal	Pistol
9 mm	9 mm	Pistol
Five-seveN FN Herstal	5.7x28 mm	Pistol
Magnum 44 - Magnum Research Inc. Desert Eagle Pistol	44 cal	Pistol
SP101 Sturm, Ruger CO inc.	.22 cal	Pistol
AK-47 Model 56S Norinco	7.62x39 mm	Rifle
M4 Carbine	5.56 mm	Rifle
M4 Carbine - COLT'S MFG. CO. LLC.	.22 cal	Rifle

4.2.2 Results

Each recording was post-processed and inputted in the MATLAB DoA estimator. In this case, directional and frequency response of the actual sensors were already embedded in the recorded time series. The MATLAB script basically performed the fast Fourier Transform (FFT) of the signals and applied the arctan estimator.

The results shown in Figure 4.7 are representative of all the DoA measurements that were taken. Each data point represents one live-fire gunshot received with the system oriented to given incident DoA. Figure 4.7 shows the data from one of the 9mm handgun DoA data tests.

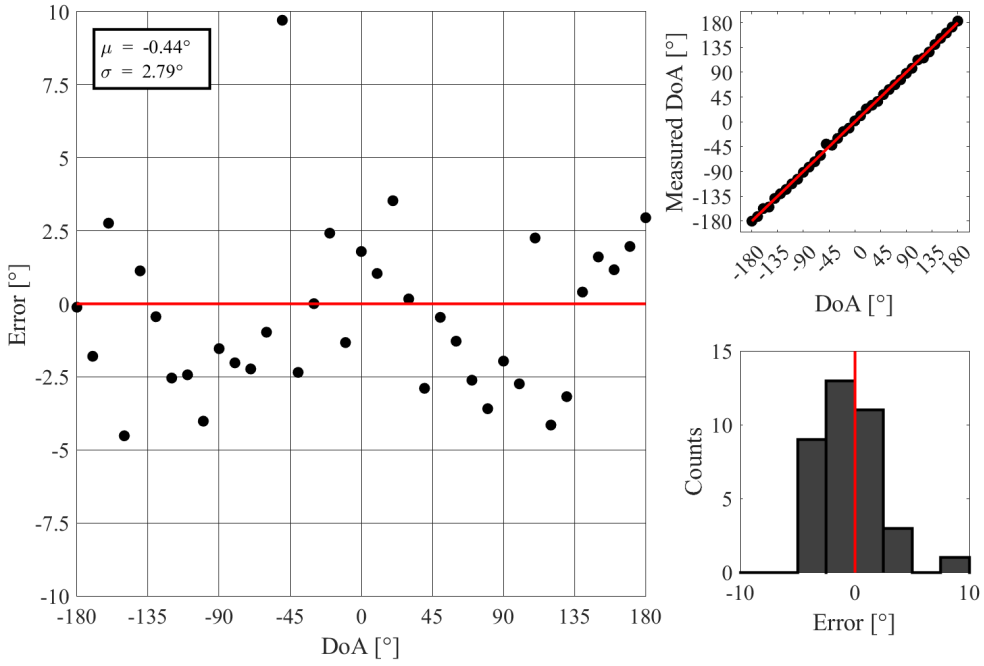

Figure 4.7. DoA error for the 9 mm handgun collected during the Paso Robles field test. A cloth cover was required to dampen noise due to high wind as well as decrease signal to avoid saturation.

4.2.3 Discussion

Error has increased as expected, but interestingly still loosely fits a normal distribution and follows a sinusoidal pattern with incident angle. One outlier exists at $\theta_i = -50°$ with an error of approximately 10° which is about 3.5σ away from true DoA. All other DoAs are will within 2σ. Additionally, the mean incident angle is only $\mu = -0.44$ suggesting that the 0° reference is true.

One important factor to note is the sensitivity of the sensor. At the shown range of approximately 200 m the sensor was easily saturated by the smallest firearm—the 9 mm handgun. This indicates that detection can be done in a much longer range than 200 m. These limits were not tested due to restrictions in the firing range. Furthermore, the wind was quite strong during the tests. Both of these issues were addressed by covering the sensor housing with sound attenuating fabric.

4.3 Correction Factor Test: Anechoic Chamber

4.3.1 Description and Setup

Anechoic Chamber Setup

The acoustic signatures for the guns listed in Table 4.1 and gathered during the Paso Robles field test provided the required audio to fully test the DoA determination algorithms including the correction factor in the anechoic chamber at NPS.

The first step was acquiring a high resolution frequency sweep of both sensors to measure the frequency response of the sensor and build the correction factor discussed in Section 3.4.3. The experimental setup for this test is shown in Figure 4.8(a). Visuals of the instruments and the chamber interior are shown in Figure 4.9.

The frequency sweep was conducted for normal incidence of both sensors as well as for the 45° of each quadrant. Frequency was stepped from 400 Hz to 1100 Hz in 1 Hz intervals in order to achieve a high enough resolution for use in the correction factor.

After the frequency sweep, DoA data was acquired using the sensor and the audio recordings from Paso Robles. To do this, the gunshot acoustic signatures were passed directly through

the speaker by a computer that also controlled the DAC instrument, responsible for reading the sensors' outputs, as shown in Figure 4.8(b). The Sensor was then rotated using the turntable in 10° increments for one full rotation. Incident angles of 45° were also measured for each quadrant. This process was repeated for every acoustic signature, including adjusting the required volume adjustments to avoid saturation of the sensors.

At the conclusion we had eight sets of 360° worth of data points in 10° increments with the 45° included. This data was sufficient for further DoA determination algorithm testing.

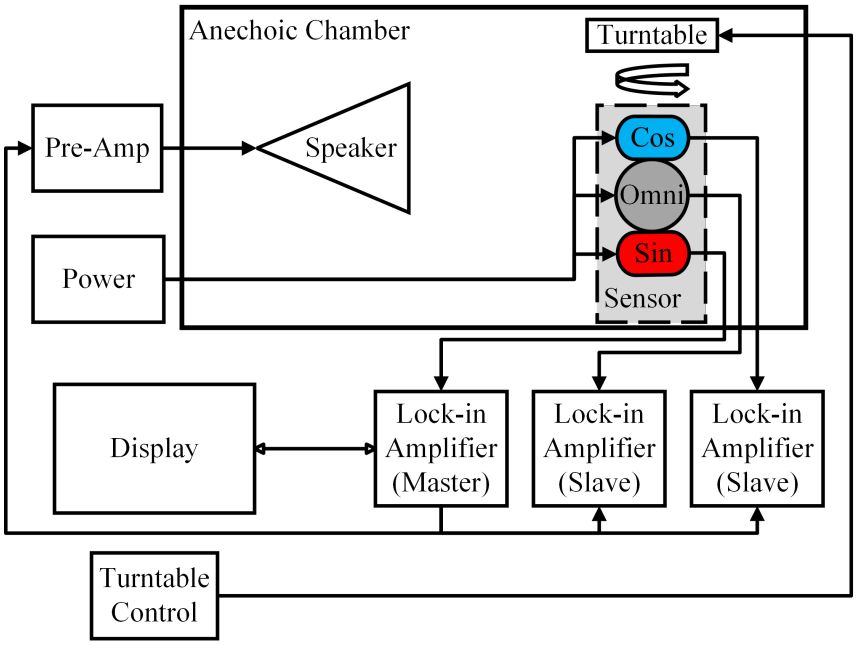

(a)

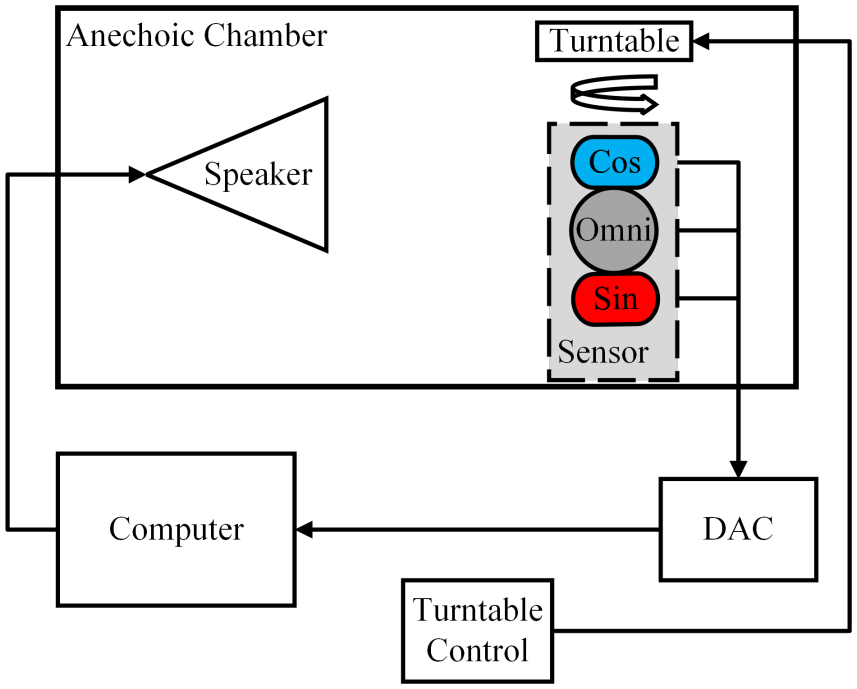

(b)

Figure 4.8. Block diagram depicting anechoic chamber setups.

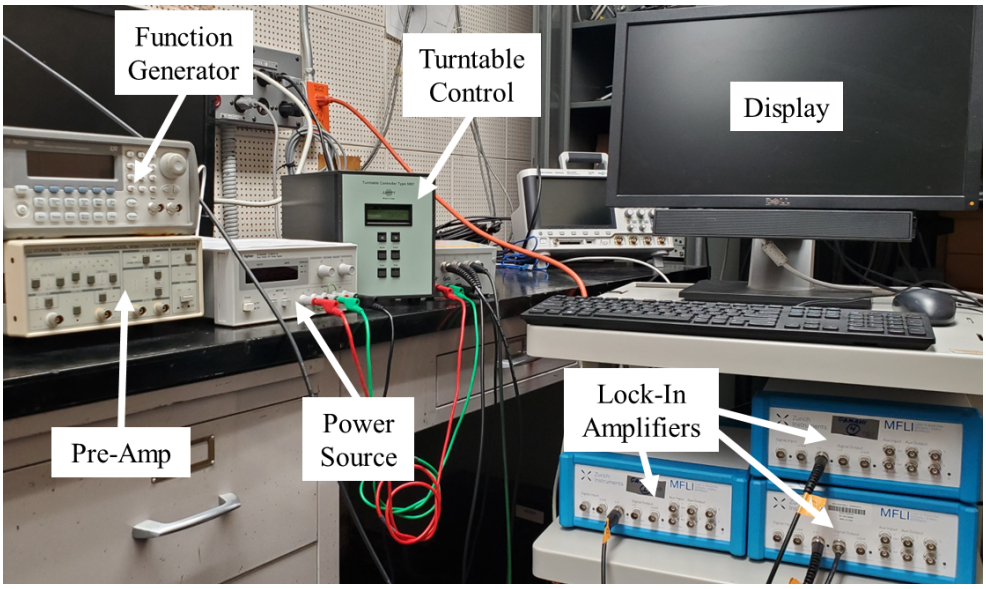

(a)

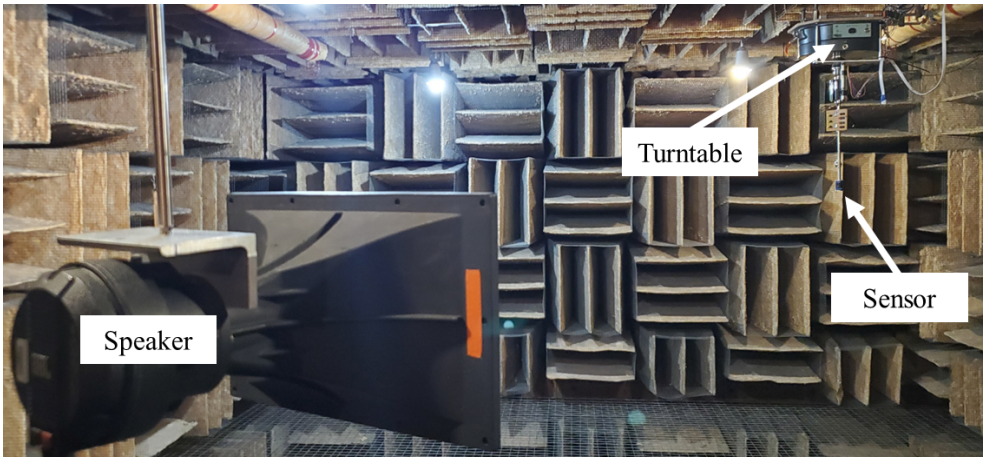

(b)

Figure 4.9. Control room instrumentation (a) and experimental setup inside the anechoic chamber (b).

4.3.2 Algorithm Setup

The acquired data was processed through two DoA determination algorithms. The first is the frequency-domain algorithm discussed in Section 3.4.2 and illustrated in block diagram form in Figure 4.2. The second includes testing the frequency-domain correction factor discussed in Section 3.4.3 and which accounts for the different frequency responses of each sensor when driven at resonance. The diagram is shown in Figure 4.10. The additions required to implement the correction are clearly visible when compared with Figure 4.2.

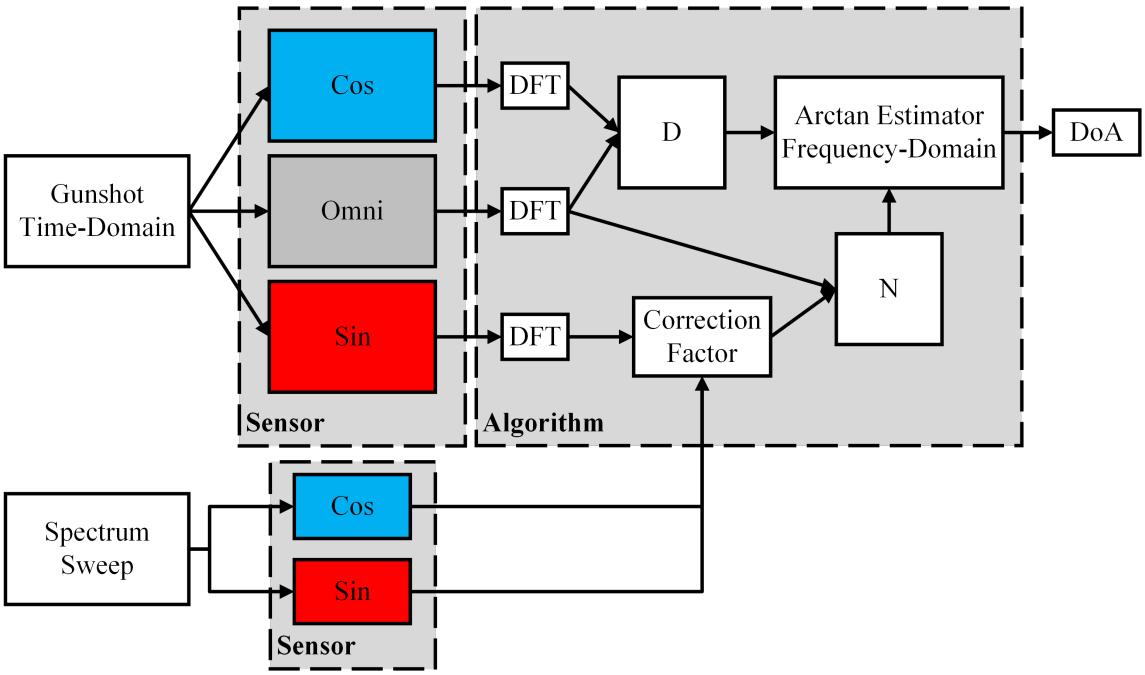

Figure 4.10. Block diagram depicting DoA determination algorithm in frequency-domain with application of the correction factor.

One key consideration when applying the correction factor is frequency matching. The frequencies acquired after passing the time-domain signal through the DFT in MATLAB are unlikely to match the 1 Hz spaced frequencies of the spectrum sweep. To overcome this, the frequency response was sampled by linear interpolation at the frequencies outputted by the DFT. The interpolated response was then used to construct the correction factor.

All eight sets of data were processed using both algorithms. Results are summarized in Section 4.3.3. Complete results are included in Appendix B.1.

4.3.3 Results

This section contains a summary of the results for all guns tested in the anechoic chamber experiment as well as detailed results of the best and worst runs. Complete results for all guns can be found in Appendix B.1.

Table 4.2. Summary of anechoic chamber results. Green denotes improvement after application of the correction factor.

	None		**Correction**	
Gun	$\sigma[^\circ]$	$\mu[^\circ]$	$\sigma[^\circ]$	$\mu[^\circ]$
45 Smith & Wesson	9.14	0.37	6.76	0.66
9 mm	21.22	0.08	11.4	-0.34
Five-seveN	2.30	-0.24	4.73	-0.07
Magnum 44	10.31	-0.45	2.21	-0.67
SP101	14.94	1.27	12.00	1.28
AK-47	3.01	0.21	4.10	0.16
M4 Carbine	4.95	0.01	3.03	-0.09
M4 .22 Carbine	15.76	0.51	8.74	0.54
Average	**10.20**	**0.22**	**6.62**	**0.18**

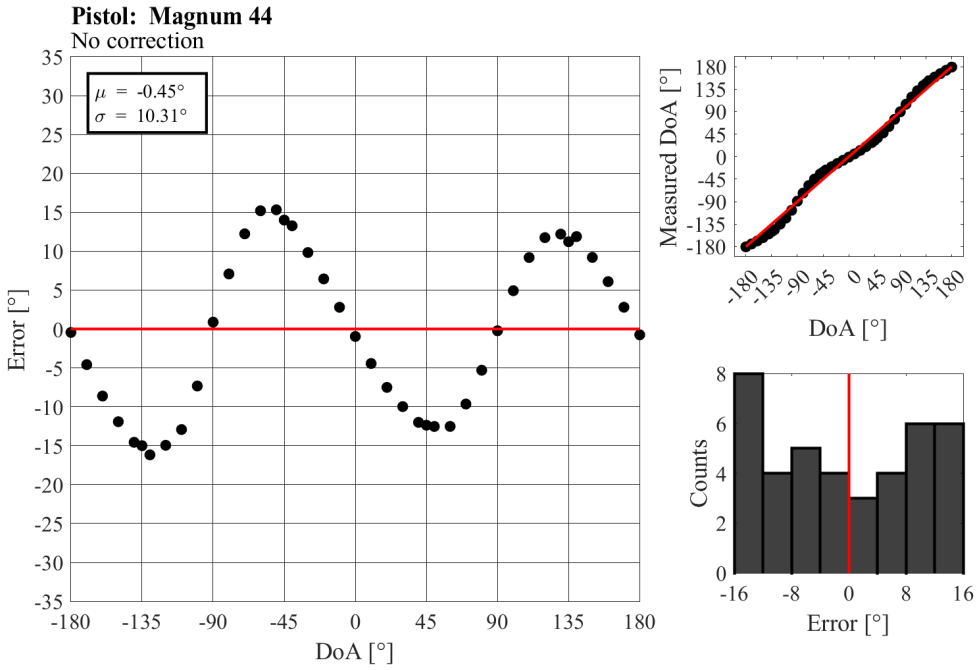

(a)

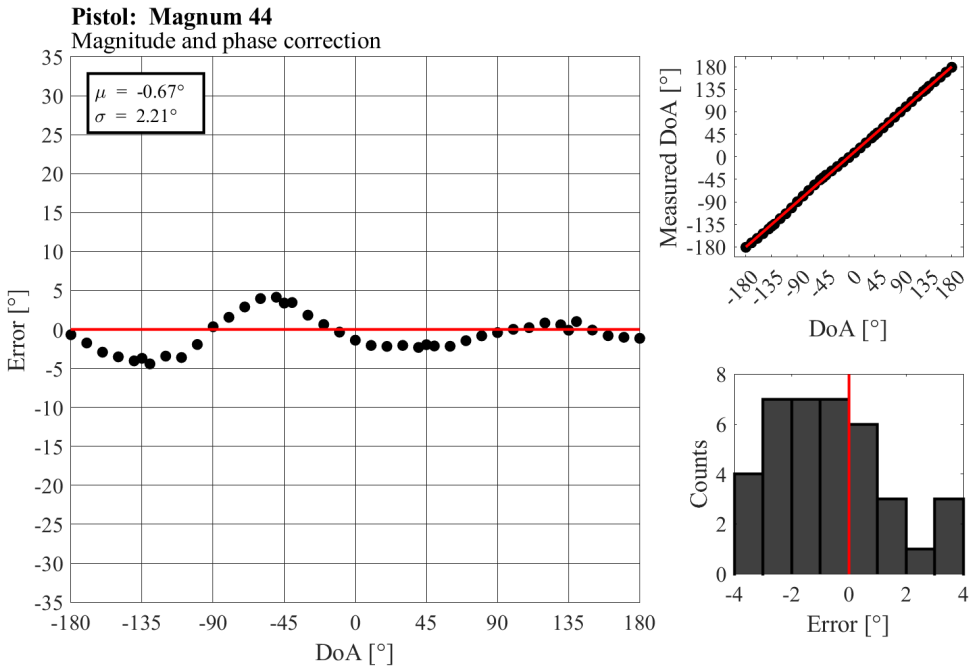

(b)

Figure 4.11. Best results using [48] approach without (a) and with (b) magnitude and phase correction.

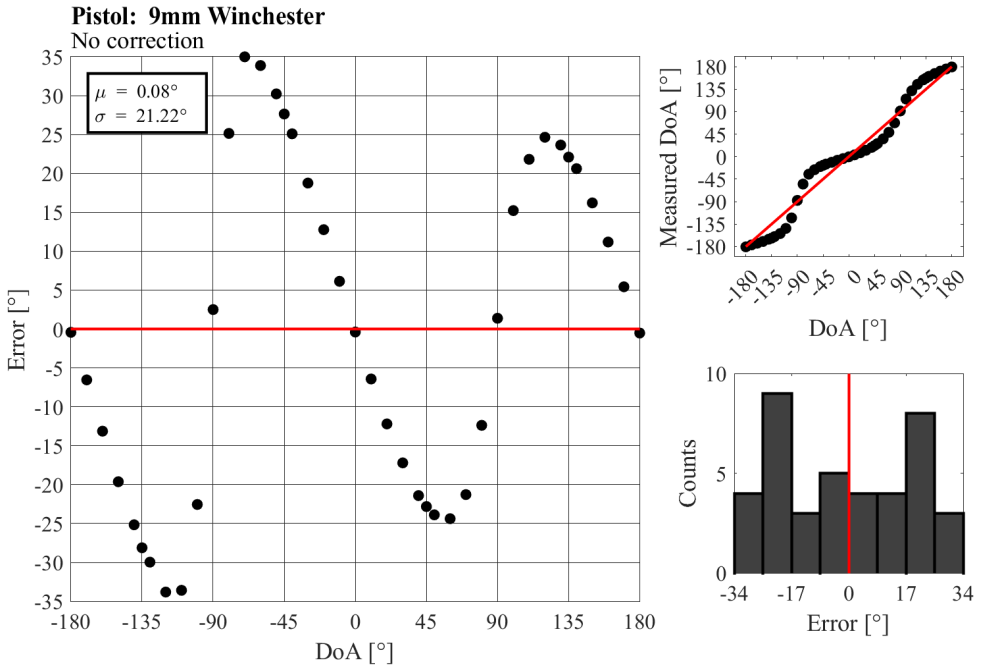

(a)

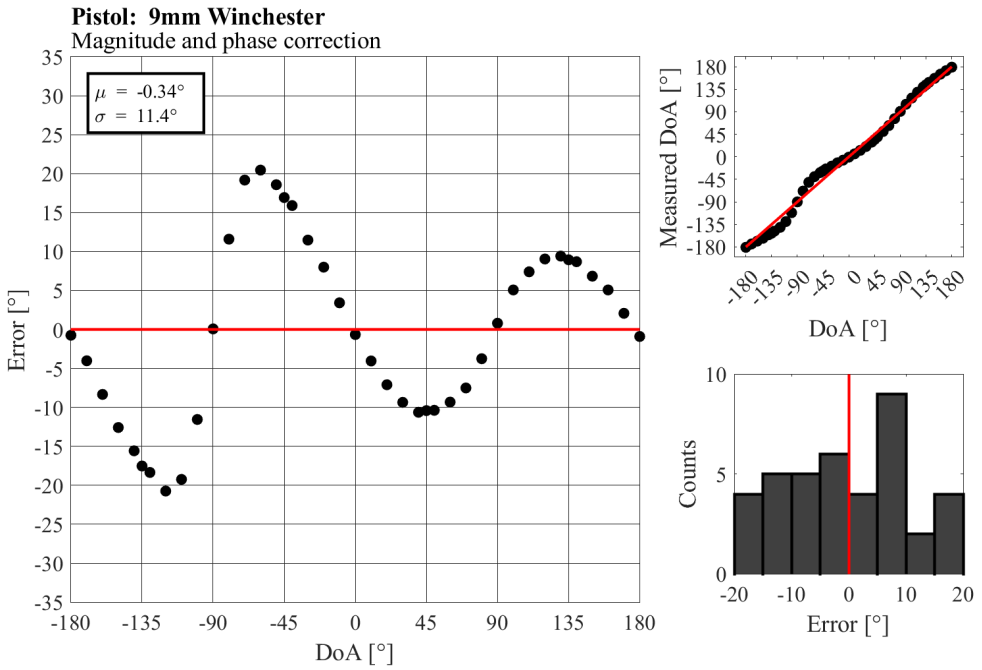

(b)

Figure 4.12. Worst results using [48] approach without (a) and with (b) magnitude and phase correction.

4.3.4 Discussion

The results acquired using [29], [47] DoA determination approach are much less accurate than expected based on the results of Sections 4.1 and 4.2.

It is interesting to note the behavior of the error. Unlike Figure 4.7 where there is a clear presence of noise effecting a slight sinusoidal behavior, Figures 4.11 and 4.12 demonstrate an exaggerated sinusoidal behavior with little discernible noise. This behavior is present across all guns. During the Paso Robles field test, a DAC was used to collect data simultaneously from all three sensors as shown in Figure 4.6. During the anechoic chamber experiment, the setup was the same as shown in Figure 4.8(b). Both experimental setups are similar. The change from an open field environment with a long propagation path to an anechoic chamber most likely accounts for the decrease in noise.

The frequency response of the sensors which is essential for implementing the correction factor was measured separately with the lock-in amplifiers using the setup shown in Figure 4.8(a). It was determined that the lock-in amplifiers were introducing an artificial phase difference between the two MEMS sensors and the omni-directional microphone which was compromising the effectiveness of the correction factor as illustrated by the red boxes in Table 4.2.

It is important to note that the data still show plenty of promise. Though error must be reduced, the algorithm was able to successfully determine incident quadrant which is essential for unambiguous 360° DoA determination.

Since the frequency response of the sensors are not matched, the signal at ±45° and ±135° are different whereas they should be equal leading to increased error. At multiples of 90° one sensor is at maximum, thus less prone to error, whereas the other is at minimum and the noise is almost negligible.

Another explanation is that at ±45° and ±135°, $N \approx D$ in the arctan estimator of Equation 3.7 and errors in both contribute equally. At 0°, ±90°, and ±180°, either $N \rightarrow 0$ or $D \rightarrow 0$. If $N \rightarrow 0$, then the error it contributes is negligible and the limit also causes the value of D to be insignificant and vise versa. This behavior is a direct result of the dipole response of the sine and cosine sensors.

4.4 New Frequency-Domain Approach: Anechoic Chamber

4.4.1 Description and Setup

The approach and results presented in this section use the same data collected during the experiment conducted in Section 4.3.

Anechoic Chamber Setup

As described in Section 4.3.1.

Algorithm Setup

The DoA determination algorithm tested in this section is based on the approach outlined in [48] with one major difference.

The original DoA determination algorithm proposed in [47] computed DoA in the time-domain. The approach used an arctan estimator approach as described in Section 3.4.1. The approach relied on the convolution of the directional sensor's responses with the omni-directional microphone's response. This served two purposes. The first was to resolve directional ambiguity by resolving incident quadrant using the conditionals of Equation 3.7. The second was more subtle. In the time-domain, summing over the directional sensor's response alone would result in a value near zero since the signal demonstrates sinusoidal behavior. This would cause the arctan estimator and conditionals to fail. Multiplying by the omni-directional response removes the sinusoidal behavior, as shown in Figure 3.7 resulting in a non-zero value for the sums in Equation 3.5 and 3.6. Without including the omni-directional response, both the arctan estimator and the conditionals would fail.

Dini et al. [48] took the time-domain approach of [47] and transposed it into the frequency-domain. They kept the approach practically intact, including the omni-directional response in both the arctan estimator and the conditionals as seen in Equations 3.7, 3.11, and 3.12.

However, in the frequency-domain, the magnitude of the sensors' response is always positive so a sum will always yield a positive non-zero value. Therefore, the omni-directional response is not needed in calculating the reference angle. The phase of the omni-directional

response is, however, required in the conditionals. Therefore, a new approach is proposed to DoA determination where the omni-directional microphone output is only used in the conditionals. Mathematically:

$$A = \sum_{i=1}^{n_f} \left| S(\omega_i, \theta) \right| \geq 0 \tag{4.1}$$

$$B = \sum_{i=1}^{n_f} \left| C(\omega_i, \theta) \right| \geq 0 \tag{4.2}$$

where A and B provide the inputs to the arctan estimator of Equation 4.5. Both N and D must still be calculated as before in order to resolve quadrant ambiguity, using:

$$N = \Re \left\{ \sum_{i=1}^{n_f} S(\omega_i, \theta) O^*(\omega_i) \right\} \tag{4.3}$$

$$D = \Re \left\{ \sum_{i=1}^{n_f} C(\omega_i, \theta) O^*(\omega_i) \right\} \tag{4.4}$$

Thus the DoA can be estimated using:

$$\theta = \begin{cases} +\tan^{-1}\left(\frac{A}{B}\right), & D \geq 0, N \geq 0 \\ -\tan^{-1}\left(\frac{A}{B}\right), & D > 0, N < 0 \\ -\tan^{-1}\left(\frac{A}{B}\right) + \pi, & D < 0, N > 0 \\ +\tan^{-1}\left(\frac{A}{B}\right) - \pi, & D < 0, N < 0 \end{cases} \tag{4.5}$$

Equation 4.5 shows the new set of conditionals required to resolve directional ambiguity. Since both A and B will always be positive values, a fourth conditional is required and the $\pm$ determines the starting quadrant of the reference angle. Figure 4.13 helps illustrate the new approach highlighting the new additions in red.

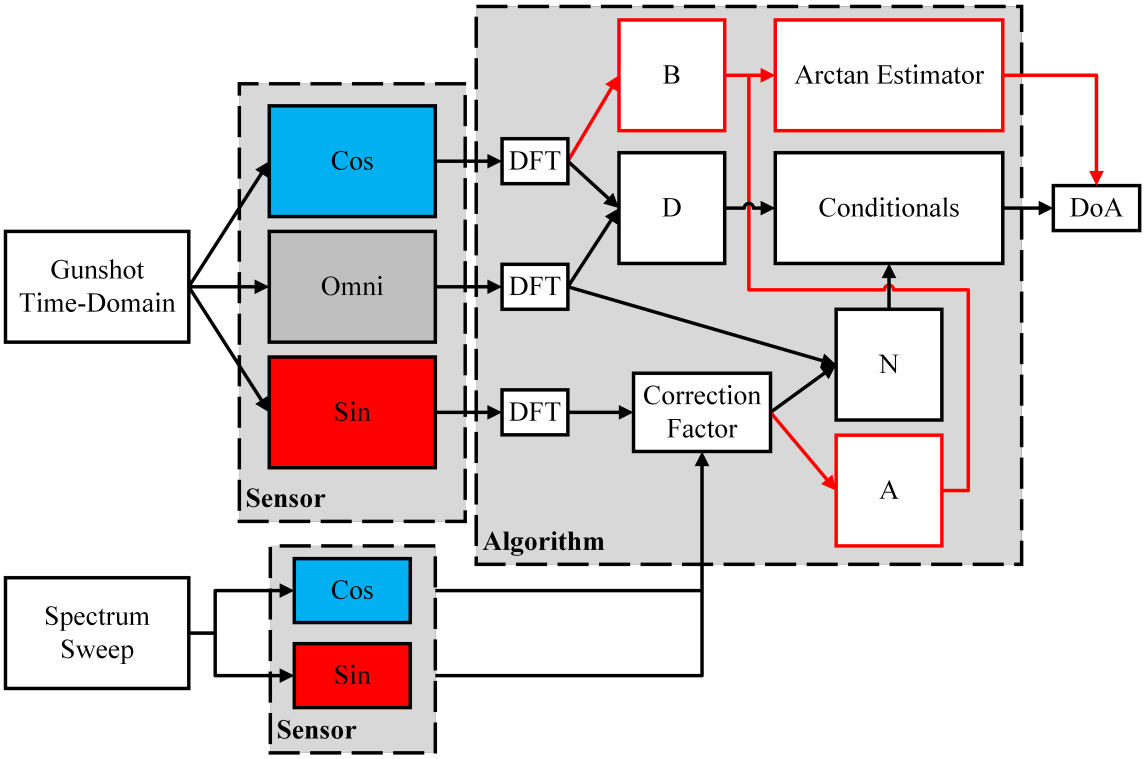

Figure 4.13. Block diagram of new approach to DoA determination algorithm in frequency-domain with application of correction factor. Red outlines indicate new components.

The omni-directional microphone was shown to introduce significant noise into the reference angle calculation of the arctan estimator. By removing it and only using its phase to determine incident quadrant, error can be significantly reduced.

Additionally, since the arctan estimator now only uses the magnitude of the frequency response, the correction factor can be simplified as shown in Equation 4.6 making it easier to implement.

$$CF_{2\to1}(\omega) = \frac{R_1(\omega)}{R_2(\omega)} = \frac{|F_1(\omega)|}{|F_2(\omega)|} \tag{4.6}$$

Furthermore, although the omni-directional response is still needed to implement the conditionals in Equation 4.5 and resolve incident quadrant, they only rely on the sign of Equations 4.3 and 4.4 and not the actual value. If either $N, D \rightarrow 0$ it is only because $A, B \rightarrow 0$, respectively. This corresponds to an incident angle along one of the axes. This also corresponds to a maximum response in the opposite sensor. Therefore, in the region of possible sign swapping that could result in incorrect quadrant determination, error is negligible. Similar behavior is noted previously in Section 4.3.3.

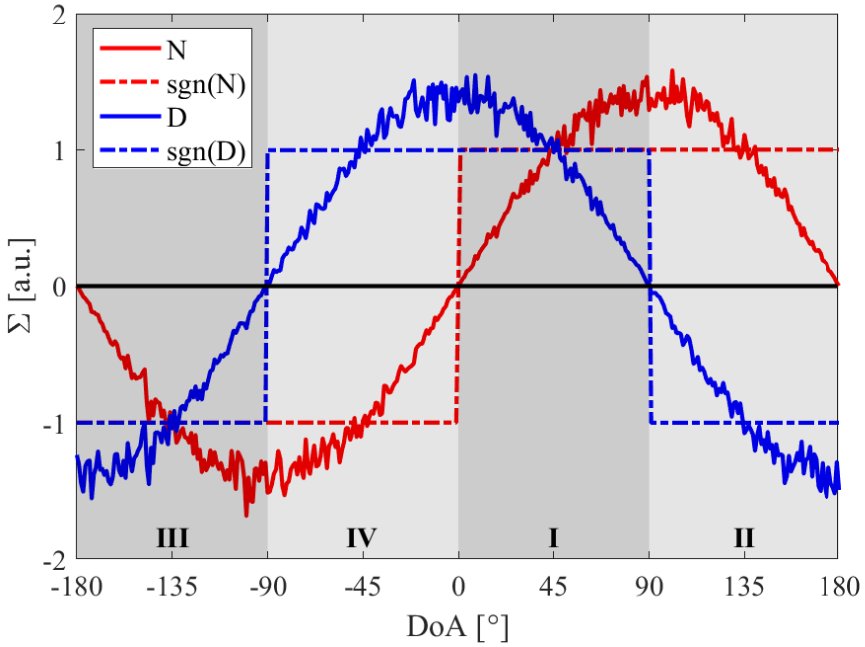

Figure 4.14. Illustration of how the sign of N and D from Equations 4.3 and 4.4 unambiguously determine quadrant. Also note how noise is minimal when $N, D \rightarrow 0$.

4.4.2 Results

This section contains a summary of the results for all guns tested using the new approach developed in Section 4.4 as well as detailed results of the best and worst runs. Complete results for all guns can be found in Appendix B.2.

Table 4.3. Summary of new approach results. Green denotes improvement after application of the magnitude only correction factor. Results are improved across the board when compared to Table 4.2.

	None		**Correction**	
Gun	$\sigma[^\circ]$	$\mu[^\circ]$	$\sigma[^\circ]$	$\mu[^\circ]$
45 Smith & Wesson	2.55	-0.31	1.13	-0.27
9 mm	6.00	-0.04	1.26	-0.15
Five-seveN	2.30	0.00	1.98	-0.02
Magnum 44	3.88	-0.25	0.80	-0.26
SP101	5.96	-0.01	1.19	-0.03
AK-47	3.56	-0.27	2.12	-0.34
M4 Carbine	3.39	-0.11	1.18	-0.17
M4 .22 Carbine	6.07	0.11	1.16	0.02
Average	**4.21**	**-0.11**	**1.35**	**-0.15**

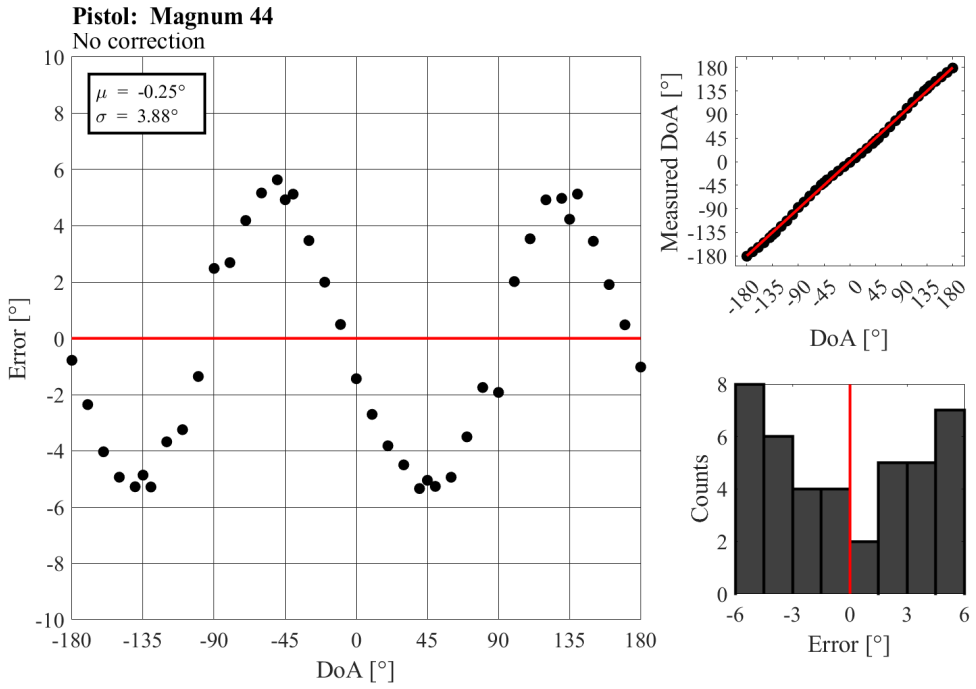

(a)

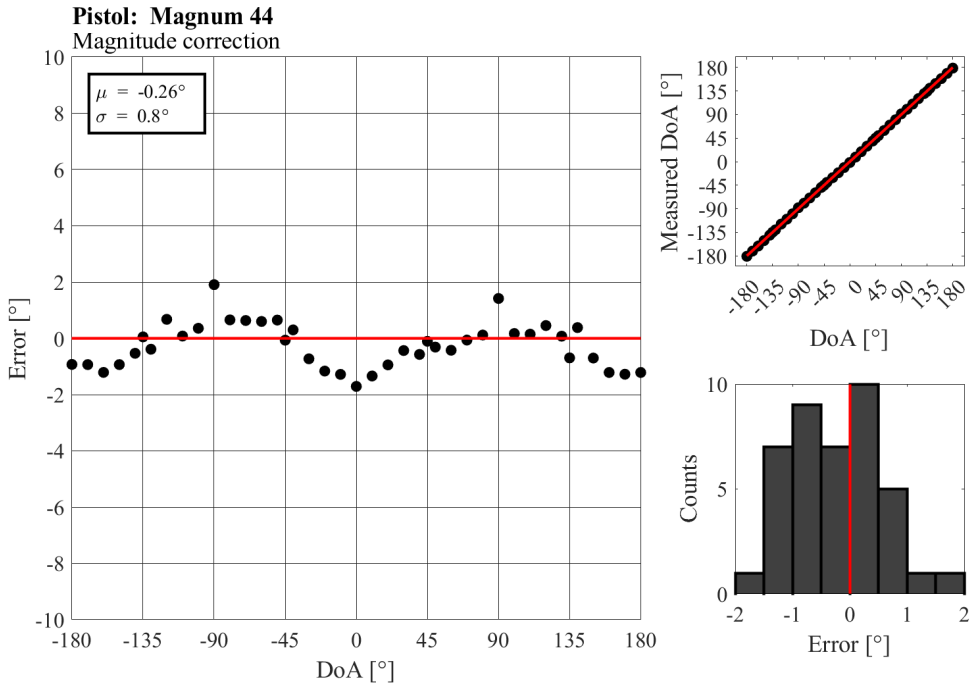

(b)

Figure 4.15. Best results using new approach without (a) and with (b) magnitude only correction.

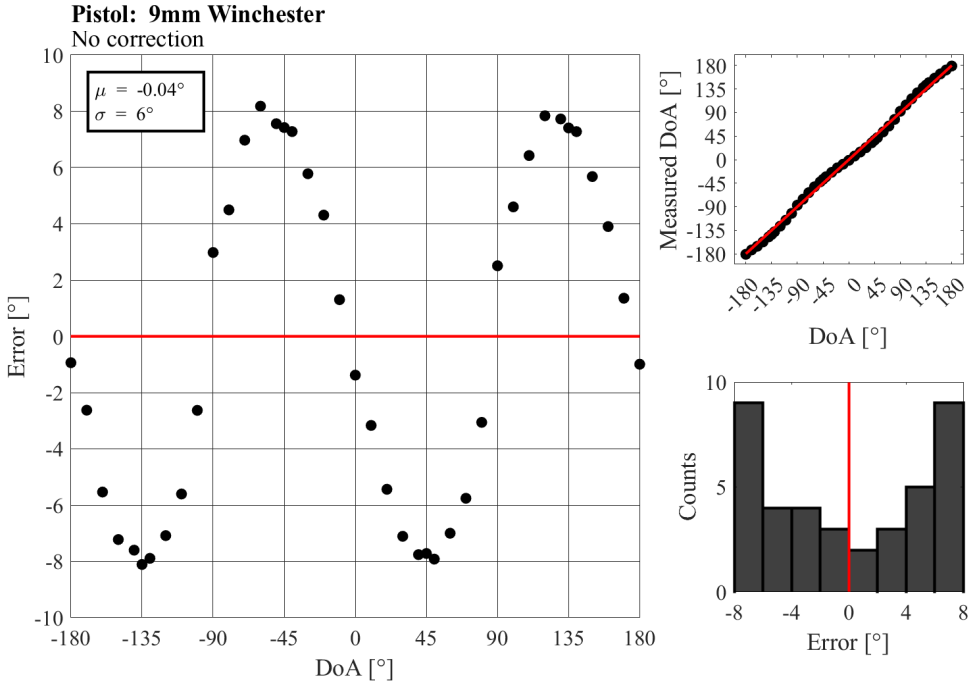

(a)

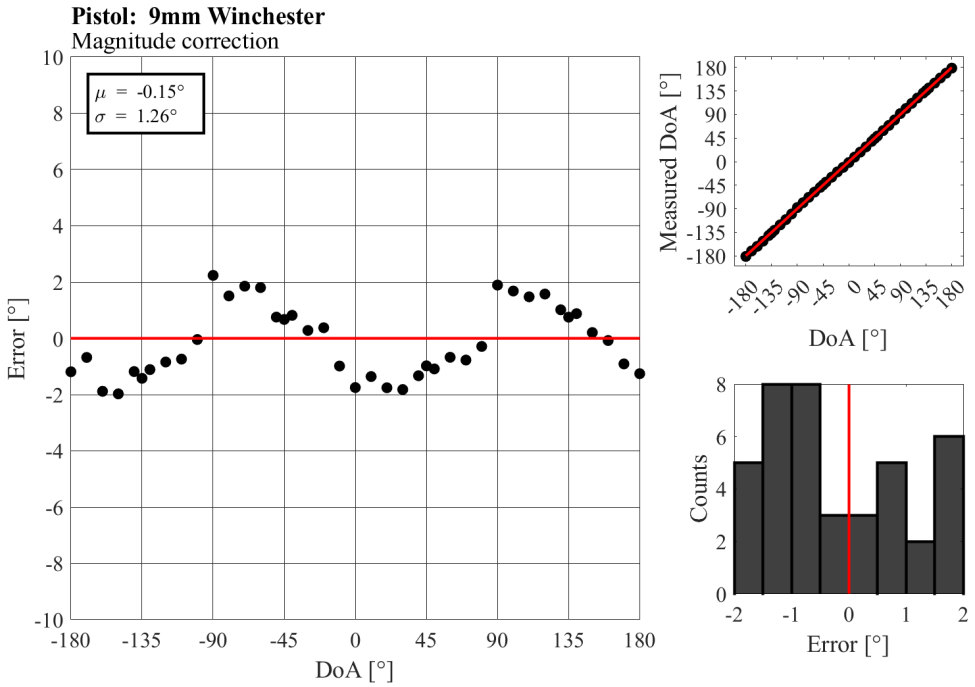

(b)

Figure 4.16. Worst results using new approach without (a) and with (b) magnitude only correction.

4.4.3 Discussion

The new approach discussed in Section 4.4.1 shows improvement across all guns when compared to the approach of [48]. In addition, the correction factor developed in Equation 4.6 improves DoA determination accuracy across all guns. The obvious improvement supports the reasoning that the noisy magnitude of the omni-directional microphone was impacting the the calculation of the reference angle in Section 4.3. By removing the omni-directional microphone from the arctan estimator, it ceased to play a role in the reference angle calculation. Its phase was still required for the conditionals to achieve unambiguous 360° DoA determination.

The underlying sinusoidal behavior is still present which makes sense since $A, B \rightarrow 0$ when $N, D \rightarrow 0$, respectively, causing the same error propagation phenomenon described in Section 4.3.4. This can probably be further improved by using a correction factor with reliable phase information.

Finally, the results in Section 4.4.2 and Appendix Section B.2 show comparable accuracy when compared to the best reported results for both the commercial and biomimetic research systems described in Section 2. This result indicates that this DoA determination approach has great potential to be employed for military or law enforcement applications.

CHAPTER 5:
Conclusions

In this research, a method of acoustically determining the direction of arrival of gunshots was developed by improving upon previous algorithms.

A sensor system consisting of a crossed-dipole of two *Ormia*-inspired MEMS sensors with one centrally collocated commercial MEMS omni-directional microphone was used. The sensors were fully characterized and algorithms for unambiguous 360° DoA determination were discussed. A correction factor was proposed to mitigate the error caused by operating two sensors on resonance with slightly different frequency responses.

The sensor system and gunshot stimulus were then simulated with artificial noise to prove the concept and to better test and understand how the DoA determination algorithms worked. Both of the proposed time-domain and frequency-domain algorithms functioned properly with little degradation in results up to a clear high-noise threshold. Afterwards, the physical system was field tested against live fire from multiple firearms. This field test successfully accomplished two goals: to achieve adequate gunshot DoA determination with the sensor in a real world environment and to create a library of gunshot audio files for later anechoic chamber testing.

The audio recordings of the various gunshot stimulus allowed further testing, conducted at NPS in the anechoic chamber. This testing was geared towards finding the true abilities and limitations of the proposed algorithms and to improve and adapt them for the specific task of gunshot DoA determination. The electronic equipment used to record the frequency response of the sensors was introducing an artificial phase delay between the MEMS sensors and the omni-directional microphone. This, unfortunately, compromised the ability of the correction factor to rectify the different frequency responses of the sensors. Additionally, it was observed that the omni-directional microphone was introducing high amounts of noise into the arctan estimator increasing DoA error.

However, a novel approach to calculating the reference angle without the omni-directional microphone was proposed. A modified set of conditionals to unambiguously resolve DoA

over 360° was tested with greatly improved results. Furthermore, the new approach allowed for a slightly simpler correction factor to be applied which successfully improved accuracy across all different guns. In fact, the achievable accuracy of $< 2°$ standard deviation is now on par with the best commercial and research systems described in Section 2.

Overall, this thesis successfully developed:

- a thorough understanding of the impact of the frequency response of the *Ormia*-inspired sensors and their differences on the accuracy of DoA determination algorithms,
- accurate and novel DoA determination algorithms as well as,
- corrective signal processing through the proposed correction factor to improve overall accuracy.

All research questions were also answered affirmatively:

1. The proposed collocated sensor combination can provide 360° DoA determination.
2. DoA can be determined in the frequency-domain and processing techniques can be applied effectively.
3. Correcting different sensor responses in the frequency-domain will increase accuracy of the DoA algorithms.
4. Achievable DoA accuracy has a standard deviation of $\sigma = 1.35°$ when averaged over all guns using the DoA algorithm and correction factor developed in Section 4.4.

5.1 Suggestions for Future Work

My suggestions for future work are:

1. Include phase information in the correction factor. Phase should be measured with precision instrumentation and reference.
2. Retest complete system and algorithm in a field-test to see how it performs outside of an anechoic chamber.
3. Explore possibilities of completely removing the need for an omni-directional microphone. This could further increase DoA accuracy as the additional microphone is an extra noise source. It would also decrease the final cost of the system.

APPENDIX A:
Gun Information

This appendix provides a compilation of all data collected on each gun recorded and used in this thesis as well as their respective ammunition.

Table A.1. Complete list of gun information for all guns recorded during the Paso Robles field test.

Gun >	Name:	**9 mm**
	Serial #:	MG460135
	Type:	Pistol
Ammo >	Manufacturer:	Winchester
	Caliber:	9 mm
	Grain:	115 Gr.
	Notes:	Full metal jacket, luger
Gun >	Name:	**M4 Carbine**
	Serial #:	W-0026028
	Type:	Rifle
Ammo >	Manufacturer:	Federal Ammunition
	Model #:	XM193AF
	Caliber:	5.56 mm
	Grain:	55 Gr.
	Notes:	MC-BT
Gun >	Name:	**M4 Carbine - COLT'S MFG. CO. LLC.**
	Serial #:	BP039678
	Type:	Rifle
Ammo >	Manufacturer:	Winchester Wildcat
	Caliber:	.22 cal
	Grain:	40 Gr.
	Notes:	Lead round nose, long rifle high velocity

Table A.1 continued from previous page

Gun >	Name:	**SP101 Sturm, Ruger CO inc.**
	Serial #:	570-55605
	Type:	Pistol
Ammo >	Manufacturer:	Winchester Wildcat
	Caliber:	.22 cal
	Grain:	40 Gr.
	Notes:	Lead round nose, 4 inch barrel, long rifle high velocity
Gun >	Name:	**Five-seveN FN Herstal**
	Serial #:	386339842
	Type:	Pistol
Ammo >	Manufacturer:	Federal Ammunition - American Eagle
	Caliber:	5.7x28 mm
	Grain:	40 Gr.
	Notes:	Full metal jacket
Gun >	Name:	**Magnum 44 - Magnum Research Inc. Desert Eagle Pistol**
	Serial #:	45200726
	Type:	Pistol
Ammo >	Manufacturer:	S & W
	Caliber:	44 cal
	Grain:	240 Gr.
	Notes:	Point bullet, centerfire cartridges
Gun >	Name:	**45 Smith & Wesson**
	Serial #:	TVB1874 Mod 4506-1
	Type:	Pistol
Ammo >	Manufacturer:	Remmington Arms
	Caliber:	45 cal
	Grain:	230 Gr.
	Notes:	Metal case, automatic (ACP) centerfire
Gun >	Name:	**AK-47 Model 56S Norinco**
	Serial #:	2766
	Type:	Rifle
Ammo >	Manufacturer:	Century Internation Arms

Table A.1 continued from previous page

	Caliber:	7.62x39 mm
	Grain:	
	Notes:	

THIS PAGE INTENTIONALLY LEFT BLANK

APPENDIX B:
Complete Results

This appendix contains complete results of all guns for the experiments conducted in Sections 4.3 and 4.4 as well as a reproduction of Tables 4.2 and 4.3 for ease of reference. Each figure contains the results without (a) and with (b) the appropriate correction factor. Figure titles contain information about the gun used and the correction factor applied if any. Mean μ and standard deviation σ information is also shown.

B.1 Correction Factor Test: Anechoic Chamber

Table B.1. Summary of anechoic chamber results. Green denotes improvement after application of the correction factor. Reproduction of Table 4.2 for ease of reference.

	None		**Correction**	
Gun	$\sigma[^\circ]$	$\mu[^\circ]$	$\sigma[^\circ]$	$\mu[^\circ]$
45 Smith & Wesson	9.14	0.37	6.76	0.66
9 mm	21.22	0.08	11.4	-0.34
Five-seveN	2.30	-0.24	4.73	-0.07
Magnum 44	10.31	-0.45	2.21	-0.67
SP101	14.94	1.27	12.00	1.28
AK-47	3.01	0.21	4.10	0.16
M4 Carbine	4.95	0.01	3.03	-0.09
M4 .22 Carbine	15.76	0.51	8.74	0.54
Average	**10.20**	**0.22**	**6.62**	**0.18**

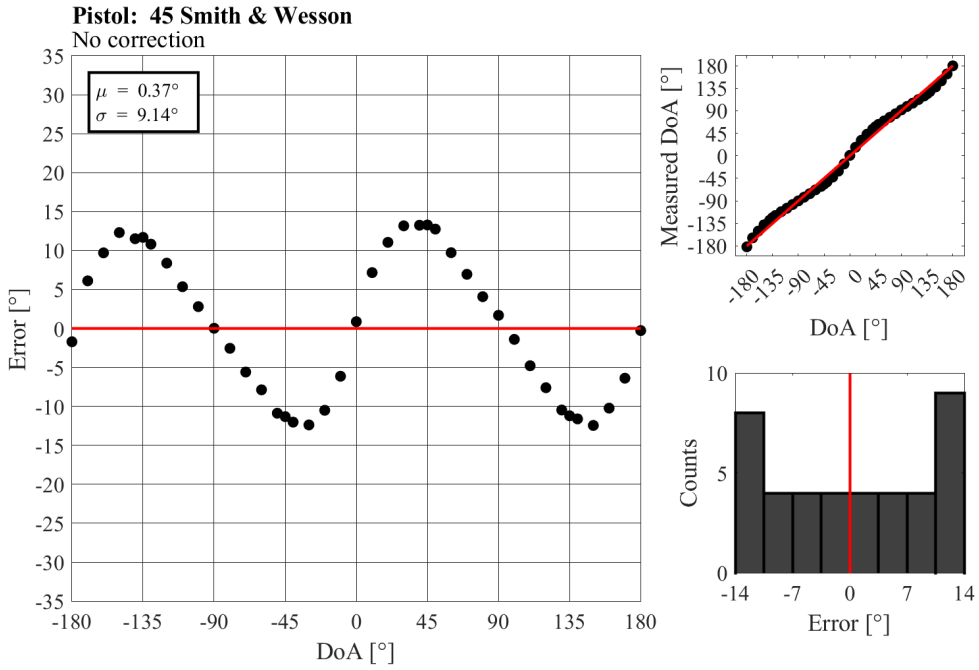

(a)

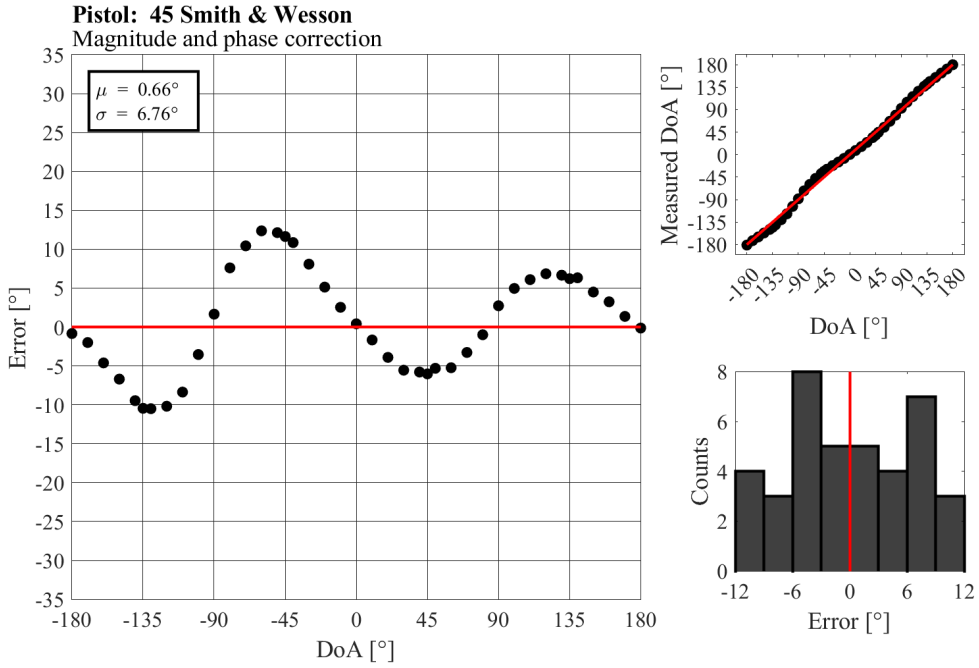

(b)

Figure B.1. Anechoic chamber results: 45 Smith & Wesson.

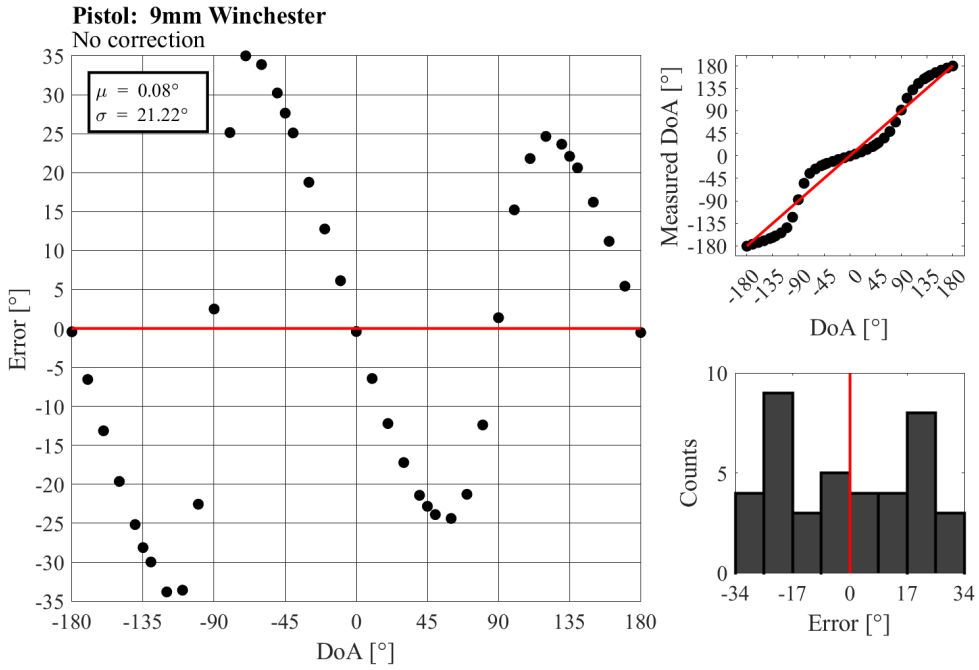

(a)

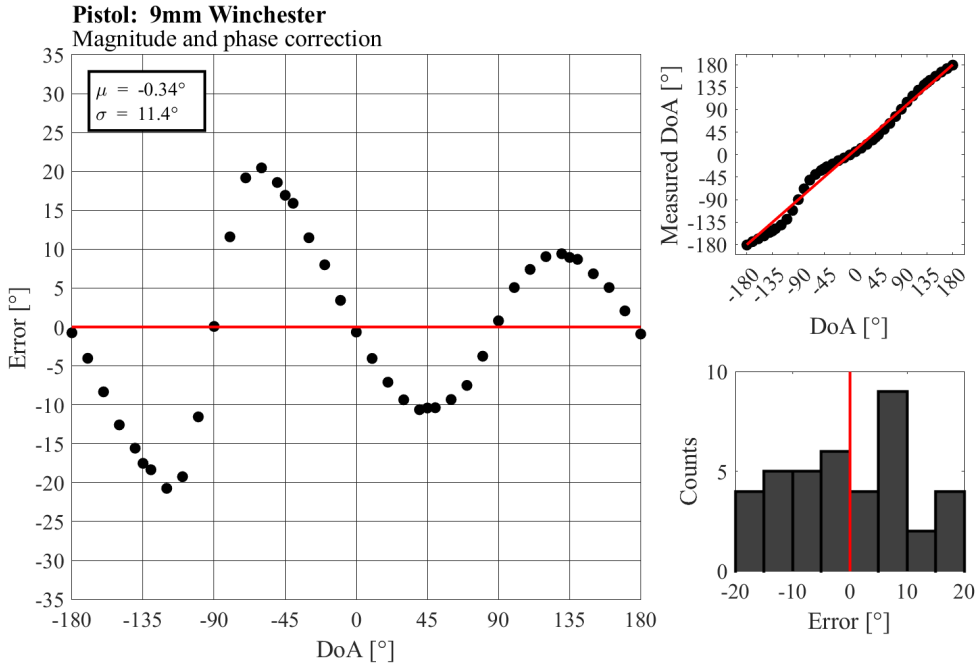

(b)

Figure B.2. Anechoic chamber results: 9mm.

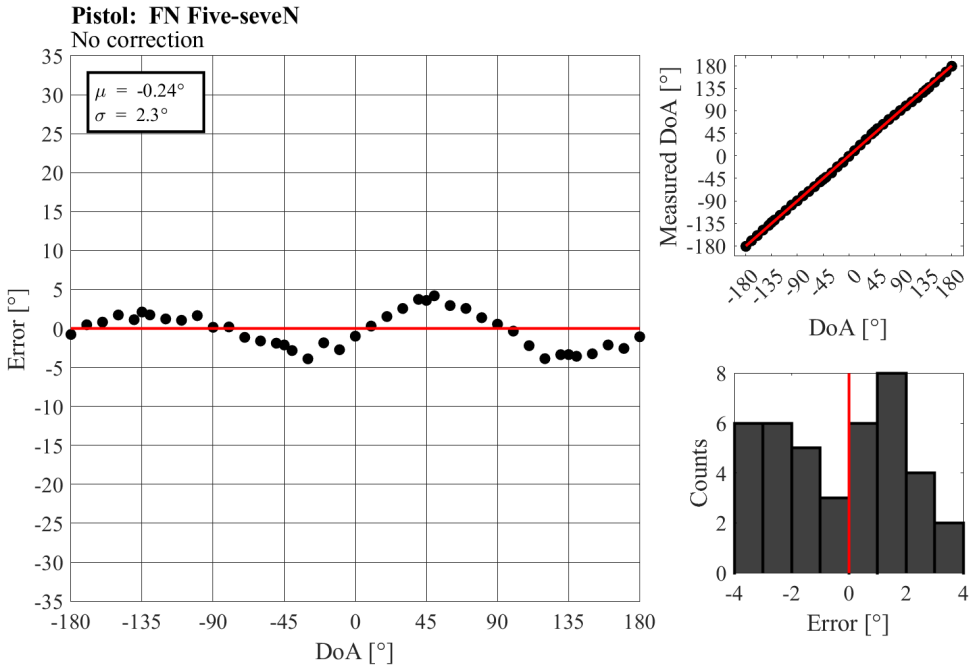

(a)

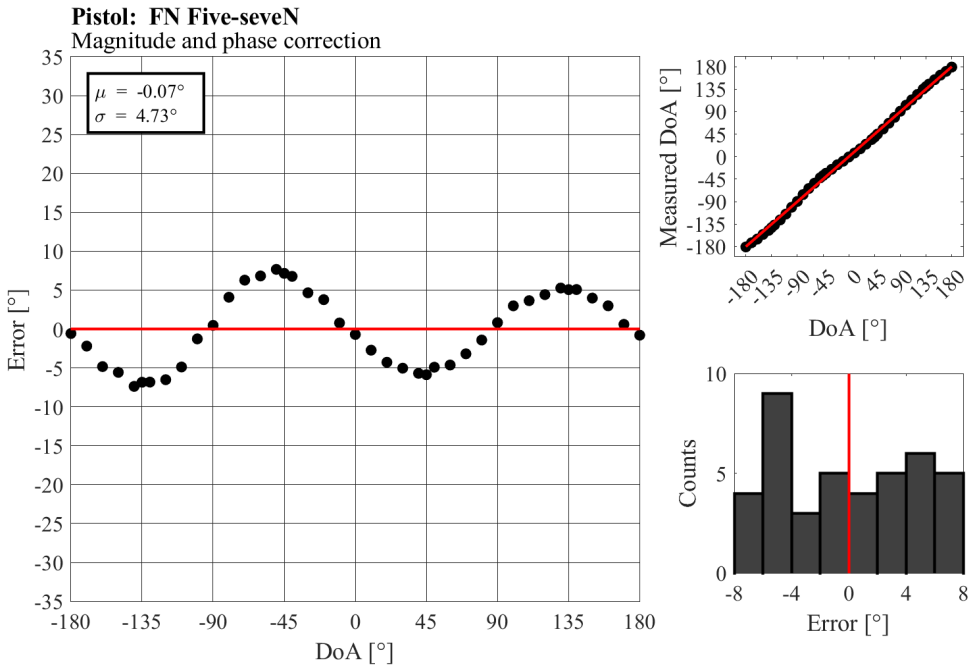

(b)

Figure B.3. Anechoic chamber results: Five-seveN.

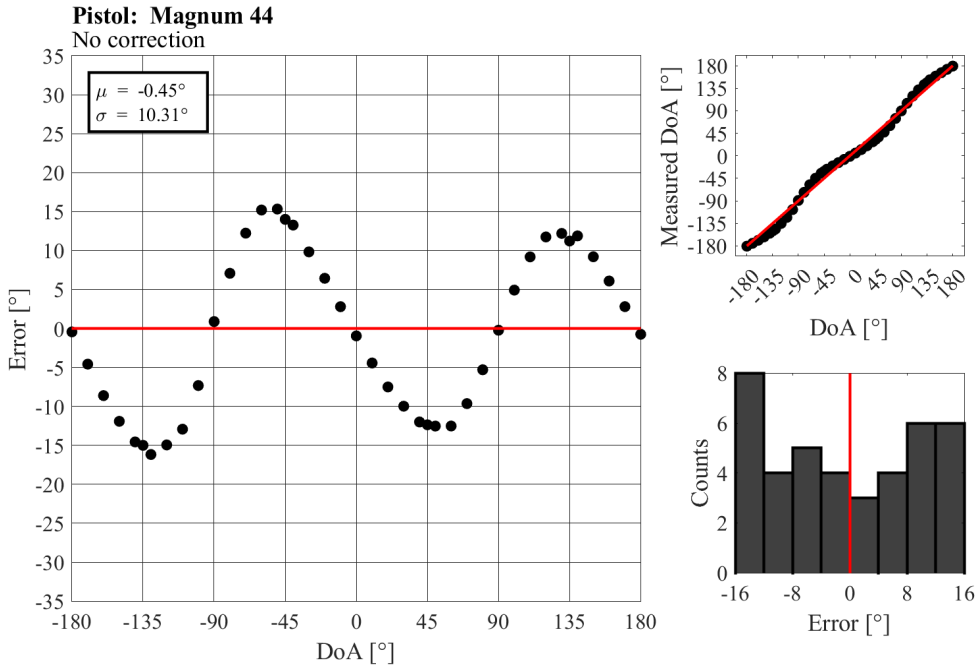

(a)

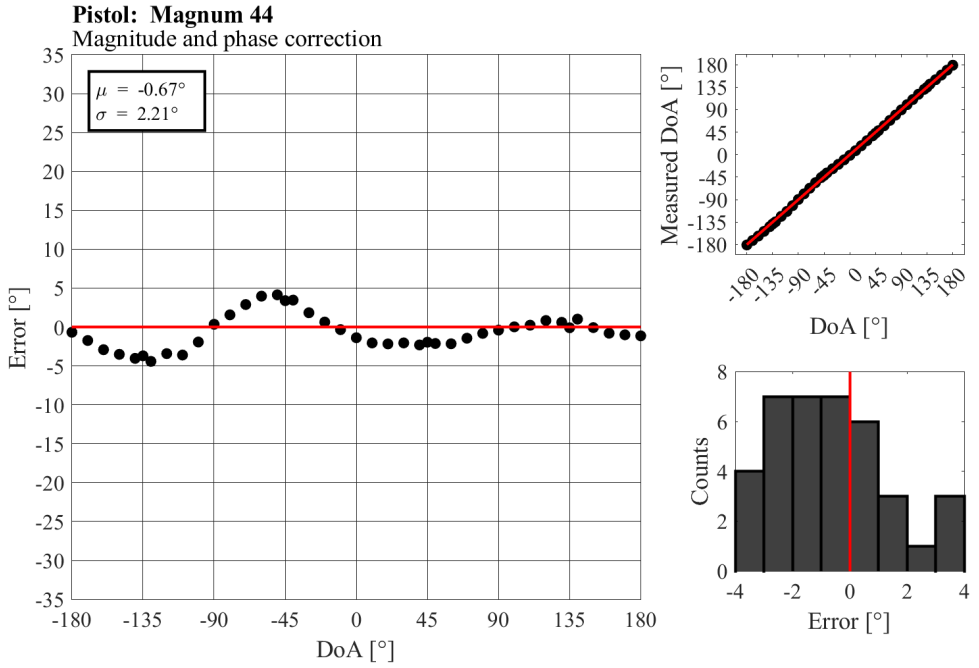

(b)

Figure B.4. Anechoic chamber results: Magnum 44.

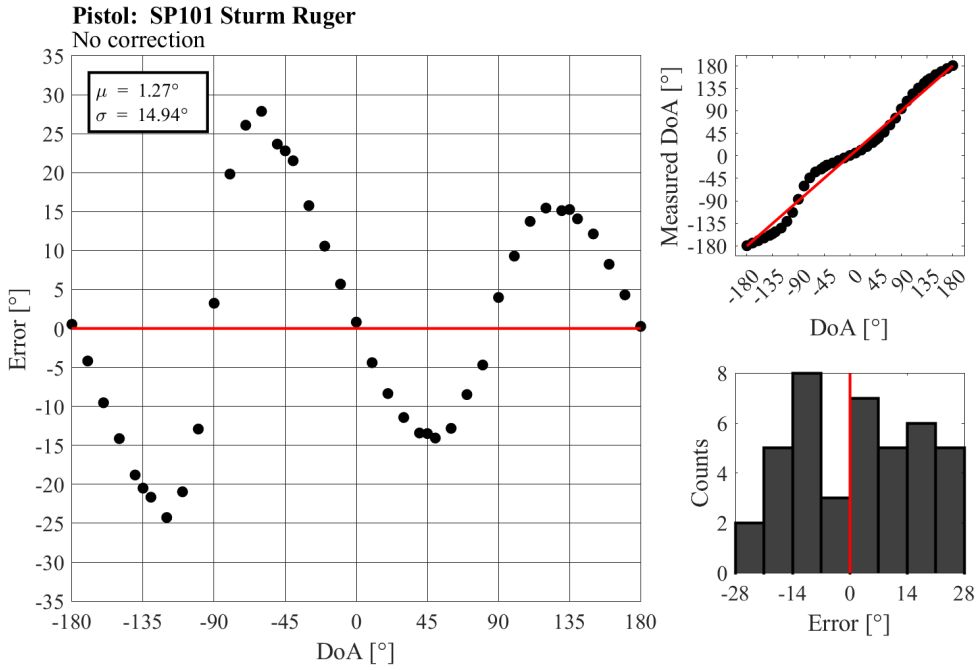

(a)

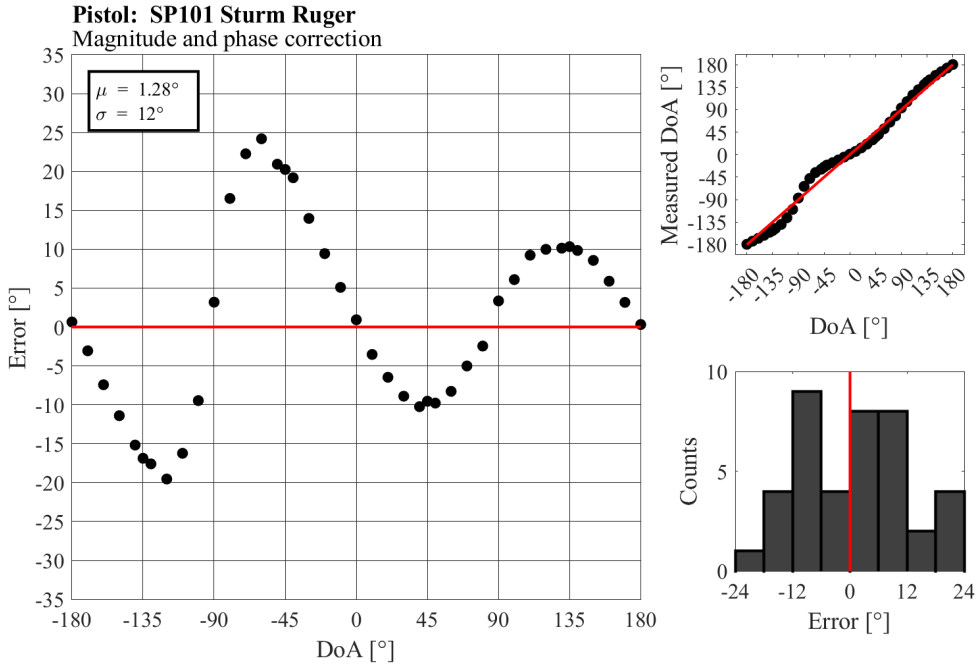

(b)

Figure B.5. Anechoic chamber results: SP101 Sturm.

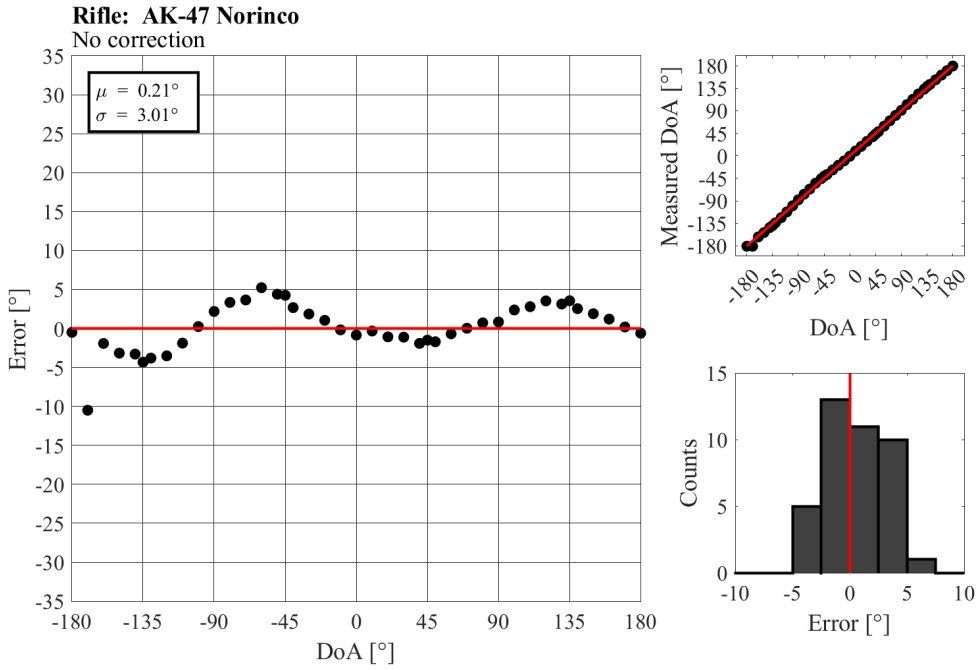

(a)

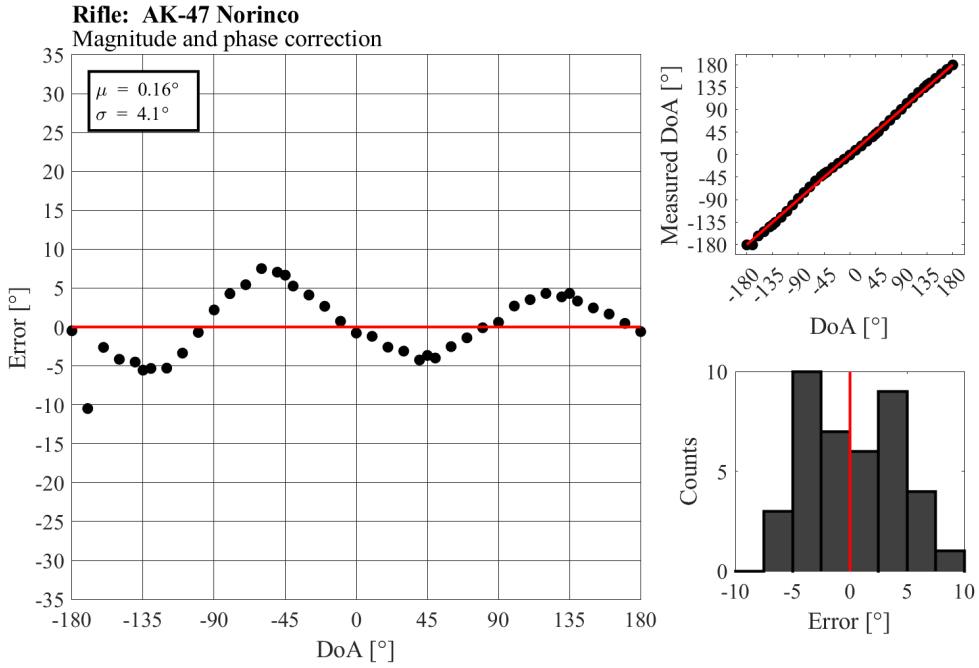

(b)

Figure B.6. Anechoic chamber results: AK-47.

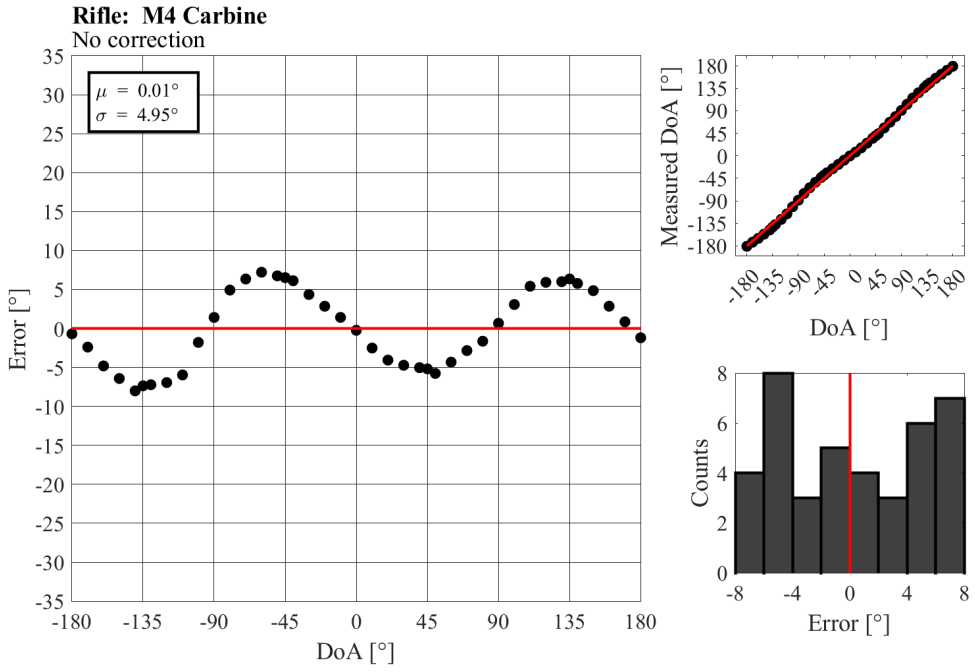

(a)

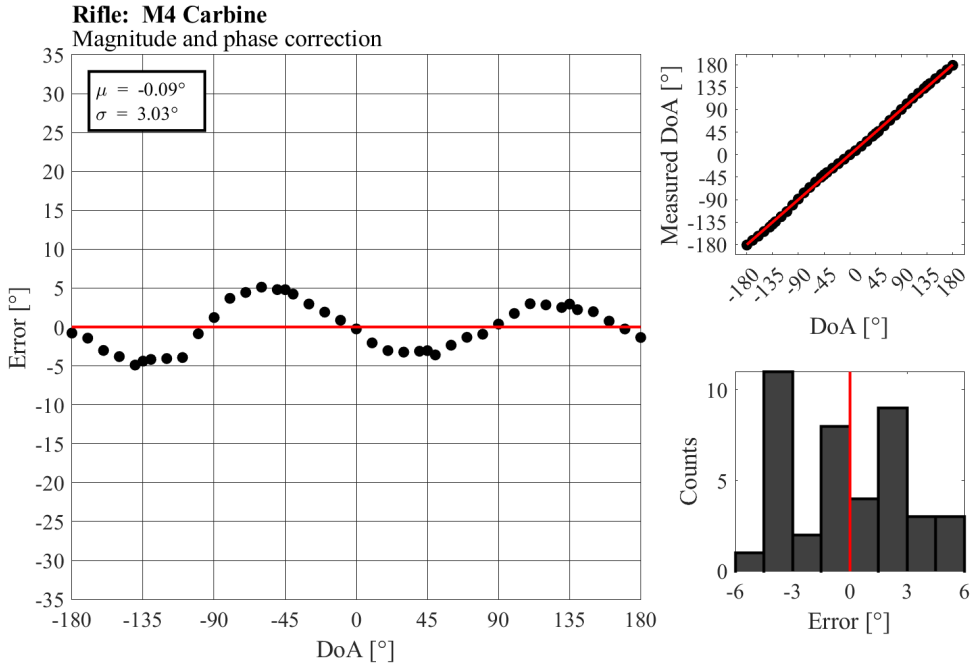

(b)

Figure B.7. Anechoic chamber results: M4 Carbine.

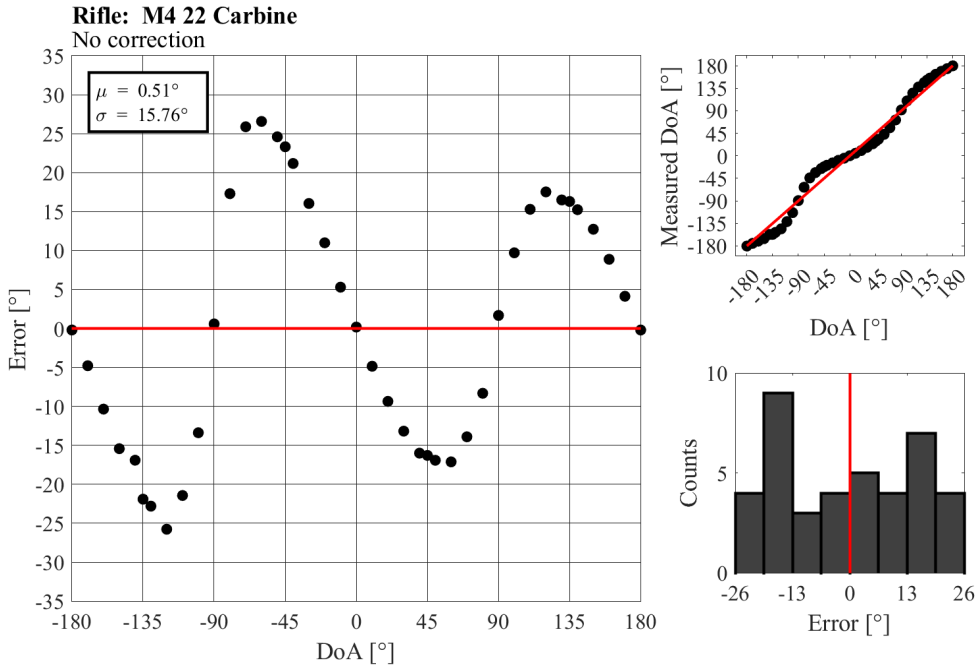

(a)

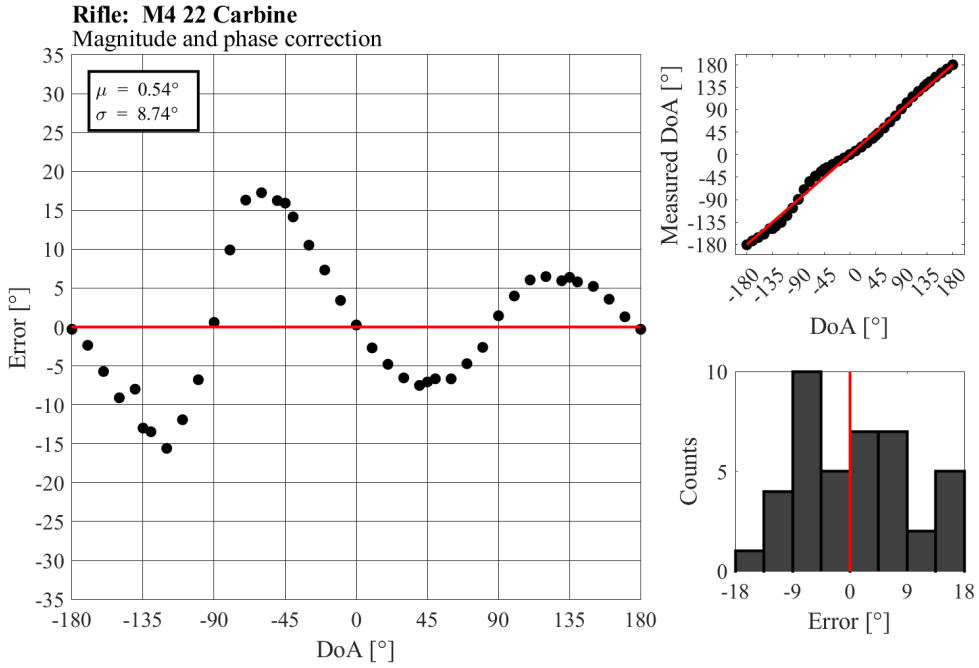

(b)

Figure B.8. Anechoic chamber results: M4 .22 Carbine.

B.2 New Frequency-Domain Approach: Anechoic Chamber

Table B.2. Summary of new approach results. Green denotes improvement after application of the correction factor. Reproduction of Table 4.3 for ease of reference.

	None		**Correction**	
Gun	$\sigma[^\circ]$	$\mu[^\circ]$	$\sigma[^\circ]$	$\mu[^\circ]$
45 Smith & Wesson	2.55	-0.31	1.13	-0.27
9 mm	6.00	-0.04	1.26	-0.15
Five-seveN	2.30	0.00	1.98	-0.02
Magnum 44	3.88	-0.25	0.80	-0.26
SP101	5.96	-0.01	1.19	-0.03
AK-47	3.56	-0.27	2.12	-0.34
M4 Carbine	3.39	-0.11	1.18	-0.17
M4 .22 Carbine	6.07	0.11	1.16	0.02
Average	**4.21**	**-0.11**	**1.35**	**-0.15**

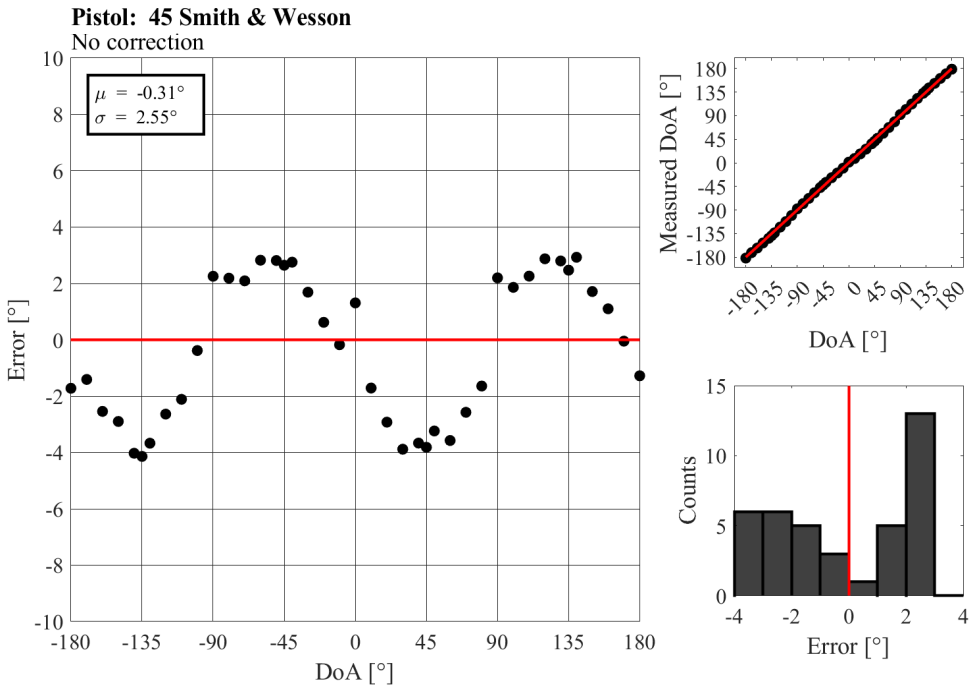

(a)

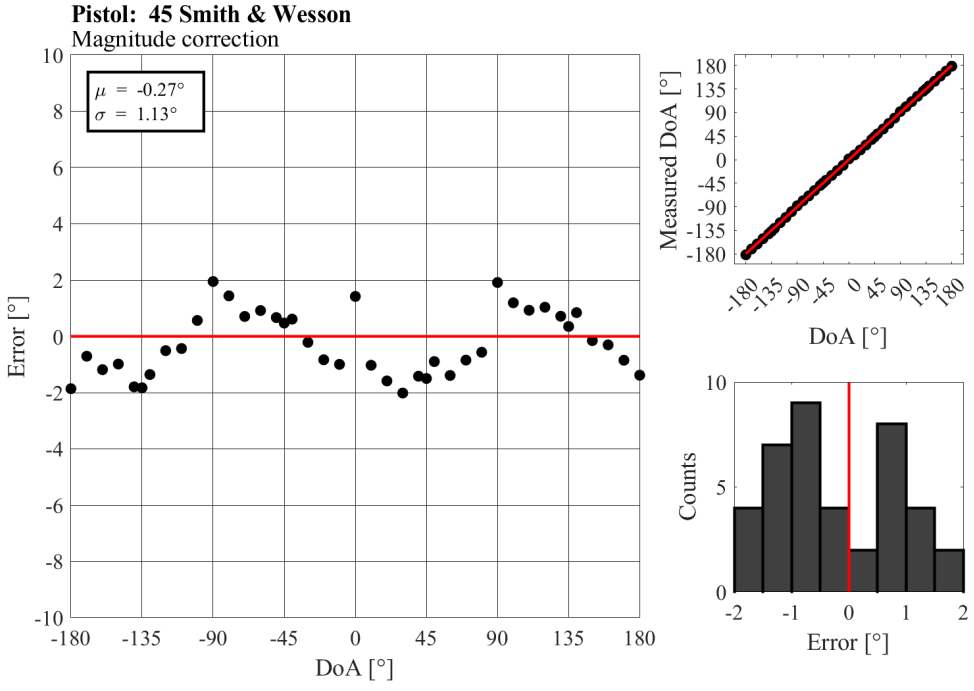

(b)

Figure B.9. New approach results: 45 Smith & Wesson

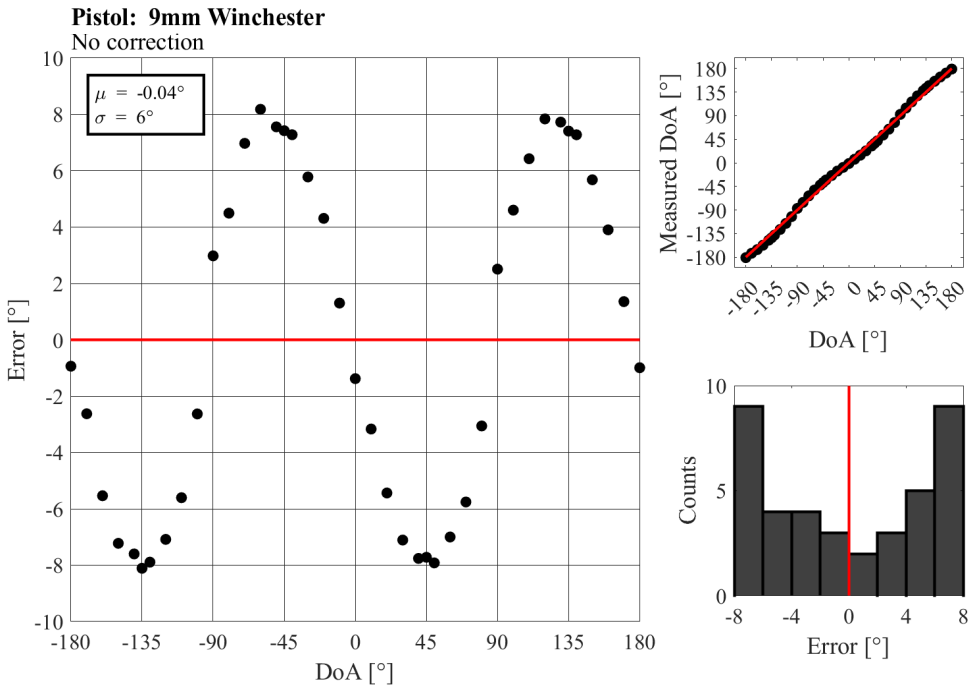

(a)

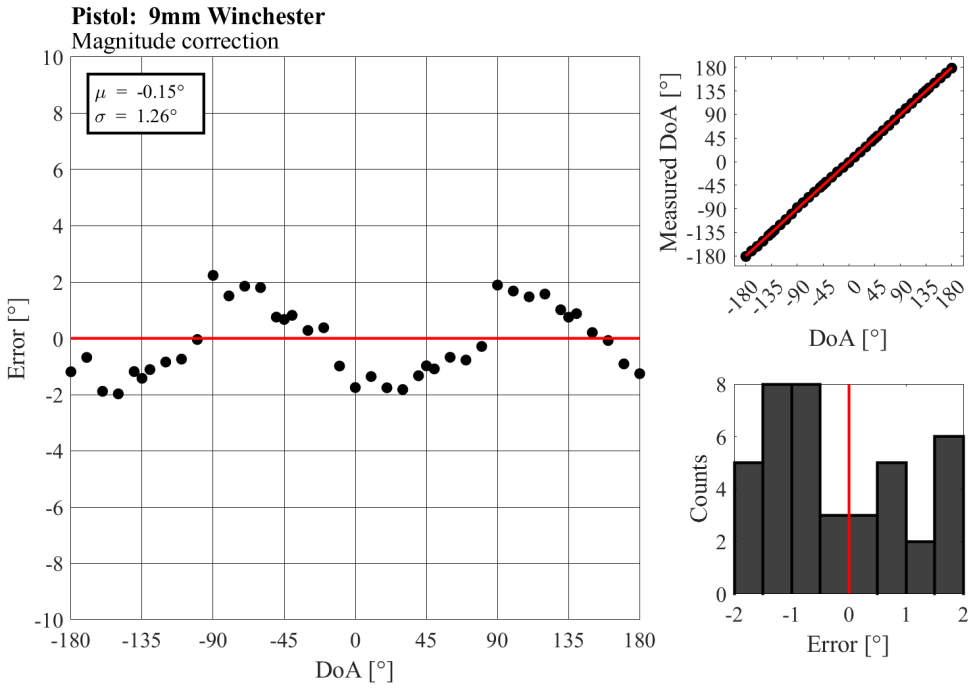

(b)

Figure B.10. New approach results: 9mm.

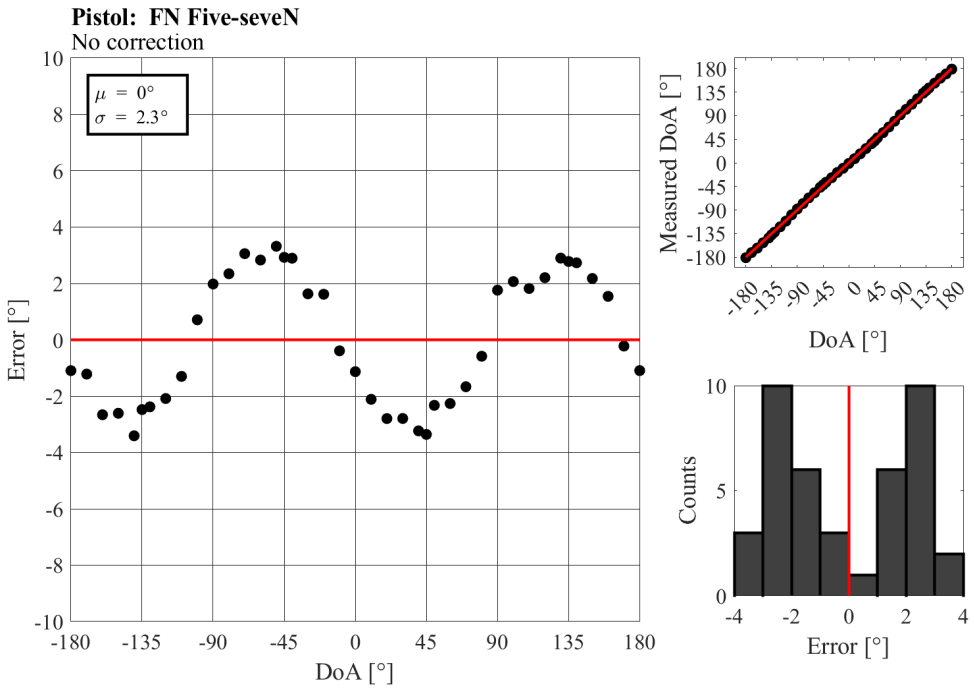

(a)

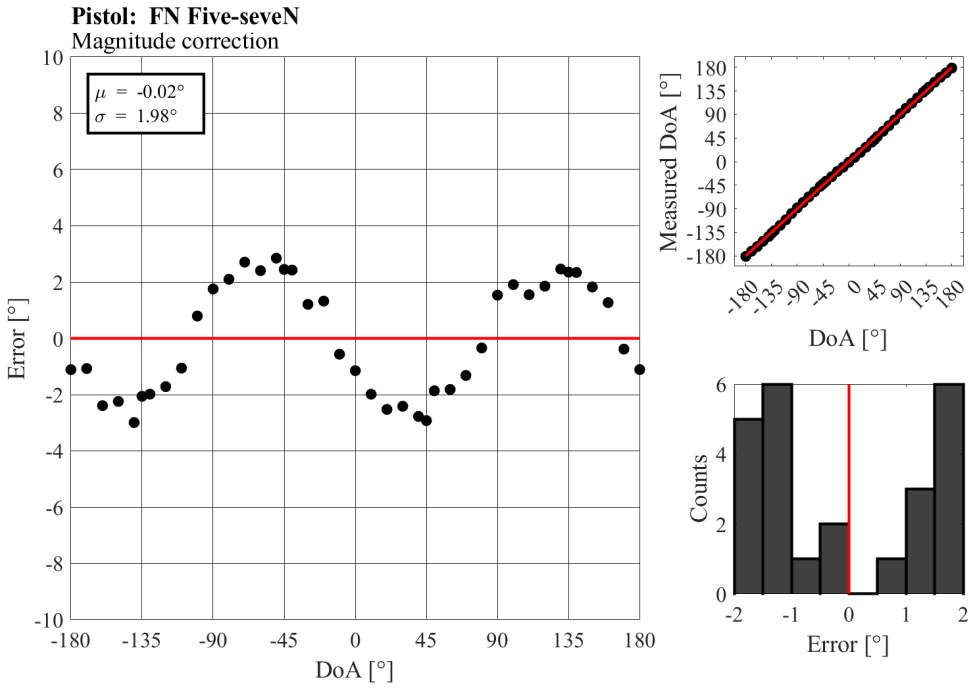

(b)

Figure B.11. New approach results: Five-seveN.

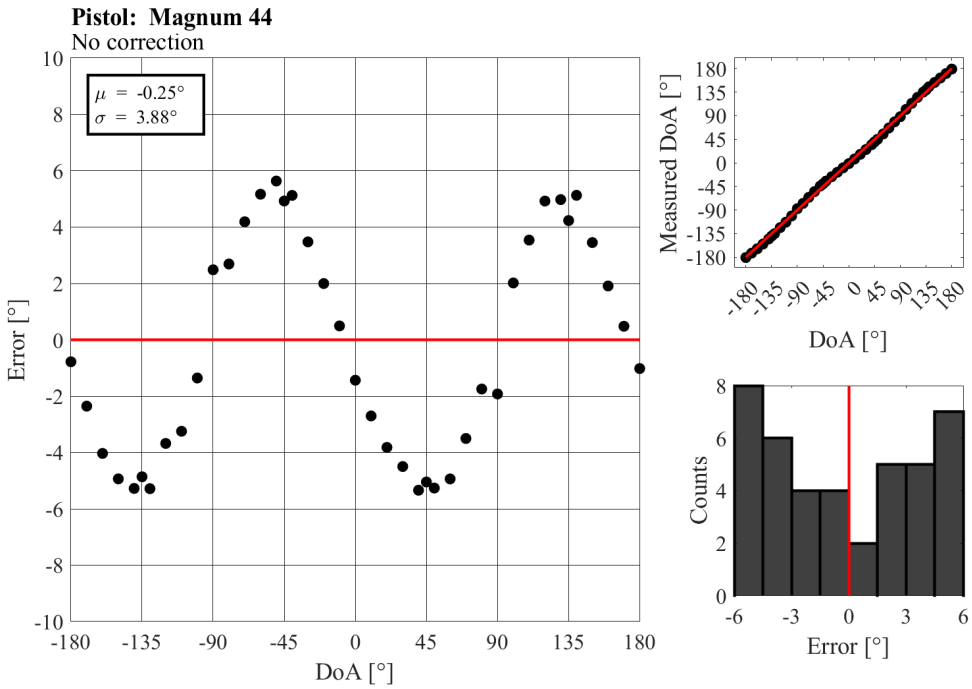

(a)

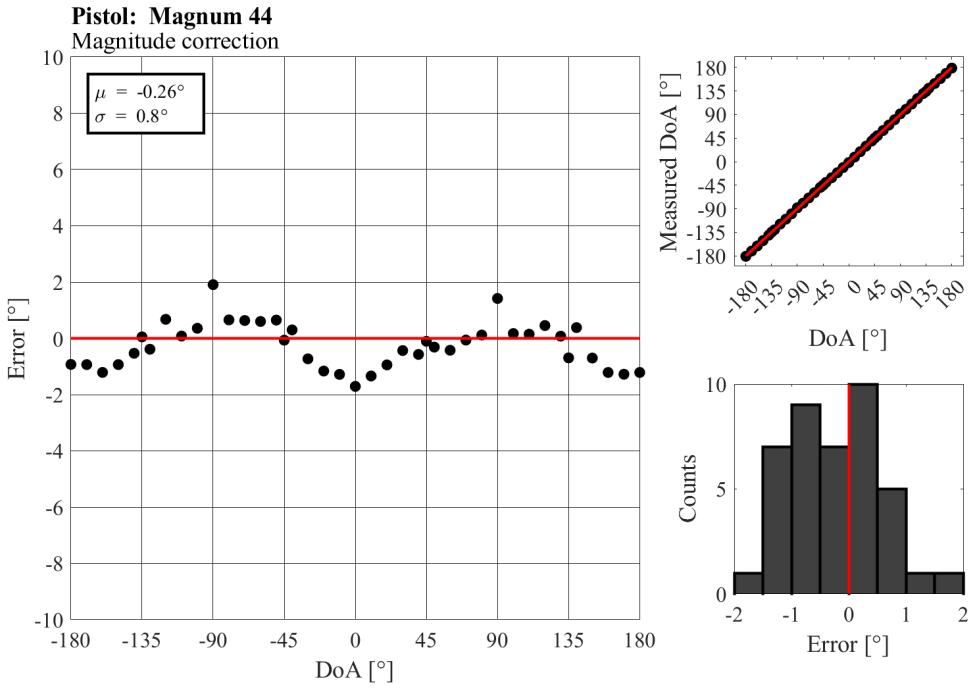

(b)

Figure B.12. New approach results: Magnum 44.

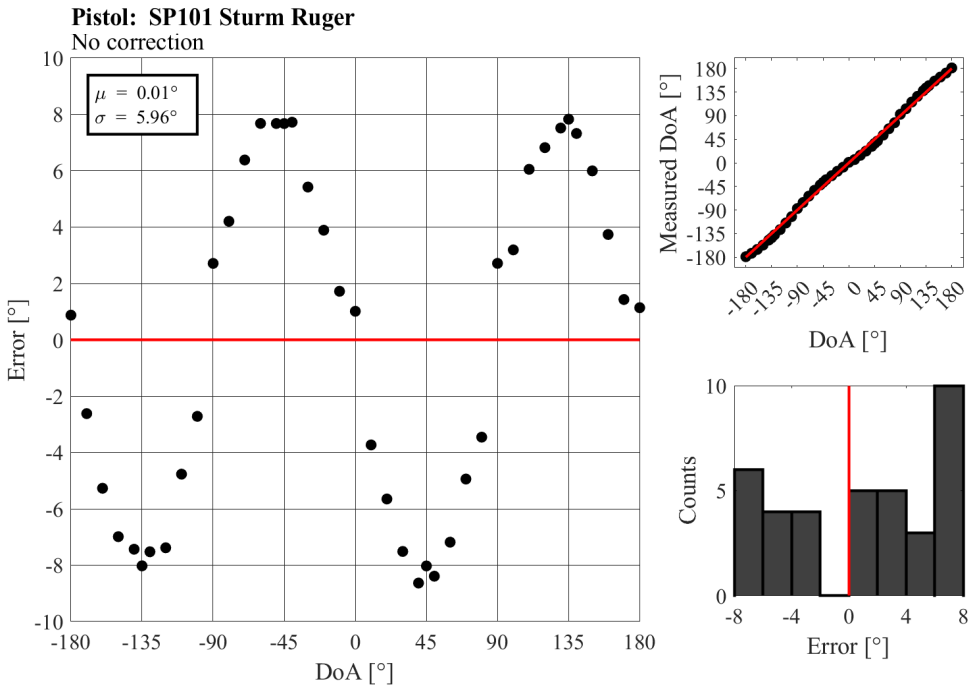

(a)

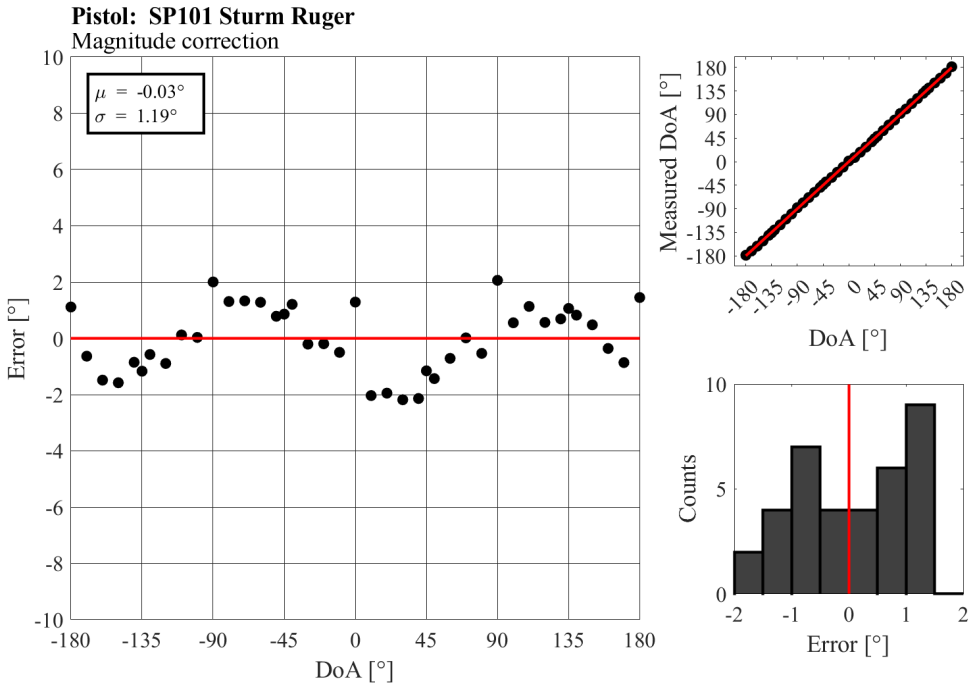

(b)

Figure B.13. New approach results: SP101 Sturm.

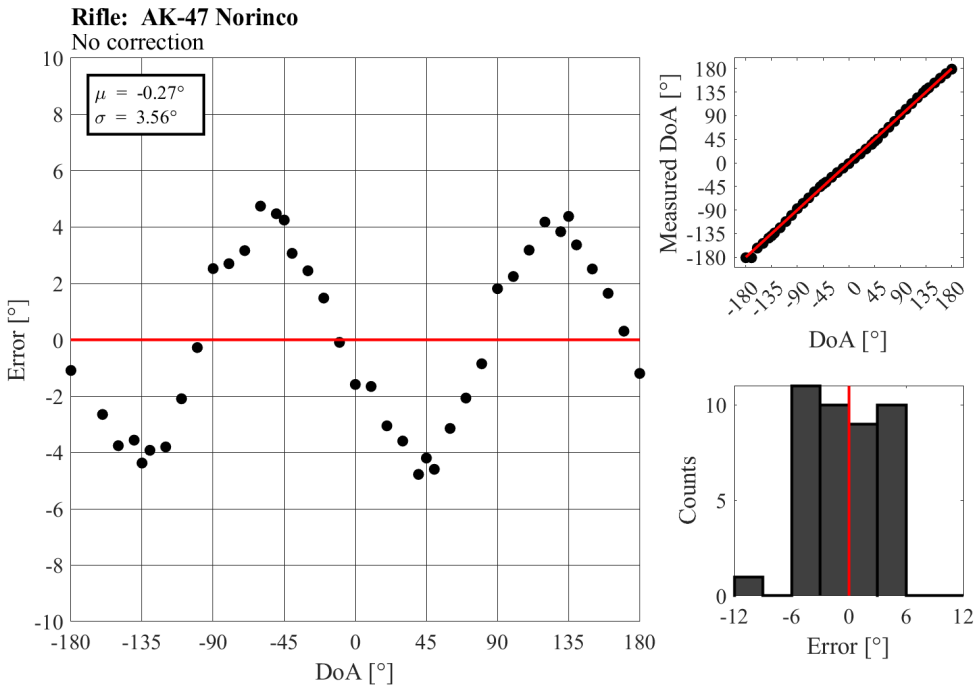

(a)

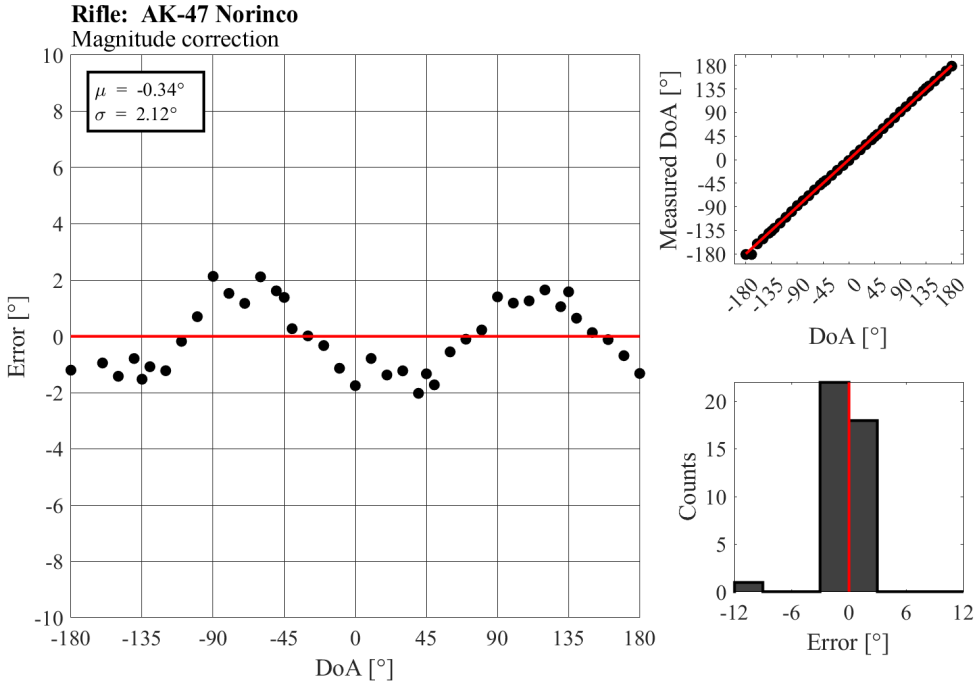

(b)

Figure B.14. New approach results: AK-47.

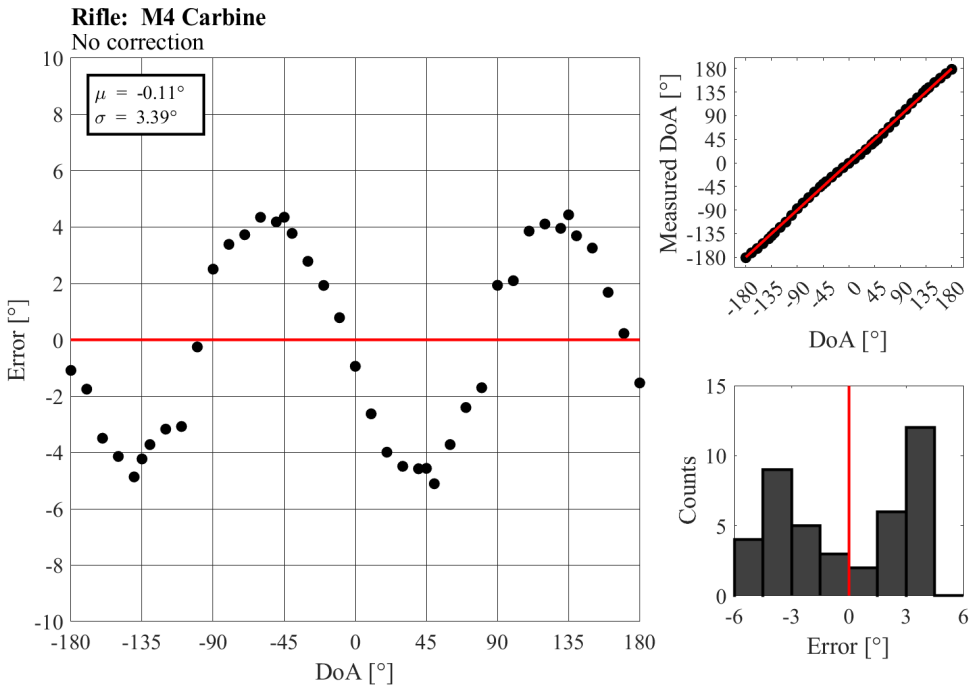

(a)

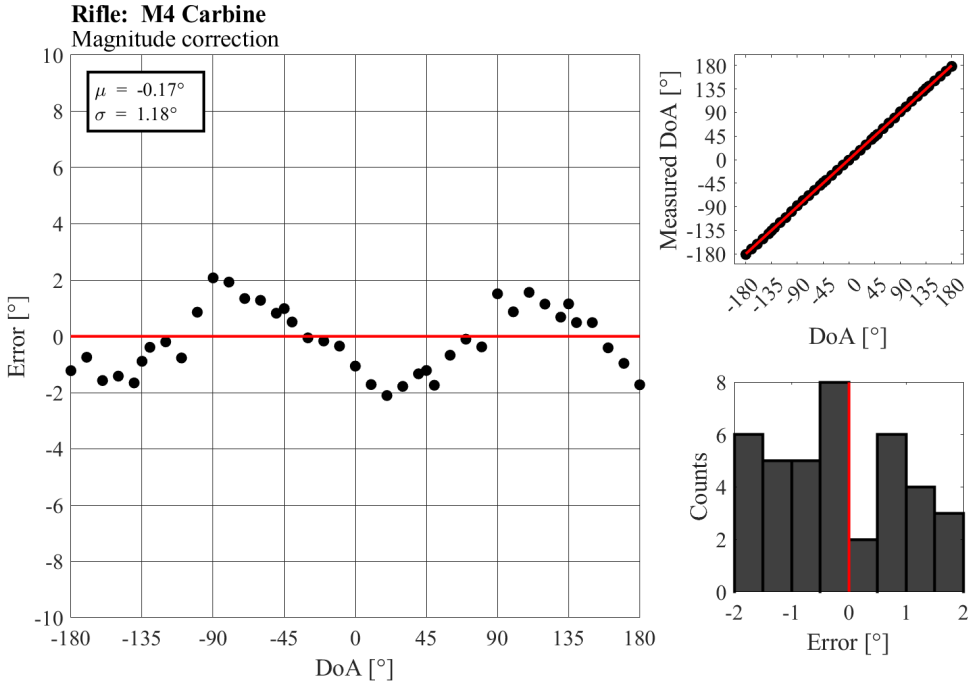

(b)

Figure B.15. New approach results: M4 Carbine.

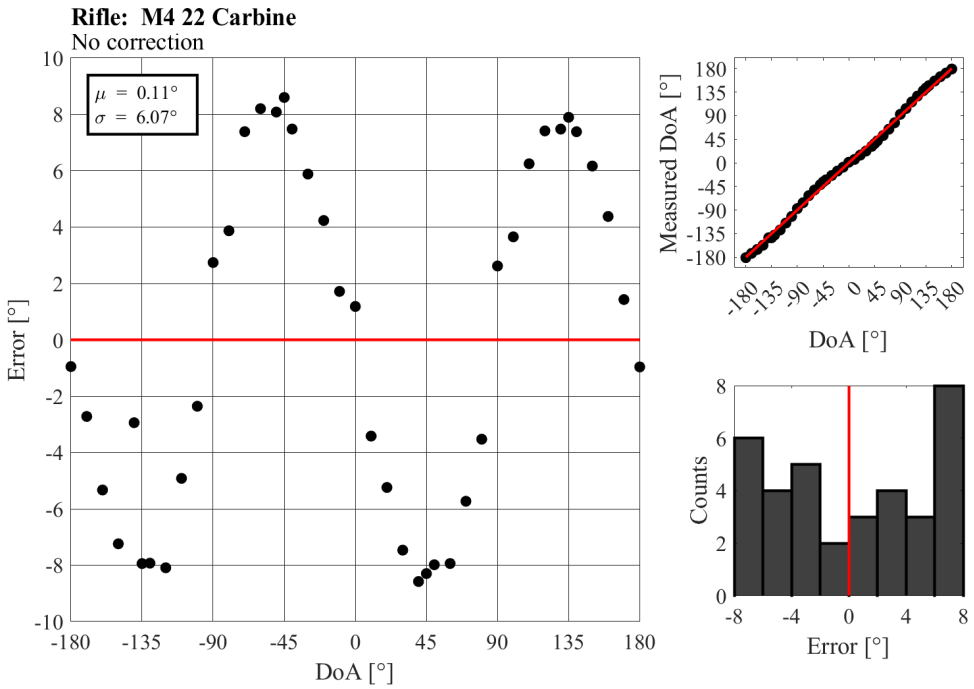

(a)

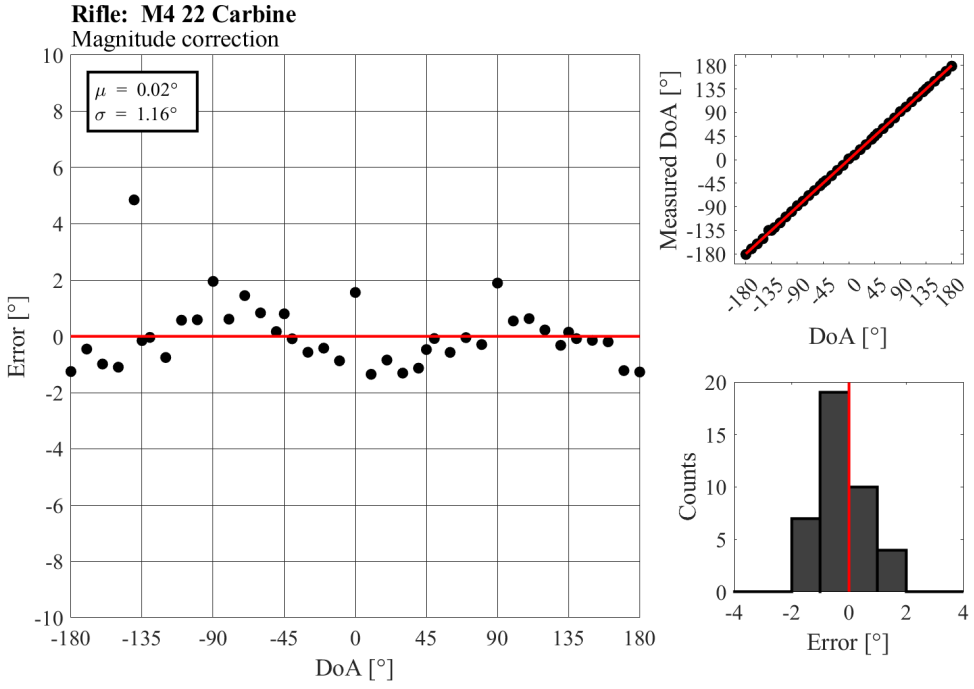

(b)

Figure B.16. New approach results: M4 .22 Carbine.

APPENDIX C:
Matlab Code

C.1 DoA Determination Algorithms

```
%% INFORMATION

% dipole_doa.m - Implements choice of two DoA determination algorithms in
%                the frequency-domain along with three possible correction
%                factors for the dipole sensor configuration. Approach one
%                is taken from literature. Approach two is a new low-noise
%                approach that achieve superior results than approach one
%                by removing the omni sensor from the reference angle
%                calculation

% ENS Ionatan A. Soule, USN
% 17JUN2022

%% SETUP
clc; clear all; close all; warning off; set(0,'DefaultLineLineWidth',2);

%% USER DEFINED PARAMETERS
phi = sort([-180:10:180 -135:90:135]); % all measured angles sorted
backtrack = 500; % # of points to backtrack from max excitation
thresh = 0.01; % trigger threshold as percent of max excitation
NP = 4096; % # of points to process once triggered
approach = 1;                   % (1) == Dini et al.'s approach
                                % (2) == Superior approach
correction = 3;                 % (0) == no correction applied
                                % (1) == magnitude only
                                % (2) == magnitude and phase
                                % (3) == magnitude and adjusted phase

%% FILEPATH AND GUN INFORMATION
folder = 'C:path\to\audio\recordings\folder\';
gunfile = ['5-7',...            % (1) ... name of audio recordingS
```

```
        '9mm',...                % (2)
        '22cal revolver',...     % (3)
        '44 Magnum',...          % (4)
        '45-ACP',...             % (5)
        'AK-47-565',...          % (6)
        'M4',...                 % (7)
        'M4-22'];                % (8)
gunname = ['FN Five-seveN',...   % (1) ... name of gun for titleS
        '9mm Winchester',...     % (2)
        'SP101 Sturm Ruger',...  % (3)
        'Magnum 44',...          % (4)
        '45 Smith & Wesson',...  % (5)
        'AK-47 Norinco',...      % (6)
        'M4 Carbine',...         % (7)
        'M4 22 Carbine'];        % (8)
typename = ['Pistol',...         % (1) ... type of gunS
        'Pistol',...             % (2)
        'Pistol',...             % (3)
        'Pistol',...             % (4)
        'Pistol',...             % (5)
        'Rifle',...              % (6)
        'Rifle',...              % (7)
        'Rifle'];                % (8)

%% LOOP THROUGH ALL GUNS
% loop to process all guns with choosen correction
for select = 1:length(gunfile)          % loop thru all guns
    path = folder+gunfile(select)+'\';  % set full path to gun folder

    ch0 = '_Ch_0.wav';              % cosine
    ch1 = '_Ch_1.wav';              % omni
    ch2 = '_Ch_2.wav';              % sine

    %% LOOP THROUGH ALL ANGLES
    % loop through all angles for each gun
    for n = 1:length(phi)           % loop thru all angles
        s = num2str(abs(phi(n)));   % create string of current angle
        neg = 'n';                  % account for negative values
        % define full path to audiorecordings
        if phi(n) < 0               % negative angles
```

```
72              ch0s = path+neg+s+ch0;
73              ch1s = path+neg+s+ch1;
74              ch2s = path+neg+s+ch2;
75          else                        % positive angles
76              ch0s = path+s+ch0;
77              ch1s = path+s+ch1;
78              ch2s = path+s+ch2;
79          end
80
81          %% FIND AND SETUP GUNSHOT IN TIME-DOMAIN
82          % read signals
83          [y0,Fs0] = audioread(ch0s); % cos sensor
84          [y1,~] = audioread(ch1s);   % omni sensor
85          [y2,~] = audioread(ch2s);   % sin sensor
86          % setup time vectors
87          ts = (1/Fs0)*length(y0);    % total time of recording
88          t = [0:ts/length(y0):ts];   % appropriately spaced time-vector
89          t = t(1:length(t)-1);       % fix vector sizing and index issues
90          % located gunshot
91          [m0,shoti0] = max(y0);      % find max excitation of cos
92          [m2,shoti2] = max(y2);      % find max excitation of sin
93          if m0 > m2                  % set reference to max excitation
94              shoti = shoti0;         % index of max excitation
95              mm = m0;                % max excitation
96          else
97              shoti = shoti2;         % index of max excitation
98              mm = m2;                % max excitation
99          end
100         r = shoti-backtrack;        % index to look for threshold
101         % locate start of gunshot
102         while abs(y0(r)) < thresh &&...
103               abs(y2(r)) < thresh   % both must meet threshold
104             r = r+1;
105         end
106         % select gunshot
107         ttr = t(r:r+NP);
108         y0tr = y0(r:r+NP);
109         y1tr = y1(r:r+NP);
110         y2tr = y2(r:r+NP);
111
```

```
%% CONVERT TO FREQUENCY-DOMAIN FOR PROCESSING
% setup frequency-domain
NFFT = length(y0tr);        % number of points in FFT
Fstep = Fs0/(NFFT-1);       % frequency resolution
Fstart = 500;               % initial frequency to process
Fstarti = Fstart/Fstep+2;   % index of initial frequency
Fstop = 900;                % final frequency to process
Fstopi = Fstop/Fstep;       % index of final frequency
% freq
F0 = ((0:1/NFFT:1-1/NFFT)*Fs0).'; % create frequency axis
F0 = F0(Fstarti:Fstopi);    % select frequencies of interest
% cos
Y0 = fft(y0tr,NFFT);        % FFT of cosine sensor
Y0 = Y0(Fstarti:Fstopi);    % select frequencies of interest
% omni
Y1 = fft(y1tr,NFFT);        % FFT of omni sensor
Y1 = Y1(Fstarti:Fstopi);    % select frequencies of interest
% sin
Y2 = fft(y2tr,NFFT);        % FFT of sine sensor
Y2 = Y2(Fstarti:Fstopi);    % select frequencies of interest

%% CORRECTION FACTOR
% Apply choosen correction factor
CRF = correctionfactor(F0,correction);  % call correction factor
Y0 = CRF.*Y0;                           % correct cosine sensor

%% FREQUENCY-DOMAIN DoA DETERMINATION ALGORITHMS
% Setup values for DoA determination algorithms
A(n) = trapz(abs(Y2));
B(n) = trapz(abs(Y0));
N(n) = real(trapz(Y2.*conj(Y1)));
D(n) = real(trapz(Y0.*conj(Y1)));

% ######################    Approach developed by Dini et al.
% #### APPROACH ONE ####    with conditionals modeled after
% ######################     Davies' time-domain approach

if approach == 1
    % Dini et al.'s arctan estimator in frequency-domain
    DoAa(n) = atan(N(n)./D(n));
```

```
152             % conditionals to resolve incident quadrant
153             if D(n)>=0                  % I & IV
154                 DoA(n)=DoAa(n);
155             elseif D(n)<0 && N(n)>=0     % II
156                 DoA(n)=DoAa(n)+pi;
157             elseif D(n)<0 && N(n)<0      % III
158                 DoA(n)=DoAa(n)-pi;
159             end
160
161         % ######################    New approach to DoA determination
162         % #### APPROACH TWO ####    in the frequency-domain with new
163         % ######################    conditionals to handle removal of
164         %                           omni sensor from arctan estimator
165
166         elseif approach == 2
167             % superior arctan estimator for sin and cos only
168             DoAa(n) = atan(A(n)./B(n));
169             % superior conditionals to resolve incident quadrant
170             if D(n)>=0 && N(n)>=0       % I
171                 DoA(n) = DoAa(n);
172             elseif D(n)<0 && N(n)>=0    % II
173                 DoA(n) = -DoAa(n)+pi;
174             elseif D(n)<0 && N(n)<0     % III
175                 DoA(n) = DoAa(n)-pi;
176             elseif D(n)>0 && N(n)<0     % IV
177                 DoA(n) = -DoAa(n);
178             end
179         end
180     end
181
182     %% FINAL PROCESSING
183     % final DoA & error processing
184     DoA_deg = -DoA*180/pi;          % radians to degrees
185     Err = (DoA_deg-phi);            % calculate error from true heading
186
187     %% PLOTS
188     if correction == 0
189         correctionstr = 'No';
190         correctionstr_ = 'none';
191     elseif correction == 1
```

```
192         correctionstr = 'Magnitude';
193         correctionstr_ = 'magnitude';
194     elseif correction == 2
195         correctionstr = 'magnitude and phase';
196     elseif correction == 3
197         correctionstr = 'Magnitude and phase';
198         correctionstr_ = 'magnitudeandphase';
199     end
200 
201     h1 = figure(10+select);
202     hold on
203     % error as a function of incident angle
204     subplot(2,3,[1,2,4,5])
205     hold on
206     box on
207     plot(phi, Err,'ko',...
208         'MarkerFaceColor','k')
209     yline(0,'r',...
210         'LineWidth',2,...
211         'Alpha',1)
212     xlabel('DoA [\circ]')
213     ylabel('Error [\circ]')
214     ttl = title(strcat(typename(select),{':  '},gunname(select)),...
215         'HorizontalAlignment','left');
216     ttl.Units = 'Normalize';
217     ttl.Position(1:2) = [0 1.05];
218     sttl = subtitle([correctionstr,' correction'],...
219         'HorizontalAlignment','left');
220     sttl.Units = 'Normalize';
221     sttl.Position(1) = 0;
222     annotation('textbox',...
223         [.145 .7 .2 .2],...
224         'String',{['\mu  =  ',num2str(round(mean(Err),2)),'\circ'],...
225                   ['\sigma  =  ',num2str(round(std(Err),2)),'\circ']},...
226         'FontName','times',...
227         'FontSize',14,...
228         'FitBoxToText','on',...
229         'LineWidth',2,...
230         'BackgroundColor','w')
231     set(gca,'XTick',linspace(-180,180,9),...
```

```
232             'YTick',linspace(-35,35,15),...
233             'XGrid','on',...
234             'YGrid','on',...
235             'GridAlpha',1)
236     axis([-180 180 -35 35])
237     % calculated DoA as a function of actual DoA
238     subplot(2,3,3)
239     hold on
240     box on
241     plot(phi,DoA_deg,'ko',...
242         'MarkerFaceColor','k')
243     plot(phi,phi, '-r')
244     xlabel('DoA [\circ]')
245     ylabel('Measured DoA [\circ]')
246     set(gca,'XTick',linspace(-180,180,9),...
247             'YTick',linspace(-180,180,9));
248     % error histogram
249     subplot(2,3,6)
250     hold on
251     box on
252     histogram(Err,...
253         linspace(-roundup2even(max(abs(Err))),...
254                   roundup2even(max(abs(Err))),9),...
255         'FaceColor','k',...
256         'FaceAlpha',.75,...
257         'LineWidth',2)
258     xline(0,'r',...
259         'LineWidth',2,...
260         'Alpha',1)
261     xlabel('Error [\circ]')
262     ylabel('Counts')
263     set(gca,'XTick',linspace(-roundup2even(max(abs(Err))),...
264                               roundup2even(max(abs(Err))),5),...
265             'XLimSpec','tight')
266 end
267
268 %% FUNCTIONS
269 function y = roundup2even(x)
270     x = floor(x);
271     for xx = 1:length(x)
```

```
        if x(xx)<=1
            x(xx) = 2;
        end
    end
    y = mod(x,2)+x;
end
```

C.2 Correction Factor

```
%% INFORMATION

% correctionfactor.m - creates correction mask for dipole configuration

% Inputs:       fs              - frequency (single value or array)
%               type            - type of correction factor
% Calls:        spectrumdata    - high res. sensor freq. response data
% Outputs:      correction      - mask to correct cos signal

% ENS Ionatan Soul, USN
% 17 June, 2022

function [correction] = correctionfactor(fs,type)
    %% IMPORT FREQUENCY RESPONSE FROM DATA
    % load data
    load('C:\path\to\spectrumdata.mat');
    % assign variables
    fr = n_cos.cos.frequency;           % frequecny - same for all runs
    Vcr = n_cos.cos.r;                  % cos response
    Vcp = unwrap(n_cos.cos.phase);      % cos phase
    Vcx = n_cos.cos.x;                  % cos real
    Vcy = n_cos.cos.y;                  % cos imaginary
    Vsr = n_sin.sin.r;                  % sin response
    Vsp = unwrap(n_sin.sin.phase);      % sin phase
    Vsx = n_sin.sin.x;                  % sin real
    Vsy = n_sin.sin.y;                  % sin imaginary
    Vosr = n_sin.omni.r;                % sin response
    Vosp = unwrap(n_sin.omni.phase);    % sin phase
    Vosx = n_sin.omni.x;                % sin real
```

```
30      Vosy = n_sin.omni.y;                % sin imaginary
31      Vocr = n_cos.omni.r;                % cos response
32      Vocp = unwrap(n_cos.omni.phase);    % cos phase
33      Vocx = n_cos.omni.x;                % cos real
34      Vocy = n_cos.omni.y;                % cos imaginary
35
36      %% INTERPOLATE VALUES FOR MASK
37      Vcrm = interp1(fr,Vcr,fs);          % cos response interp
38      Vcpm = interp1(fr,Vcp,fs);          % cos phase interp
39      Vcxm = interp1(fr,Vcx,fs);          % cos real interp
40      Vcym = interp1(fr,Vcy,fs);          % cos imaginary interp
41      Vsrm = interp1(fr,Vsr,fs);          % sin response interp
42      Vspm = interp1(fr,Vsp,fs);          % sin phase interp
43      Vsxm = interp1(fr,Vsx,fs);          % sin response interp
44      Vsym = interp1(fr,Vsy,fs);          % sin phase interp
45
46      %% ATTEMPT TO ADJUST PHASE APPROPRIATELY
47      [~,mci] = max(Vcr);         % find maximum amplitude response
48      [~,msi] = max(Vsr);         % find maximum amplitude response
49      Vcpp = Vcp-Vocp;            % subtract omni phase from cos phase
50      Vspp = Vsp-Vosp;            % subtract omni phase from sin phase
51      cc = Vcpp(mci)-pi/2;        % shift peak phase response down to...
52      cs = Vspp(msi)-pi/2;        % mimic phase response of SHO
53      Vcpp = Vcpp-cc;             % shift phase response down so that...
54      Vspp = Vspp-cs;             % peak response is at -pi/2
55      Vocpm = interp1(fr,Vcpp,fs);% interpolate for mask
56      Vospm = interp1(fr,Vspp,fs);% interpolate for mask
57
58      %% CREATE AND OUTPUT SELECTED CORRECTION FACTOR
59      if type == 0        % no correction
60          correction = 1;
61      elseif type == 1    % magnitude only
62          correction = Vsrm./Vcrm;
63      elseif type == 2    % magnitude and phase w/o attempted phase correction
64          correction = -(Vsxm+1i.*Vsym)./(Vcxm+1i.*Vcym);
65      elseif type == 3    % magnitude and phase w/ attempted phase correction
66          correction = (Vsrm.*exp(1i.*Vospm))./(Vcrm.*exp(1i.*Vocpm));
67      end
68  end
```

THIS PAGE INTENTIONALLY LEFT BLANK

List of References

[1] R. C. Maher, "Acoustical characterization of gunshots," in *2007 IEEE Workshop on Signal Processing Applications for Public Security and Forensics*, 2007 [Online]. Available: https://ieeexplore.ieee.org/document/4218954

[2] I. Freire and J. Apolinario Jr., "Gunshot detection in noisy environments," in *Anais de VII International Telecommunications Symposium*. Sociedade Brasileira de Telecomunicações, 2010 [Online]. Available: http://biblioteca.sbrt.org.br/articles/506

[3] M. Hrabina and M. Sigmund, "Acoustical detection of gunshots," in *2015 25th International Conference Radioelektronika (RADIOELEKTRONIKA)*. Pardubice, Czech Republic: IEEE, Apr. 2015 [Online], pp. 150–153. Available: http://ieeexplore.ieee.org/document/7128993/

[4] M. Kastek, R. Dulski, H. Madura, P. Trzaskawka, G. Bieszczad, and T. Sosnowski, "Electro-optical system for gunshot detection: Analysis, concept, and performance," in *International Symposium on Photoelectronic Detection and Imaging 2011: Advances in Infrared Imaging and Applications*. SPIE, Sep. 2011 [Online], vol. 8193, pp. 1059–1068. Available: https://www.spiedigitallibrary.org/conference-proceedings-of-spie/8193/81933W/Electro-optical-system-for-gunshot-detection--analysis-concept-and/10.1117/12.900968.full

[5] G. Tidhar, O. Aphek, and M. Gurovich, "An update on TED gunshot detection system development status," in *Infrared Technology and Applications XXXV*, 2009 [Online], vol. 7298, pp. 530–540.

[6] Raytheon Intelligence and Space, "Boomerang," 2022 [Online]. Available: http://www.raytheonintelligenceandspace.com/what-we-do/modernization-mission-support/mission-support/boomerang

[7] A. Sinha and T. Singh, "Acoustic localisation of gunshots in the presence of obstacles," in *2018 AIAA/CEAS Aeroacoustics Conference*, 2018 [Online]. Available: https://arc.aiaa.org/doi/pdf/10.2514/6.2018-3123

[8] Y. Arslan, "Impulsive sound detection by a novel energy formula and its usage for gunshot recognition," *CoRR*, p. 4, June 2017 [Online]. Available: https://doi.org/10.48550/arXiv.1706.08759

[9] R. Lilien, "Development of computational methods for the audio analysis of gunshots," U.S. Department of Justice, Chicago, IL, USA, Tech. Rep. Rep. 252947,

2019 [Online]. Available: https://www.ojp.gov/ncjrs/virtual-library/abstracts/development-computational-methods-audio-analysis-gunshots

[10] Raytheon Intelligence and Space, "Boomerang gunshot detection," July 2020 [Online]. Available: https://prd-sc101-cdn.rtx.com/-/media/ris/what-we-do/modernization-mission-support/mission-support/boomerang/2020-10/files/boomerang_data.pdf?rev=b3b7837160db47cca32e50a01a7d175b

[11] Security Update, "Gunshot detection technology: Hearing is believing," Feb. 2018 [Online]. Available: https://securityupdate.in/gunshot-detection-technology-hearing-is-believing/

[12] ShotSpotter, "Reduce gun crime with proven gunshot detection technology," 2022 [Online]. Available: https://www.shotspotter.com/law-enforcement/gunshot-detection/

[13] ShotSpotter, "Gunshot detection technology," Sep. 2014 [Online]. Available: https://www.shotspotter.com/system/content-uploads/mediakit/Gunshot-detection-WP.pdf

[14] QinetiQ, "EARS gunshot localization systems," 2022 [Online]. Available: https://www.qinetiq.com/en/what-we-do/services-and-products/ears-gunshot-localization-systems

[15] QinetiQ, *EARS SWATS*, 2021 [Online]. Available: https://www.qinetiq.com/-/media/e634d3dd156c48c48781d53665128cb9.ashx

[16] Jay Chang, William Mendyk, Lisa Thier, Paul Yun, Andy LaRow, Scott Shaw, and William Schoenborn, "Early Attack Reaction Sensor (EARS), A man-wearable gunshot detection system," in *Sensors, and Command, Control, Communications, and Intelligence (C3I) Technologies for Homeland Security and Homeland Defense V*, 2009 [Online]. Available: https://doi.org/10.1117/12.665978

[17] Metravib, *PEARL*, 2017 [Online]. Available: https://storage.googleapis.com/aco-metravib-defence.appspot.com/1/2021/03/EN-PEARL.pdf

[18] Metravib, *PILAR Helicopter*, 2017 [Online]. Available: https://storage.googleapis.com/aco-metravib-defence.appspot.com/1/2021/03/EN-PILAR-Helicopter.pdf

[19] Metravib, *PILAR V*, 2017 [Online]. Available: https://storage.googleapis.com/aco-metravib-defence.appspot.com/1/2021/03/EN-PILAR-V-Integrated.pdf

[20] F. Magand, A. Donzier, and F. Molliex, "PILAR acoustic gunshot detection & localization system: Principles of acoustic localization of small caliber gunshots," in *CFA/DAGA'04*, 2004 [Online]. Available: http://www.conforg.fr/cfadaga2004/master_cd/cd1/articles/000658.pdf

[21] P. Valpolini, “Acoustic gunshot detection systems,” *Armada International*, Aug. 2013 [Online]. Available: https://www.thefreelibrary.com/Acoustic+Gunshot+detection+systems.-a0364331354

[22] Microflown AVISA, “Microflown AVISA acoustic vector sensor technology,” 2022 [Online]. Available: https://www.microflown-avisa.com/technology

[23] Microflown AVISA, *Microflown AVISA leaflet ACLOGUS*, 2020 [Online]. Available: https://www.microflown-avisa.com/assets/uploads/Product-Leaflets/Microflown_AVISA_Leaflet_ACLOGUS_November_2020.pdf

[24] R. P. Fernandes, A. L. L. Ramos, and J. A. A. Jr, “Airborne DoA estimation of gunshot acoustic signals using drones with application to sniper localization systems,” in *Sensors, and Command, Control, Communications, and Intelligence (C3I) Technologies for Homeland Security, Defense, and Law Enforcement Applications XVI*, 2017 [Online]. Available: https://www.spiedigitallibrary.org/conference-proceedings-of-spie/10184/101840F/Airborne-DoA-estimation-of-gunshot-acoustic-signals-using-drones-with/10.1117/12.2262782.full

[25] R. C. Maher and E. Hoerr, “Audio forensic gunshot analysis and multilateration,” in *Audio Engineering Society Convention 145*, 2018 [Online]. Available: https://www.aes.org/e-lib/browse.cfm?elib=19826

[26] J. Svatos and J. Holub, “Smart acoustic sensor,” in *2019 IEEE 5th International forum on Research and Technology for Society and Industry (RTSI)*, 2019 [Online]. Available: https://ieeexplore.ieee.org/document/8895591

[27] T. C. Tran, M. N. Bui, and H. H. Nguyen, “A modified localization technique for pinpointing a gunshot event using acoustic signals,” in *Industrial Networks and Intelligent Systems*, N.-S. Vo and V.-P. Hoang, Eds., 2020 [Online]. Available: https://link.springer.com/chapter/10.1007/978-3-030-63083-6_11

[28] J. H. Park, W. Cho, and S.-C. Kim, “Improving acoustic localization accuracy by applying interaural level difference and support vector machine for AoA outlier removal,” in *2021 International Conference on Electronics, Information, and Communication (ICEIC)*, 2021 [Online]. Available: https://ieeexplore.ieee.org/document/9369732

[29] J. Ding, B. Ren, and N. Zheng, “Microphone array acoustic source localization system based on deep learning,” in *2018 11th International Symposium on Chinese Spoken Language Processing (ISCSLP)*, 2018 [Online]. Available: https://ieeexplore.ieee.org/document/8706599

[30] C. M. J. Galangque and S. A. Guirnaldo, "Gunshot classification and localization system using artificial neural network (ANN)," in *2019 12th International Conference on Information & Communication Technology and System (ICTS)*, 2019 [Online]. Available: https://ieeexplore.ieee.org/document/8850937

[31] C. Knapp and G. Carter, "The generalized correlation method for estimation of time delay," *IEEE Transactions on Acoustics, Speech, and Signal Processing*, vol. 24, no. 4, pp. 320–327, Aug. 1976 [Online]. Available: https://ieeexplore.ieee.org/document/1162830

[32] R. N. Miles, D. Robert, and R. R. Hoy, "Mechanically coupled ears for directional hearing in the parasitoid fly *Ormia ochracea*," *The Journal of the Acoustical Society of America*, vol. 98, no. 6, pp. 3059–3070, Dec. 1995 [Online]. Available: https://doi.org/10.1121/1.413830

[33] D. Wilmott, F. Alves, and G. Karunasiri, "Bio-inspired miniature direction finding acoustic sensor," *Scientific Reports*, vol. 6, no. 1, p. 29957, Sep. 2016 [Online]. Available: http://www.nature.com/articles/srep29957

[34] R. C. Rabelo, F. D. Alves, and G. Karunasiri, "Electronic phase shift measurement for the determination of acoustic wave DOA using single MEMS biomimetic sensor," *Scientific Reports*, vol. 10, no. 1, p. 12714, Dec. 2020 [Online]. Available: http://www.nature.com/articles/s41598-020-69563-1

[35] G. Karunasiri, F. Alves, and W. Swan, "MEMS directional acoustic sensor for locating sound sources," in *Fourth Conference on Sensors, MEMS and Electro-Optic Systems*, 2017 [Online]. Available: https://doi.org/10.1117/12.2244387

[36] G. Karunasiri, F. Alves, and W. Swan, "MEMS direction finding acoustic sensor," in *Smart Sensors, Actuators, and MEMS VIII*, 2017 [Online]. Available: https://doi.org/10.1117/12.2264952

[37] M. L. Kuntzman and N. A. Hall, "Sound source localization inspired by the ears of the O *rmia ochracea*," *Applied Physics Letters*, vol. 105, no. 3, p. 033701, July 2014 [Online]. Available: http://aip.scitation.org/doi/10.1063/1.4887370

[38] A. Ishfaque, A. Rahaman, and B. Kim, "Bioinspired low noise circular-shaped MEMS directional microphone," *Journal of Micro/Nanolithography, MEMS, and MOEMS*, vol. 18, no. 1, pp. 1–4, Feb. 2019 [Online]. Available: https://doi.org/10.1117/1.JMM.18.1.010501

[39] A. Rahaman and B. Kim, "Sound source localization by Ormia ochracea inspired lownoise piezoelectric MEMS directional microphone," *Scientific Reports*, vol. 10, no. 1, p. 9545, June 2020 [Online]. Available: http://www.nature.com/articles/s41598-020-66489-6

[40] Y. Zhang, R. Bauer, J. C. Jackson, W. M. Whitmer, J. F. C. Windmill, and D. Uttamchandani, "A low-frequency dual-band operational microphone mimicking the hearing property of Ormia Ochracea," *Journal of Microelectromechanical Systems*, vol. 27, no. 4, pp. 667–676, Aug. 2018 [Online]. Available: https://doi.org/10.1109/JMEMS.2018.2845680

[41] R. N. Miles, W. Cui, Q. T. Su, and D. Homentcovschi, "A MEMS low-noise sound pressure gradient microphone with capacitive sensing," *Journal of Microelectromechanical Systems*, vol. 24, no. 1, pp. 241–248, Feb. 2015 [Online]. Available: https://doi.org/10.1109/JMEMS.2014.2329136

[42] A. P. Lisiewski, H. J. Liu, M. Yu, L. Currano, and D. Gee, "Fly-ear inspired microsensor for sound source localization in two dimensions," *The Journal of the Acoustical Society of America*, vol. 129, no. 5, pp. EL166–EL171, May 2011 [Online]. Available: https://doi.org/10.1121/1.3565473

[43] A. Ishfaque and B. Kim, "Fly Ormia Ochracea inspired MEMS directional microphone: A review," *IEEE Sensors Journal*, vol. 18, no. 5, pp. 1778–1789, Mar. 2018 [Online]. Available: https://doi.org/10.1109/JSEN.2017.2787862

[44] A. Rahaman and B. Kim, "Microscale devices for biomimetic sound source localization: A review," *Journal of Microelectromechanical Systems*, vol. 31, no. 1, pp. 9–18, Feb. 2022 [Online]. Available: https://doi.org/10.1109/JMEMS.2021.3129282

[45] F. D. Alves, G. Karunasiri, and R. C. Rabelo, "Dual band Ormia-inspired MEMS directional acoustic sensor for near resonance operation," unpublished.

[46] QinetiQ, *EARS Fixed Site System*, 2021 [Online]. Available: https://www.qinetiq.com/-/media/aa67285e3c1c499681548796019d3b4b.ashx

[47] S. W. Davies, "Bearing accuracies for arctan processing of crossed dipole arrays," in *OCEANS '87*, 1987 [Online]. Available: http://ieeexplore.ieee.org/document/1160847/

[48] D. H. Dini and D. P. Mandic, "An enhanced bearing estimation technique for DIFAR sonobuoy underwater target tracking," in *Sensor Signal Processing for Defence (SSPD 2012)*, 2012 [Online]. Available: https://doi.org/10.1049/ic.2012.0115

THIS PAGE INTENTIONALLY LEFT BLANK

Initial Distribution List

1. Defense Technical Information Center
   Ft. Belvoir, Virginia

2. Dudley Knox Library
   Naval Postgraduate School
   Monterey, California